AD-A039 118 HUGHES RESEARCH LABS MALIBU CALIF F/G 20/6
DEVELOPMENT OF A COLOR SYMBOLOGY AC LIQUID CRYSTAL LIGHT VALVE.(U)
APR 77 A D JACOBSON, W P BLEHA N00024-75-C-7187
UNCLASSIFIED NL

1 OF 2
AD A039118

AD A039118

(20) 14

DEVELOPMENT OF A COLOR SYMBOLOGY AC LIQUID CRYSTAL LIGHT VALVE

FINAL TECHNICAL REPORT
FOR PERIOD 1 NOVEMBER 1974 THROUGH 12 JUNE 1976

APRIL 1977

Prepared under Contract N00024-75-C-7187

Approved for public release; distribution unlimited.

For the
DEPARTMENT OF THE NAVY
NAVAL SEA SYSTEMS COMMAND
Washington, DC 20362

Prepared by
A.D. Jacobson and W.P. Bleha
Hughes Research Laboratories
a division of Hughes Aircraft Company
Malibu, CA 90265

AD No. /
DDC FILE COPY

DDC
MAY 6 1977
B

HUGHES

HUGHES AIRCRAFT COMPANY
RESEARCH LABORATORIES

DEVELOPMENT OF A COLOR SYMBOLOGY AC LIQUID CRYSTAL LIGHT VALVE

APRIL 1977

Prepared Under

CONTRACT N00024-75-C-7187

FINAL TECHNICAL REPORT
FOR PERIOD 1 NOVEMBER 1974 TO 12 JUNE 1976

Prepared by

A.D. Jacobson and W.P. Bleha

Hughes Research Laboratories
Malibu, CA 90265

ACCESSION for
NTIS White Section
DDC Buff Section
UNANNOUNCED
JUSTIFICATION
BY
DISTRIBUTION/AVAILABILITY CODES
Dist. AVAIL. and/or SPECIAL
A

Prepared for

Department of the Navy
Naval Sea Systems Command
Washington, DC 20362

See 1473

Approved for public release; distribution unlimited.

ABSTRACT

The development of a reflective-mode liquid-crystal light valve suitable for large-screen dynamic color-symbology projection display is described. The light valve is a sandwich structure of a thin-film photoconductor, light-blocking layer, broad visible spectrum dielectric mirror, and liquid crystal between two glass electrodes with transparent conductive electrodes. There are no matrix elements to define resolution. Because of the insulating characteristics of the dielectric mirror, ac voltages must be used to operate the light valve. The CdS photoconductor operates as a high-resolution, imaging light-activated voltage gate for the liquid crystal. The light-blocking layer and the dielectric mirror reflect the projection light and prevent it from reaching the visible sensitive photoconductor. Imaging on the light valve is done with a low-intensity P-1 CRT with a fiber-optic faceplate and a light valve constructed on a mating fiber optic faceplate.

The report details the development of the ac light valve with two liquid-crystal modes: tilted perpendicular birefringent field effect and hybrid field effect (HFE). These field-effect modes allow white, yellow, magenta, blue, and green symbols to be projected on a black background. The black background also allows the superposition of static imagery, such as maps, on the color symbology. The various colors and white are selected by the value of the image light intensity.

The light valve was developed in two phases. The first concentrated on the tilted perpendicular device. The discussion of this phase considers the development of liquid crystal, alignment techniques, and CdS photoconductors and with dielectric mirror fabrication and light valve device physics. Also discussed are a new cell-holder design improvements in substrate uniformity and cosmetic quality. Finally, the performance of the two tilted perpendicular light valves, delivered to the Naval Electronics Laboratory Center, San Diego, California, is described.

The second phase, a continuation of the first, concentrated on the HFE light valve. The application of the HFE mode to color symbology is described, and final delivery to NELC is detailed.

PRECEDING PAGE BLANK-NOT FILMED

TABLE OF CONTENTS

PRECEDING PAGE BLANK-NOT FILMED

LIST OF ILLUSTRATIONS

PRECEDING PAGE BLANK-NOT FILMED

SECTION 1

INTRODUCTION AND PROGRAM SUMMARY

A. HISTORICAL BACKGROUND

This final report covers work done on Contract N00024-75-C-7187, entitled "Development of a Color Symbology Liquid Crystal Light Valve." That contract was a follow-on to Contract N00024-73-C-1185, "Development of a Reflection Mode Liquid Crystal Light Valve." The goal of the earlier program was to develop an ac version of the liquid-crystal light valve (LCLV)[1] that had been reduced-to-practice on an IR&D program at Hughes Research Laboratories (HRL) early in June 1972. The ac LCLV incorporates a dielectric mirror and a light-blocking layer to permit reflection-mode operation. In this way, the read-out light can be separated from the input image light so that very high intensity, white read-out light can be used for projecting images onto a large screen. All of the initial work on the program was organized around the dynamic scattering mode (DSM) electro-optic effect. Although this approach was effective in developing the novel ac LCLV substrate (the ITO/CdS/CdTe/dielectric mirror thin-film sandwich), we came to realize that DSM presented several drawbacks for the application of the LCLV to large screen display because it

- Was limited to projecting black symbols on a bright background, which is an undesirable format for many Navy applications
- Had relatively low contrast—never better than 13:1 and typically 5:1 or 6:1
- Had poor physical characteristics (e.g., slow speed of response, limited sensitivity, short lifetime, difficult cosmetics).

Fortunately, a parallel IR&D program at HRL, a program to examine alternative liquid-crystal electro-optic effects for the LCLV, bore fruit early in 1974. At that time we demonstrated for the Navy the new tilted perpendicular birefringent field-effect LCLV.[2] This device

offered the solution to most of the problems with the DSM device. It presented white symbols on a dark background, provided contrast in excess of 100:1, and led to substantially improved physical characteristics of the device. But perhaps most important, it was able to project multi-color symbology onto a large screen with a single device. This new capability was felt to be very desirable for many Navy applications. As a result of this demonstration, the Navy authorized Hughes to extend the scope of the initial contract to permit Hughes to fabricate and deliver a tilted perpendicular field-effect light valve for evaluation. After completing this evaluation, the Navy initiated the follow-on contract with Hughes to develop a color-symbology light valve. This report describes the work done on and the results obtained from that follow-on contract.

B. DESCRIPTION OF THE PROGRAM

The principal initial task for this program was to perfect the tilted perpendicular birefringent field-effect mode for application to the projection of color symbology imagery onto a large screen. The birefringent field effect uses the liquid crystal essentially as a uniaxial birefringent single crystal with birefringence which is variable in response to an applied electric field. A typical characteristic curve of a liquid-crystal layer used in such a mode is shown in Figure 1. (The birefringent effect discussed and its realization with liquid crystals is discussed in the proposal, No. 74M-5260/C6321-3, associated with this contract and will not be repeated here.) Under the influence of an applied field, the liquid crystal, when placed between crossed polarizers, rotates the polarization of the incoming light so that a portion of the light passes through the polarization analyzer. Initially, at low applied voltage, the polarization of each wavelength in the incident light is affected equally. Hence, at low applied voltage, white light emerges from the analyzer. However, as voltage increases, the birefringence of the liquid-crystal layer increases and dispersive effects occur. These effects cause the polarization associated with different wavelengths (colors) to be rotated by different amounts. It is this effect which permits different colors to be selected for projection onto the screen. The light valve controls the

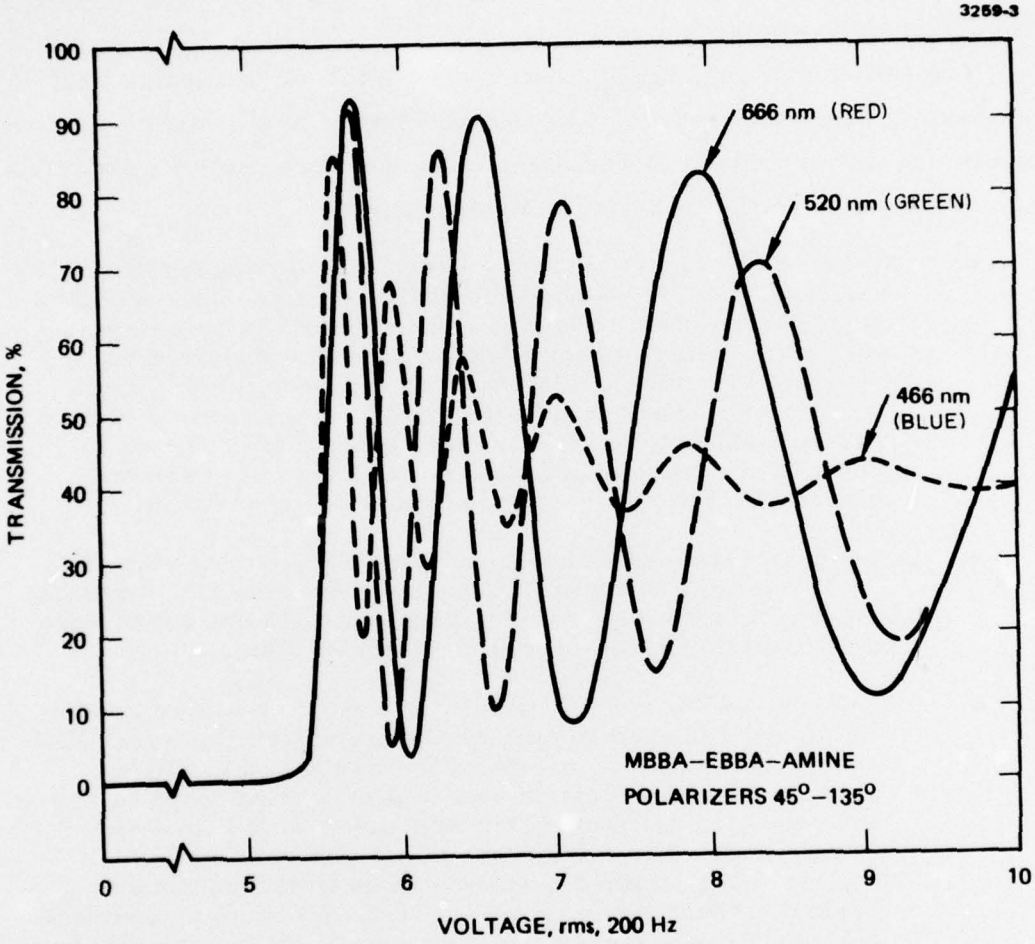

Figure 1. Birefringent liquid crystal response characteristics.

selection of color by selectively applying the correct voltage to the liquid crystal at each resolution element across the aperture of the device. The voltage distribution is established by the distribution of the intensities of the input light that falls on the CdS photoconductor from the primary image source.

The initial program tasks, which were intended to realize useful performance from this device, were related to the performance parameters of resolution, speed of response, and cosmetic quality. Briefly, these tasks included the following considerations:

- Resolution—The resolution of the color-symbology imagery was limited by the so-called outline effect. This effect is caused by the low voltages at the edge of the color symbol where the voltage changes from the value required to generate the color symbol to that required for the black background. This causes white light transmission rather than no light transmission. This outline effect tends to spread the apparent line thickness of the color symbol, leading, thereby, to an apparent loss of resolution.

- Speed of Response—The color symbols occur at very high tilt of the liquid-crystal molecules. As a result, the time required for the liquid crystal to decay from a color state to the background state was undesirably long.

- Cosmetics—The most difficult task (and the major accomplishment) realized in making the transition from the DSM to the birefringent field-effect light valve on the IR&D program mentioned above was in discovering ways to prevent unwanted artifacts from appearing in the imagery. Such artifacts can arise from misalignment and from electric-field-induced discontinuities in the response characteristics of the liquid crystal. Moreover, cosmetic problems in this device were increased by the great sensitivity of the eye to color contrast. Quite small variations in device uniformity are visible because they often lead to local differences in color. Thus, both cosmetic point defects and local variations in alignment must be carefully controlled in the birefringent field-effect color-symbology light valve.

The program was organized to attack these particular tasks and thereby to develop an operational color-symbology light valve. The details of and results from that program are given in this report. Section 1.C summarizes the key results. Section 1.D describes the LCLV and its operation.

C. PROGRAM SUMMARY

This program was highly successful. We were able to establish control of the new technology required to implement the ac light valve with field-effect-mode liquid-crystal electro-optic effects. The most significant result from the program was the application of a new liquid-crystal electro-optic effect to the display of color symbology.[3,4] That effect was originally developed for use with spatially coherent laser read-out light. By making the transition from the tilted perpendicular birefringent field effect to the new effect — the hybrid field effect (HFE)[5] — we were able to avoid several limitations of the tilted perpendicular effect. The primary limitation was short device lifetime caused by a photochemically induced instability in the tilt angle of the birefringent field-effect device. By using the HFE, we were able to increase the speed of response, sensitivity, and resolution of the light valve. However, we paid a penalty in device performance for this transition to the HFE. The transmission efficiency of the new electro-optic effect is somewhat lower than is that of the birefringent effect. Moreover, it requires larger switching ratios to present white (as well as colored) symbols on a black background than does the tilted perpendicular light valve, and very large switching ratios to provide black and white continuous tone images. It also does not provide as high contrast as does the tilted perpendicular device. Nevertheless, the substantially greater device stability and lifetime — lifetime as great as 2,000 hr at full read-out light throughput have already been measured in the laboratory — and the very effective color symbology performance more than outweigh the sacrifices in performance mentioned above. Therefore, we regard the introduction of the HFE color-symbology light valve to be a major step forward in the development of the color-symbology liquid-crystal light valve. Since the HFE device was introduced near the end of the program, additional work remains to complete the development of the color symbology light valve.

We conclude this section by comparing and discussing the program device performance goals and the characteristics of the final LCLV

delivery. This is followed by a brief discussion of the additional tasks that are required to complete the development of the HFE color-symbology light valve.

Table 1 compares the program goals with the characteristics of the final HFE mode color symbology LCLV device delivered to NELC. (Complete specifications for this device are given in Section 3. B.)

We exceeded program goals in many areas. The device sensitivity achieved (100 $\mu W/cm^2$) is sufficiently high that the present CRT technology is capable of driving the light valve through the complete range of colors. We also achieved a remarkably high contrast ratio (120:1) for an HFE mode device. This resulted from the transmission null in the HFE characteristics that we discovered during the program. As mentioned above, we have made significant gains in operating lifetime (>1,000 hr), projection light capacity (>2,000 lumen), and stability by using the HFE mode. During the program, cosmetic quality, light-intensity variation, and packaging have also been improved, so much so that manufacturing technology can be effectively applied to produce an LCLV monochrome symbology product. However, because of the great sensitivity of the eye to small color variations, more work is still necessary to display uniform color across the entire working aperture.

Additional effort is also needed to improve response time, resolution, intensity of the color peaks, and the generation of a white-on-black gray scale. Although the observed response times of 125 msec rise and 140 msec decay are close to 100 msec goals for the white-on-black symbology, the response time (in particular the rise time) for the selection of color peaks needs further improvement. The slow rise is caused primarily by the slow rise at low-imaging light intensities of the thick CdS photosensor used in the device. This area requires further work in the on-going multimode LCLV program. Similarly, the symbol outline that limits resolution is primarily a problem of gaining further linearization of the photosensor. As is discussed in

Table 1. Comparison of Program Goals and Characteristics of Final LCLV Delivery

	Goals	Final Delivery
Sensitivity, $\mu W/cm^2$ at 525 nm	150	100
Resolution		
White on black	60 lines/mm	Symbol: 51 lines/mm
Color on black	40 lines/mm	Symbol w/ outline: >18 lines/mm
Contrast (W/B)	20:1	120:1
Grayscales (W/B)	8	0
Reflectivity, %	80	85
Speed, msec		
Excitation (W/B)	100	125
Extinction (W/B)	100	140
Excitation (Color)	100	800 to 2200
Extinction (Color)	100	150 to 220
Color Content	White, blue, green, magenta on a black background	White, yellow, magenta, blue and green on a dark background
Lifetime, hr	1000	>1000
Projection-light capacity, lumen	1000	>2000
Cosmetic Quality	No more than 5 point defects over the aperture	4 point defects: 3 mm, 2.5 mm, 2.5 mm, and 0.8 mm diameter. Small area of fine, low-contrast scratches
Uniformity, %		
Max. intensity variation	>60	88
Max. color variation	>90	75 of aperture one color
Packaging	Hermetic sealing, thickness tuning	Hermetic sealing, thickness tuning

Sections 2.A and 2.B, the thicker CdS photosensor allowed using the HFE operating mode for color symbology, but did not give the additional performance gain needed to minimize the outline effect effectively. To do this will require implementing the composite graded band-gap photosensor being developed in the multimode LCLV program. However, because of the reversal of selection of the color peaks in the HFE mode as compared with the tilted perpendicular, the symbol outline is not white but is a lower intensity color. Thus, the outline is not as obvious and has less effect on apparent symboi resolution.

Finally, methods of optimizing the intensity of the color peaks must be pursued through a study of the electro-optic behavior of the HFE mode. Since this mode is very complex, it will not be possible to construct a simple model, such as was done with the tilted perpendicular field-effect mode, to provide a basis for the experimental work. Therefore, we plan to study the electro-optic behavior both by computer simulation and direct experimentation. We believe that the implementation of the program just outlined will result in the development of a truly practical color-symbology LCLV.

D. DESCRIPTION AND OPERATION OF THE LCLV

1. Configuration

The LCLV device is the thin-film multilayer structure shown schematically in Figure 2. The components of the light valve are the

- Primary electrode
- Counterelectrode
- Liquid-crystal layer.

The primary electrode consists of a fiber-optic faceplate substrate and a multifunction stack of vacuum-deposited thin films. This stack includes a transparent electrode, a photosensor, a projection light blocking layer, a dielectric mirror, and a liquid-crystal alignment

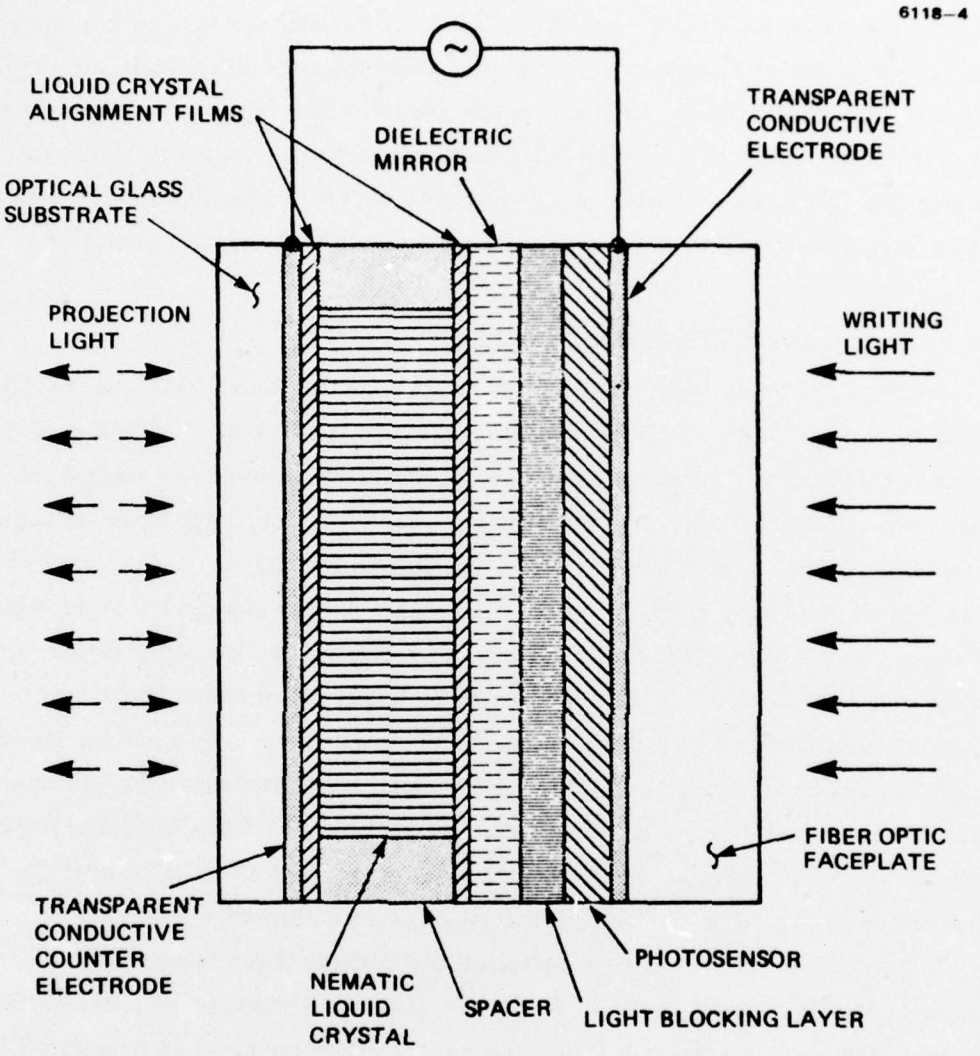

Figure 2. Schematic of the photoactivated LCLV.

film. The counterelectrode forms the cover of the device. It consists of an optical glass substrate on which a thin-film structure has been deposited; this structure consists of a transparent electrode, a liquid-crystal alignment film, and a spacer layer. The spacer, confined to the circumference of the optical aperture of the device, is used to define the thickness of the liquid-crystal layer. The liquid-crystal layer is sandwiched between the primary and the counterelectrode.

2. Description of the LCLV Layers

This section, with reference to Figure 2, describes the LCLV structure in detail. Transparent conductive electrodes made of indium-tin oxide (ITO) are used to apply an ac voltage across the sandwich structure. The photosensor CdS film converts the input light image that is incident on the fiber-optic faceplate into an electrical signal that can drive the liquid crystal.[5,7] Peak photosensitivity is at 525 nm in the green. The dielectric mirror and the light-blocking layer optically protect the photosensor from the output projection light beam, which is incident on the device from its other side. The CdTe light-blocking layer provides >4 neutral-density (ND) isolation between the photosensor and the read-out light. The characteristics of the layer are shown in Figure 3, in which the absorption of the CdTe and the photoresponse of the CdS are plotted as a function of wavelength.

The dielectric mirror reflects the output light beam back through the counterelectrode and out of the device. It consists of alternating optical films of sputtered TiO_2 and SiO_2. The mirror is designed to provide greater than 90% reflectivity across the visible spectrum; alternatively, it can be tuned to reflect a specific spectral region at a higher reflectivity if that is required for a specific application. The combination of the light-blocking layer and dielectric mirror give us a total factor of 10^6 isolation of the photosensor from the projection light. Thus, the light valve can handle high projection light intensities without performance degradation.

Sputter-deposited films of SiO_2 are used to overcoat both the dielectric mirror and the counterelectrode. These films provide a

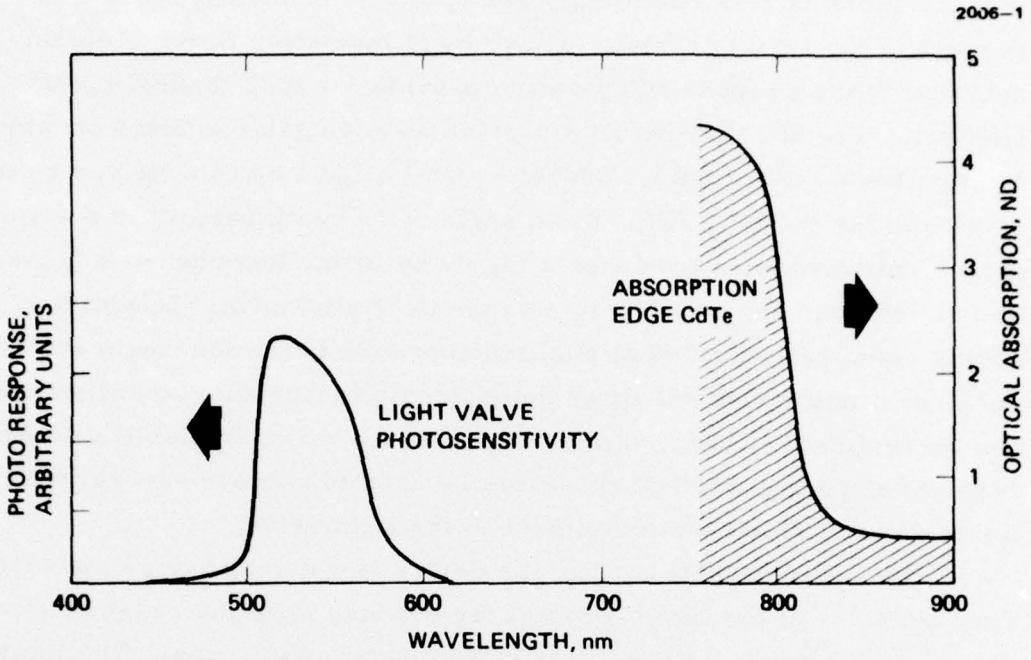

Figure 3. Comparison of photo-response of CdS compared with optical absorption spectrum of CdTe light-blocking layer.

surface which is both chemically and electro-chemically inert with respect to the liquid crystal. These inert insulating films in combination with the ac mode of operation provide for long liquid-crystal lifetime. The SiO_2 layers also provide an acceptable surface on which to align the liquid crystal. Liquid crystal alignment is achieved by ion-beam etching the SiO_2 films at an angle of 20^o with respect to the surface. This technique produces a highly uniform, homogeneous (parallel) or twisted homogeneous ("twisted nematic") alignment. In addition, by adding chemically bonded aliphatic compounds to the ion-beam etched surface, a unidirectional tilted homeotropic (perpendicular) alignment can be realized. These alignment techniques make available a complete range of alignment modes; these can be used to achieve several different liquid-crystal electro-optic effects in the light valve.

The liquid crystal used in the device is a nematic-type material. The thickness of the liquid-crystal layer, which is in the range of 2 to 12 μm, is chosen to suit the particular device application. The liquid cyrstal electro-optic effects used in the light valve are discussed in more detail in Section 3.

3. Operation of the LCLV

Two device layers, the CdS photosensor and the liquid-crystal layer, control the operation and performance of the light valve.[7] An ac voltage power supply is applied to the sandwich by means of the two ITO transparent electrodes. In the absence of an input-imaging light (i.e., in the off-state of the device), most of the power-supply voltage drops across the photosensor, and the liquid crystal remains below the activation threshold. When the input-imaging light is turned on, the photosensor impedance is substantially lowered and most of the voltage is switched across the liquid-crystal layer. This causes the liquid crystal to become electro-optically activated and thereby to modulate the projection light.

The most important feature of the thin-film structure is that it preserves the spatial resolution of the image. In other words, a small

spot of light in the input image generates an equally small spot of activated liquid crystal. Image resolution is maintained through the device because the photocurrent that is created when the input light strikes the photoconductor does not spread as it passes through the device. This very desirable phenomenon is due to the physical structure of the device and also to the focusing effect of the electric field across the device. The complete device thin-film structure is less than 0.05 mm thick and is 50 mm in diameter. Therefore, the impedance through the device is much lower than the lateral impedance over the face of the device. Also, the field which results from the applied voltage is directed across the device and thus forces the photocurrent to flow through the films rather than along the film interfaces. Therefore, if a complex distribution of light (i.e., a high-resolution input image) is focused onto the CdS photoconductor, the device converts that image into an exact replica (high resolution) electro-optic activation image in the liquid crystal. The electro-optic image in the tilted perpendicular mode has been discussed in detail in the final report of Contract N00024-73-C-1185. The novel HFE mode, used for the first time for color symbology in this program, is discussed in Section 3.A.

To read out the replica image which has been created in the liquid crystal, a projection or output light is passed through the liquid-crystal layer, reflected from the dielectric mirror, and then passed back through the liquid crystal and out of the device. The light is then projected to the screen by means of the projection read-out optics shown in Figure 4.

The reflection-mode structure of the device has three important advantages:

- The read-out beam is blocked from the photoconductor, which prevents overwriting the photoconductor by the read-out source. This feature permits using a very high brightness, broad bandwidth projection light.

- The dielectric mirror blocks the flow of any dc current components. This is vital to the realization of long liquid-crystal lifetime.

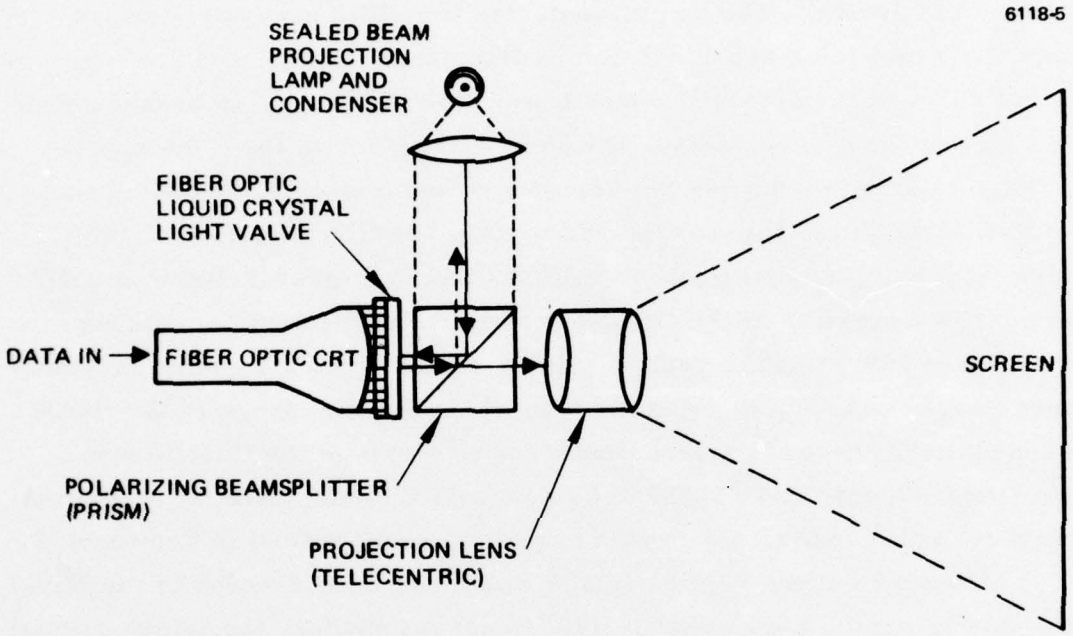

Figure 4. Liquid-crystal large-screen display projector.

- The double pass of the read-out light through the liquid-crystal layer enables us to reduce the thickness of the liquid crystal by a factor of two. This increases the speed of response of the liquid crystal by a factor of four.

SECTION 2

THE FIRST PHASE—THE TILTED PERPENDICULAR COLOR-SYMBOLOGY LIGHT VALVE

This section summarizes the progress made in this program to develop a tilted perpendicular color-symbology light valve. This work is a continuation of the color-symbology light-valve program supported by NAVSEA Contract N00024-73-C-1185. We report here the results of a study to determine the causes of the color-symbology outline effect and to formulate approaches to reduce the magnitude of the effect. This is followed by a report of the work done to improve the light-valve substrate including improvements in the dielectric mirror, blemish density and also the development of an extended switching ratio photosensor.

Next, we detail the development of new liquid crystals and of alignment techniques. This development will provide stable, controllable tilted perpendicular alignment. Finally, we describe an improved cell holder design and record the properties of two interim devices delivered to NELC that represent the state of the art of the particular light valve configuration.

A. DEVICE PHYSICS

In this section we analyze the physical factors, related to both the light valve and the primary image source, that lead to the color symbol edge outline that is present in the light valve projected image. The purpose of this analysis is to understand fully the causes of the outline and to find solutions to minimize the effect. Below, we detail the five primary causes of the outline that we have identified so far, along with possible solutions for each. Finally, we discuss the immediate approach we plan to take, based on our analysis of the feasibility and impact of the various possibilities.

PRECEDING PAGE BLANK-NOT FILMED

1. Causes of Color-Symbology Outline Effect

The color-symbol outline manifests itself as a white border around the edges of a symbol projected from the tilted perpendicular color-symbology light valve. Presently, this border limits color symbology to 15 lines/mm resolution with a 100% MTF input image.* The reason for the broad spectral character of the outline is the nature of the color transmission characteristics of the tilted perpendicular aligned liquid crystal. As was detailed in the Final Technical Report of Contract N00024-73-C-1185, at low $V_{LC}/V_{threshold}$ values, where V_{LC} is the voltage applied across the liquid-crystal layer and V_{th} is the threshold voltage for the liquid-crystal electro-optic effect, the separation of the birefringent color peaks is very small, thus giving a white broadband transmission. This voltage image corresponds to low imaging light intensity activation of the light valve photosensor. As V_{LC}/V_{th} increases, corresponding to increased levels of imaging light, the birefringent colors separate to form the distinct color symbols. Thus, the white border around the color symbols is the result of a low level activation of the liquid crystal in the transition region between the center of the symbol and the black background. To minimize this effect, it is necessary to provide the liquid crystal with as steep a voltage gradient as is possible to prevent low values of V/V_{th} from giving a broad white outline around the symbol.

We have identified five possible mechanisms that tend to reduce the steepness of the voltage gradient:

- The CRT spot shape
- The photosensor nonlinearity
- Saturation of the photosensor switching ratio with increasing imaging light

---

*This border effect is different from the character edge effect (called "black lines") which results from reverse tilt of the liquid-crystal molecules. The blackline artifact can be eliminated by increasing the liquid crystal pre-tilt angle beyond a minimum value so that reverse tilt of the molecules cannot occur.

- Image spreading in the liquid crystal
- Image spreading in the photosensor.

These effects and their estimated relative contribution to the overall outline effect are briefly summarized below.

a. The CRT Spot Shape

The electron-beam (E-beam) activation of the phosphor in the CRT, which is the primary display for the light valve, produces a Gaussian-shaped light-intensity pattern. Thus, the light in the wings of the Gaussian curve produces a low-level activation of the light valve that contributes to the outline effect. This effect is enhanced by the nonlinearity of the photosensor film (see below). A direct solution is to alter the shape of the CRT spot to provide a spot profile that more closely approximates a step function. Two approaches to this are to use a laminar flow gun CRT and/or to reduce the scattering and spreading of light in the phosphor.

b. Photosensor Nonlinearity

Photosensor nonlinearity refers to the property of the CdS film that leads to increased photocurrent at low levels of light excitation. This is illustrated in Figure 5, which shows that 10% of the input imaging light required to generate a green symbol generates a photocurrent that is 50% of the green symbol photocurrent (solid grid lines). This shows that only 2% of the input light that is required to generate a green symbol will generate a white symbol outline. This is a principal reason why the wings of the Gaussian CRT spot contribute so effectively to broadening the outline effect. The solution to this problem is to linearize the photosensor response – a linear response would result in a 10X improvement in the magnitude of the outline. Another approach is to operate the light valve far below threshold so that low light levels do not excite the liquid-crystal molecules. Both of these approaches can be implemented by recourse to a photosensor that has substantially higher switching ratios than those that we presently use. This is discussed further in the following paragraph.

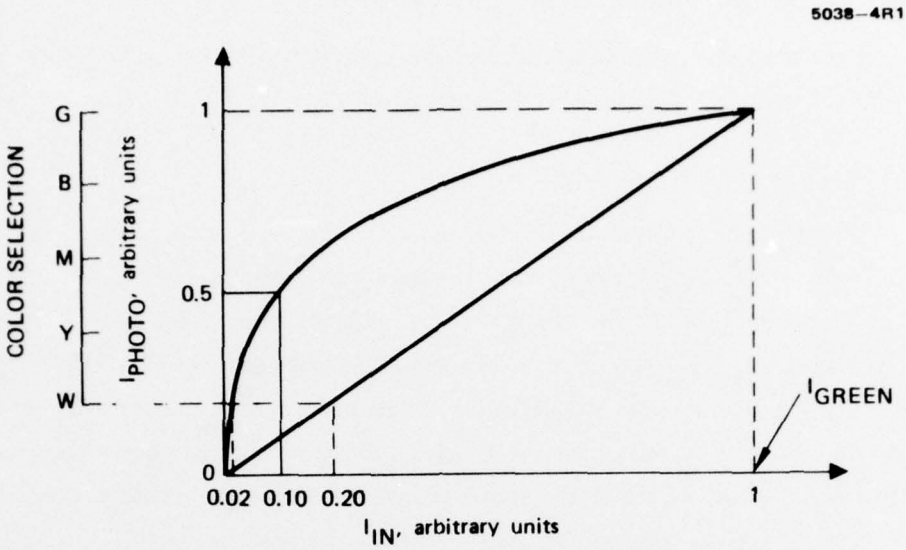

Figure 5. Photocurrent as a function of input imaging intensity for CdS light valve photosensor.

c. Photosensor Thickness

Another effect, closely related to photosensor nonlinearity, is a saturation effect that limits the available switching ratio of the light valve. This effect results from loading the light valve impedance by the liquid-crystal layer and the dielectric mirror as we now describe. The switching ratio SwR is defined as

$$SwR = \frac{Z_{CdS} + Z_{load}}{Z'_{CdS} + Z_{load}} ,$$

where

Z_{CdS} = impedance of photosensor in dark

Z'_{CdS} = impedance of photosensor with imaging light

Z_{load} = impedance of liquid crystal and dielectric mirror.

Under the present operating conditions, Z'_{CdS} becomes much less than Z_{load} for input light levels that produce white symbology. As a result, the switching ratio changes slowly with increased imaging light intensity. This effect contributes to the nonlinearity mentioned above. The solution to this problem is to increase Z_{CdS} and Z'_{CdS} by increasing the CdS photosensor thickness; then, for a given switching ratio, the operation of the light valve is further removed from saturation region. The factors that limit the thickness of the CdS are the effects of increased photosensor thickness on light-valve resolution, sensitivity, and optical quality.

d. Photocurrent Spreading in the Substrate

This effect relates to the spatial resolution limits of the substrate. In general, we can expect some spreading of the photo electrons as they traverse the stack of thin films to activate the

liquid crystal. This spreading can occur both in the film and along surface channels. The ratio

$$Z_{\perp} / Z_{\parallel} \quad ,$$

where

$Z_{\perp}$ = impedance of the substrate perpendicular to the substrate plane

$Z_{\parallel}$ = impedance parallel to the substrate plane,

determines the magnitude of the spreading. One possible solution is to increase $Z_{\parallel}$. We can accomplish this by increasing the sheet resistivity of the most conductive film of the substrate, the CdTe light blocking layer, and also by eliminating any conductive junction surface channels that may exist at the CdS/CdTe interface. The other approach is to decrease $Z_{\perp}$ by maximizing the light valve operating frequency. Increasing the frequency increases the capacitive current, thereby reducing the operating impedance level of the light valve relative to the sheet resistivity of the films. We have already observed some improvement in the outline by operating the light valve at 100 kHz compared with 10 kHz.

e. Image Spreading in the Liquid Crystal

The final contributing effect we have analyzed is image spreading in the liquid crystal. Similar to spreading in the substrate, this will contribute reduced resolution and thus an increased outline effect. To ascertain the magnitude of this effect, we have constructed and tested cells that allow us to activate the liquid crystal with an image without using a substrate. To do this we fabricated the image pattern into the electrodes of the cell. Since we did not observe an outline effect, it appears that this is not a contributing factor to the outline

effect in the present light valve. Nevertheless, the liquid crystal can be used to reduce the outline effect. By developing high-birefringence, low-viscosity materials, we will be able to operate the light valve in the color mode with a lower switching ratio. This will improve the overall linearity of the device because it will permit us to use a smaller, and thus more linear, portion of the curve shown in Figure 5.

2. Summary and Approaches to Outline Reduction

Table 2 summarizes the causes of the outline effect and the possible approaches for improvement. Based on this analysis, we believe that the best and most direct approach to reducing the outline effect is to improve photosensor linearity. This could provide up to a tenfold reduction in the spread of the outline. To implement this approach, we plan to develop the technology to increase the thickness of the CdS photosensor from the present value of 15 μm. The advantage of thicker CdS is to reduce the dark current without reducing the on current. This will increase the switching ratio. We will also evaluate the thick composite photosensor structure of the type CdS/Cd_xSS_{1-x} presently being developed on a Hughes IR&D program. We expect the limit on CdS thickness will be determined by the loss of resolution and sensitivity and caused by surface roughness from the increased grain growth that occurs in the thick films. The results of this program are reported in Section 2.3.

B. SUBSTRATE TECHNOLOGY

1. Light Valve Cosmetics and Uniformity

The program to improve the uniformity and cosmetic quality of the color-symbology light valve focussed on three areas. In the first two areas, we approached the cosmetic program of eliminating point defects in the light-valve substrate. These point defects originate in the light-valve thin films through the disruption of the film growth caused by substrate imperfections and foreign particles on the surface

Table 2. Factors Contributin to Color Symbology Outline Effect

Factor	Approach for Improving
CRT spot shape	Beam Profile Shaping
CdS photosensor non-linearity	Thicker film
Switching ratio saturation	Thicker film; graded image light absorption
Liquid crystal properties	High Δn, low η liquid crystal
Photocurrent spreading	High sheet ρ blocking layer Eliminate channel effects High-frequency operation

of the substrate, and also by the inclusion of the dust or of unwanted source material particles during the deposition processes. In particular, we devised a sputtering target polishing technique that has reduced the density of point defects in the photosensor film by a factor of ten, and we have implemented a procedure to minimize defects in the sputtered mirror. In the third area, that of light-valve uniformity, we improved the uniformity of the liquid-crystal spacer to provide less than 5% variation in the spacer thickness around the light-valve aperture. We also studied the problem of achieving uniform color responses across the device aperture.

a. Photosensor Sputtering Target Polishing

Sputtering targets are generally made from hot pressed powders of a high-purity material. This is the only practical technique for forming large-area targets with a semiconductor like CdS, which is used in the light valve as the input photosensor. However, pressed targets have the severe drawback that powder particles can be ejected from the sputtering target during the deposition process and become embedded in the growing film. This ejection process can occur even though the process is performed in the "sputter-up" mode — a mode that prevents gravitational forces from depositing particles on the

substrates. Once particles are attracted and adhere to the substrate surface, they cause the growth of a conical-shaped nodule which creates a gross point defect in the film. For example, a 0.5-μm particle embedded in the film near the start of the deposition process will grow to a defect ~15 μm in diameter in a 15-μm-thick film. Thus, this mechanism causes large defects that are quite visible in the projected image. Generally, the number of defects is between 50 and 100 for a 2 in. diameter aperture substrate.

We determined that the physical mechanism which causes particles to be ejected from the target is the microscopically uneven erosion of the sputtering target that occurs with continued use. As the target surface is sputtered away, some powder particles, or groups of particles, do not sputter as rapidly as others, and eventually are left protruding from the surface. Then, because good thermal contact to the target is lacking, they become hot and are explosively ejected from the surface of the target onto the substrate. The approach that we took to solving this problem was to eliminate the particles from the target surface before deposition begins. Our process for doing this is to polish the target surface optically before each deposition run. We use 600 grit silicon carbide polishing paper, then clean the surface thoroughly to remove any residual powder. To avoid contaminating the vacuum system with fine residual particles from this polishing procedure, we devised a demountable target assembly that allows us conveniently to remove the target from the system. This procedure has substantially improved the cosmetic quality of the substrate by removing these defects, which were the largest (and most visible) point defects found in the light valve. When the process is performed carefully, this type of defect can be completely eliminated.

b. Sputtered Dielectric Mirror Defects

Point defects in the dielectric mirror and liquid-crystal alignment film are particularly detrimental to the operating life of the light valve because they allow the liquid crystal to react electrochemically with the CdS and CdTe films below them. Our analysis of the

defects in the mirror has indicated that most of the defects originate from dust and foreign particles present in the sputtering chamber and not from particles ejected from the sputtering targets. Equipment limitations aggravate this situation by limiting us to sputtering down; gravity then deposits particles on the substrate surfaces. To prevent these inclusions from propagating a defect through the complete mirror stack, we modified the deposition process to permit the substrates to be removed several times during a run to clean the surfaces. This procedure allows us to remove included particles and permits subsequently deposited layers to coat the craters left by the removed particles. Although this process has improved the defect density in the mirror, it should be considered an interim procedure until manufacturing technology methods can be applied to develop improved techniques.

c. Liquid Crystal Spacer Uniformity and Design

In the color-symbology light valve, the thickness uniformity of the liquid crystal is critical to achieving uniform color activation over the entire aperture. The degree of uniformity is controlled by two principal factors:

- The absolute thickness variation in the deposited spacer that defines the liquid-crystal layer thickness
- The flatness of the substrate and counterelectrode.

To achieve the necessary high degree of uniformity, a flat-plate planetary-motion substrate holder (see Figure 6) was installed in the dielectric film, E-beam deposition system. This system allows us to deposit uniform SiO_x spacers on as many as five substrates at a time. In operation, the variation in thickness around a given spacer, or between different spacers in a particular deposition run, is less than 5%, which is the accuracy of the thickness measurement.

The spacer design was modified to allow the excess liquid crystal to flow readily from between the electrodes while the cell is being fabricated. We have found that trapping of the liquid crystal by the spacer design used previously, which has two small exit ports, led to a pressure

distortion of the glass surface and thus to nonuniformity in the thickness of the liquid crystal. Moreover, the distortion changed with time as the liquid crystal slowly flowed out through the small ports after the device was in use. The new spacer design, which consists of sixteen 0.20 in. diameter circular pedestals around the circumference of the 2 in. circular aperture, permits the liquid crystal to readily flow from the aperture. Thus the cell is in a stable, non-distorted condition at the time of cell fabrication.

d. Uniformity and Flatness of the Liquid Crystal Layer

This section reports on a study of the causes of liquid crystal thickness non-uniformity. This area is particularly important because, without high uniformity of the layer thickness, uniform color response across the device aperture cannot be achieved.

The overriding factor in determining thickness uniformity is the flatness of the substrate and of the counterelectrode. In general, we would like to maintain an optical flatness of $<\lambda/4$ for both components. Mating the components would then result in a maximum cell nonuniformity of $\sim\lambda/2$. Thus, the variation would be $\sim 4\%$ for a 6 μm liquid crystal thickness, which is adequate for the color-symbology display. The counterelectrode has never presented any problem in maintaining the required flatness specification. The BK-7a optical glass used is strain free and maintains its flatness through the processing steps of indium-tin oxide deposition, SiO_2 deposition, and ion-beam etching. The substrate, however, does not behave similarly. Because of the high stress buildup in the CdS sputtered photosensor film (see Final Technical Report, Contract N00024-73-C-1185, Section III-C) during deposition, the substrate is warped by the film. In practice, if we start with a substrate optical flatness of $<\lambda/4$, the figure will warp to $\sim 4\lambda$, convex, after the deposition of the conventional CdS film. By using previously unused optical glass from a previously unused fiber-optic faceplate, the surface can initially be polished 4λ, concave, to give a first order compensation to the resultant bowing of the substrate. This procedure generally results in a final substrate figure in the range of

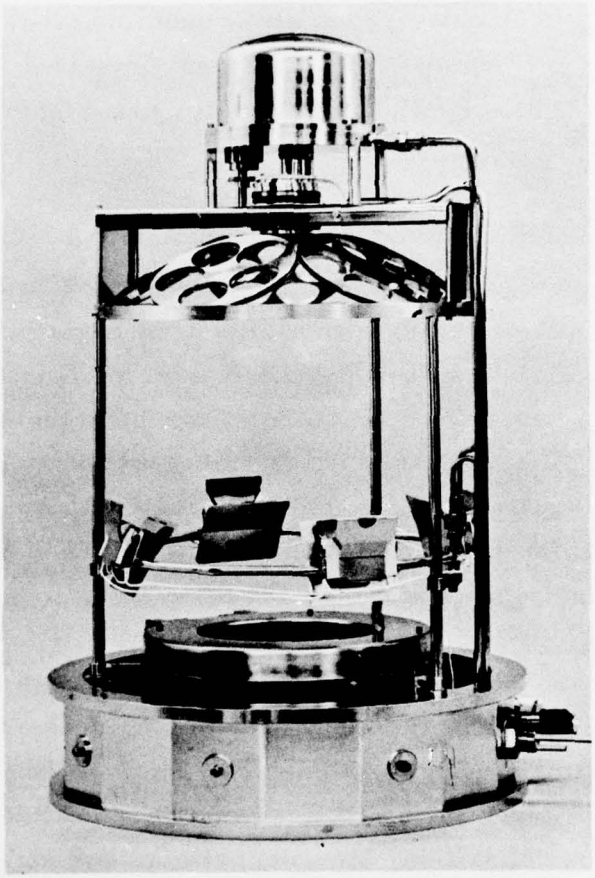

Figure 6. Flat plate planetary motion substrate holder.

$\sim\lambda/2$, which is adequate for black and white symbology. A further complication arises with the re-use of the fiber-optical faceplates for new light valves, a procedure that is necessary because of the high initial cost of the plates. The results of prior light-valve processing steps is to create a random residual strain in the used faceplate which does not even permit the use of the polishing compensation technique. (Because of possible long-term drift in the faceplate figure, it will be desirable to anneal out this residual strain.) We have not attempted to develop an annealing procedure (a logical plate to optimize this type of process will be in the Manufacturing Technology Program presently proposed to the Navy).

Thus, we have two reasons to develop a new polishing process: (1) the previously used polishing compensation technique was not accurate enough for color symbology and (2) the residual fiber-optic strain causes a random variation of the surface figure of the substrate. The most practical point at which to re-polish the fiber-optic faceplate with the CdS film is before any additional films are deposited. This is because the thickness of the CdS film is seven times greater than that of any other film in the light valve, and thus is more amenable to polishing. An additional advantage of polishing at this point is that the chemo-mechanical polish step already used to remove surface structure from the CdS film can then be used to remove polishing damage. To re-acquire the flatness, we used a hard-pitch lap with a suitable polishing powder to optically polish the CdS surface. With this procedure, it is possible to return the faceplate/film combination to a flatness of $<\lambda/4$ with the removal of <2 μm of material. However, yield on this process has not been high and it is still difficult to achieve good color uniformity consistently. We also still have a problem with residual gross scratches on the polished film surface. These scratches are caused by particles of CdS or of polishing particle agglomerates on the hard lap being forced across the soft CdS surface during polishing, thereby causing a groove. Again, these are areas well suited to optimization in a manufacturing technology program.

2. Sputtered Dielectric Mirror Development

The sputtered TiO_2/SiO_2 dielectric mirror, developed under contract N00024-73-C-1185, was made of a part of the standard light valve device during this program. This step was taken because we confirmed the long operating lifetime of both TiO_2 and SiO_2 in contact with the liquid crystal and thus the complete superiority of this system over ZnS and Na_3AlF_6 was demonstrated. In addition, we completed two other important areas of development: (1) extension of the spectral width of the high reflectivity region and (2) development of an improved optical monitor for accurately measuring the thickness of the sputtered films.

a. Sputtered Dielectric Mirror Operating Life Tests

The life tests performed in this program were concerned primarily with the TiO_2 mirror component; the SiO_2 component, which is in direct contact with liquid crystal, had previously not shown any tendency to degrade the liquid crystal material. However, the role of the SiO_2 surface in the problem of tilted perpendicular alignment stability has not yet been determined. The life tests on TiO_2 were performed with the use of test cells consisting of a TiO_2 film or TiO_2/SiO_2 alternating films and liquid-crystal layer sandwiched between ITO coated electrodes. The cells were driven at 15V rms, 10 kHz, which is a higher voltage level than that used in normal color-symbology light valve operation. After 10^3 hr of continuous operation in a dark environment, there was no evidence of catastrophic degradation of the liquid-crystal material or of the interface films. Similar tests performed with liquid crystal in the presence of the ZnS and the cryolyte films had shown that gas bubbles and film reduction occurred very rapidly after voltage was applied. Again, the complex question of the surface effects of alignment stability have not been dealt with; however the inertness of the liquid crystal in contact with these materials, which is so important for device lifetime, was clearly demonstrated.

b. Extended Spectral Range Dielectric Mirror

In a parallel IR&D program, we have designed (by computer) and fabricated extended-range dielectric mirrors that provide less than 2% total visible light transmission of a filtered Xenon arc lamp in the spectral band from 400 to 750 nm. A typical deposited mirror spectrum is shown in Figure 7, which includes a theoretical curve calculated by computer. These results are reported because they are relevant to the high-brightness Navy color-symbology light valve. In projecting $>10^3$ lumens from a LCLV, Hughes-Fullerton found deleterious heating effects resulting from absorption of residual projection light in the lower layers of the light valve. This absorption causes a temperature gradient to develop from the center to the edge of the light valve aperture because of differences in thermal paths for heat dissipation. This gradient results in nonuniform changes in the tilt angle of the liquid crystal, which in turn causes a spatial difference in the threshold value for the activation of symbols, and a variation of off-state light transmission. Table 3 summarizes the sources and quantity of light absorption in the light valve. The major source (7%) was projection light transmission through the dielectric mirror with subsequent absorption in the CdTe light-blocking layer. Present results with the extended range mirror are also presented in Table 3. The measured mirror transmission is reduced to 1.6%, which makes it comparable to other light-valve component absorption levels. With further improvements in mirror design and monitoring (see below), we expect to reach a goal of <1% absorption. This improvement plus an expected reduction in the absorption of other elements should reduce total light-valve absorption to <3% (see Table 3). Then, using the conversion that 2×10^3 lumens corresponds to 7 W of visible light, total absorption is <0.2 W. In a 2 in. diameter cell, this corresponds to a power density of 0.07 W/in.^{2}, which is below the present acceptable maximum power dissipation limit of ~0.1 W/in.^{2}. Thus, we will be able to project up to 3×10^3 lumens without affecting the performance of the light valve.

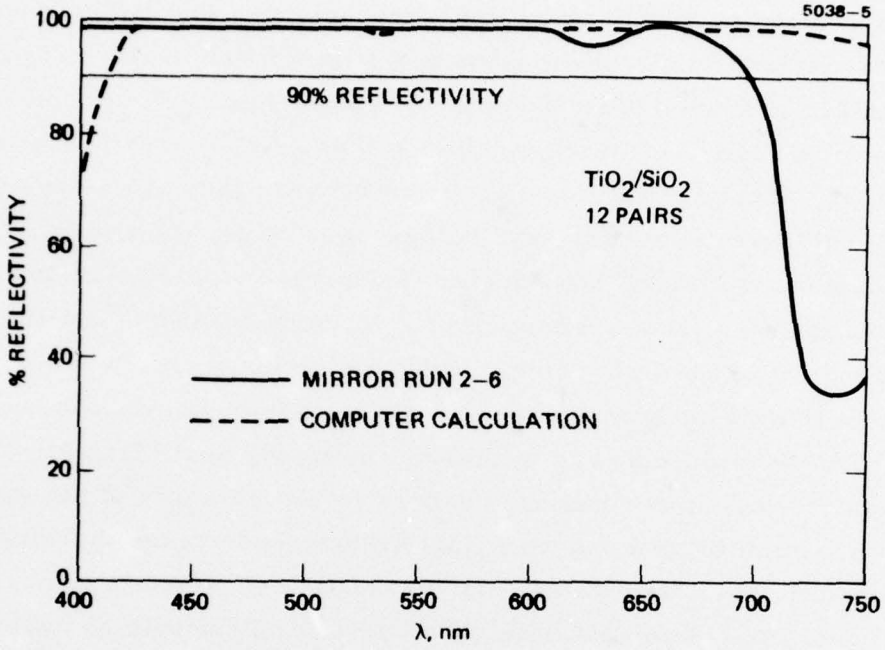

Figure 7. Spectrum of extended spectral range sputtered dielectric mirror.

Table 3. Summary of Light Valve Absorption with Extended-Range Mirror

Cell Component	Absorption %	Present Results, %	Goal, %
Dielectric mirror	7.0	1.6	1.0
ITO	2.0	2.0	1.0
Glass	0.7	0.7	0.7
Liquid crystal	0.2	0.2	<0.1
Total	9.9	4.5	2.8
Note: data taken with a filtered xenon spectrum.			

c. Improved Optical Monitoring of the Sputtering System

To achieve the optical film thickness accuracy required for depositing the extended range dielectric mirrors, we have begun, under the present contract, to develop an improved optical monitor for the dielectric mirror sputtering system. The previous monitor design, described in Section II. B of the Final Technical Report for Contract N00024-73-C-1185, used laser beams to provide a well-collimated source of light to facilitate entry and exit of the beam into and out of the confined area between the sputtering target and the substrates. Although we were able to use this monitoring technique to successfully produce the standard broadband dielectric mirror previously used, a basic problem remained. The choice of monitoring wavelengths was limited to available laser lines – typically the 6328 Å red He-Ne laser output and the 4880 Å blue and 5140 Å green Ar ion laser outputs. Because this light is not at the exact wavelengths necessary for monitoring the extended range mirror, we were not able to follow the design criterion to produce the improved mirror.

The technique we evolved to provide more versatile monitor wavelengths was to use a high-intensity white light source with narrow spectrum-width filters. With the relatively small filament size and

the high brightness available, we were able to achieve sufficient collimation and intensity to cover the path length required for the entry and exit of the light beam into and out of the sputtering system. The actual optical path in the sputtering system was horizontal, through a 1/2 in. thick glass substrate holder plate to a 45^{o} mirror prism that directed the light vertically to a thin glass cover slip in the plane of the substrate surfaces (see Figure 8). The mirror layers depositing on the cover slip provided the reflectance change that was detected after the light was reflected back through the same path and out of the system. The cover plates are manually changed when different wavelengths are monitored, or when the differential signal becomes too weak to provide high accuracy for the determination of the quarter-wave thicknesses.

In actual mirror depositions, this system has given excellent results, achieving a strong signal without the use of electronic noise reduction. We are now able routinely to monitor any given wavelength in the visible spectrum to ~1.5%. Thus it is now possible to fabricate reproducibly the extended range mirrors described above. Additional development still required for the mirror monitor system centers on the design and implementation of an automatic in situ mirror monitor slide changer. This would allow us to complete the deposition of the mirror and of the liquid-crystal alignment film without breaking vacuum.

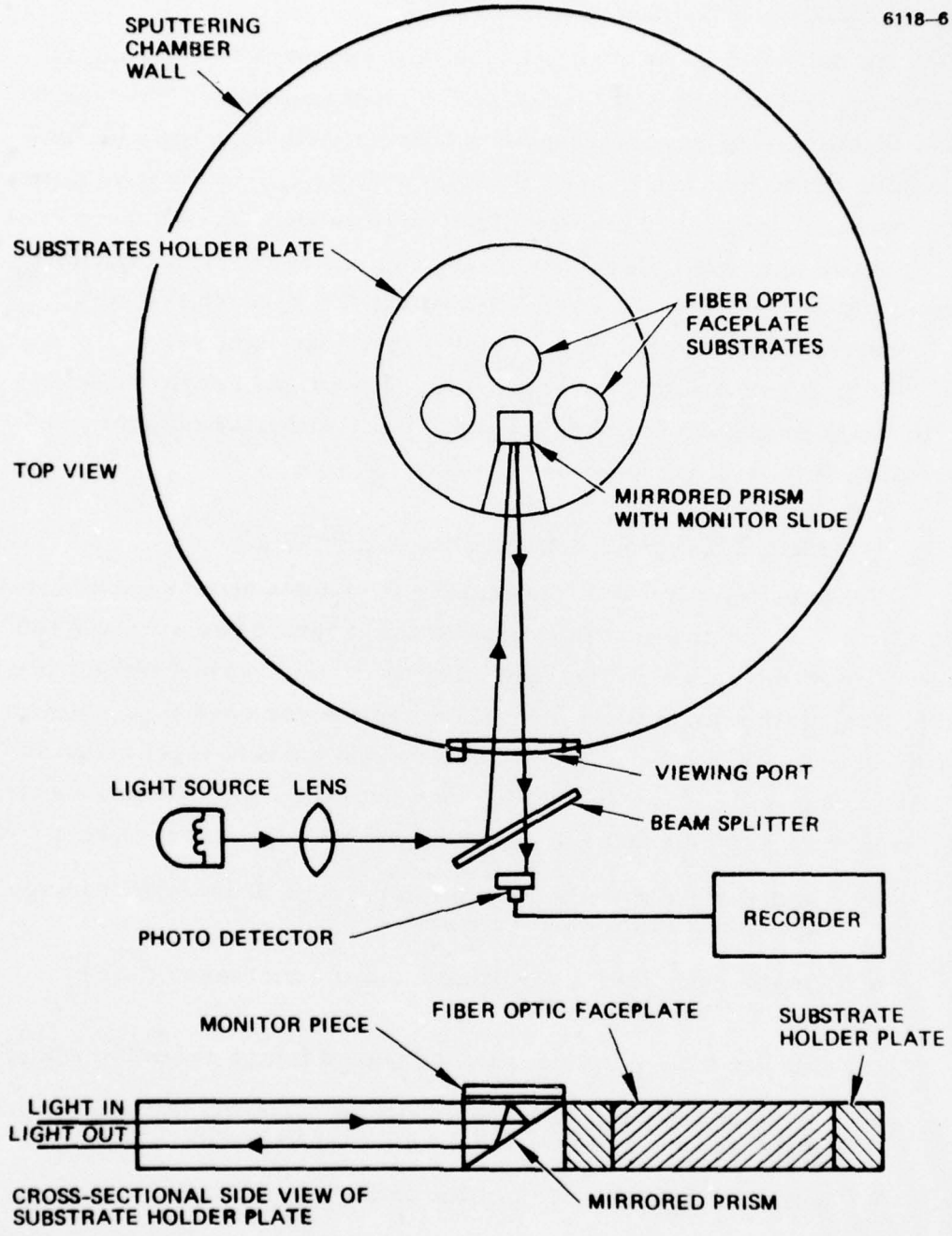

Figure 8. Schematic views of improved sputtering system optical monitor.

3. Extended Switching Ratio Photosensor

As indicated in Section 2.A, the best approach to reducing the symbology edge effect is to linearize the photoresponse. This can be done by increasing the photosensor's current switching ratio (defined as the ratio of the imaging light-activated current, I_L, to the dark current, I_D, flowing through the complete light valve sandwich). We have considered two possible approaches to increasing the current switching ratio. One is the thick CdS graded-absorption approach that was successfully implemented in the color-symbology light valve.[6,7] Another is the composite material, graded band gap approach; with further development, has the potential of providing even higher performance than with the ungraded approach.

a. CdS Photosensor with Increased Thickness

The most direct way of increasing the photosensor switching ratio is to increase the physical thickness of the layer. (The standard thickness for CdS film used in the light valve is 15 μm.) This results in a higher capacitive impedance of the layer in the dark and thus a lower dark current. Then the image light activated current level remains constant, the switching ratio I_L/I_D can be increased. Before we tried this approach, we felt that the following problems would be encountered:

- Reduced light-valve resolution because of increased image spreading in the thicker layer
- Image granularity resulting from the increased size of polycrystalline grains
- Slower time response and increased image retention effects
- Loss of imaging light sensitivity because the photo generated current is not effectively distributed in the thick layer
- Loss of adhesion of the film on the substrate.

In practice, the first three played a role in determining a usable film thickness. The experimental results are discussed below.

CdS films up to 60 μm thick were deposited. To improve the uniformity of photoelectron generation through the thickness of the film, the temperature-grading technique described in the Final Report of Contract N00024-73-C-1185 was used. In this technique, the substrate temperature is varied from a high value at the beginning of the deposition to a lower value at the end. This increases photosensitivity by producing higher optical absorption in the film closer to the CdS-CdTe junction. A detailed description of the physics of this approach is given in Appendix B. This improved absorption profile is shown schematically in Figure 9. Plots of switching ratio versus CdS thickness are shown in Figures 10 and 11 for bias frequencies of 2 and 10 kHz, respectively. Both the saturated (high imaging light intensity) and the 100 $\mu W/cm^2$ switching ratios are given. The switching ratio increases with film thickness, with the 100 $\mu W/cm^2$ value increasing at a slower rate. The lower switching ratios observed at higher frequencies result because a portion of the photogenerated carriers are unable to follow the rapidly changing electric fields associated with higher frequency operation. Although increasing the film thickness does provide the larger switching ratios needed to linearize the light-value response, eventually the trade-off factors (mentioned above) become significant. With film thicknesses above ~30 μm, we observed an objectionable granularity in the output imagery of the complete light valve; we attributed this to the growth of large crystallites in the film. The crystallite boundaries have slightly different photo response than the crystal interiors and thus the boundary pattern was visible in the output image. We attempted to inhibit the growth of the crystallites by removing the films from the sputtering station in the middle of the deposition cycle and polishing the surface. We hypothesized that this approach would cause a renucleation of the film and thus the re-start of smaller diameter crystals which would then grow through the second half of the film but not have as large a diameter as with the continuously grown film. Although this approach did eliminate the image granularity, it also resulted in a lower switching ratio and a higher photosensor response time.

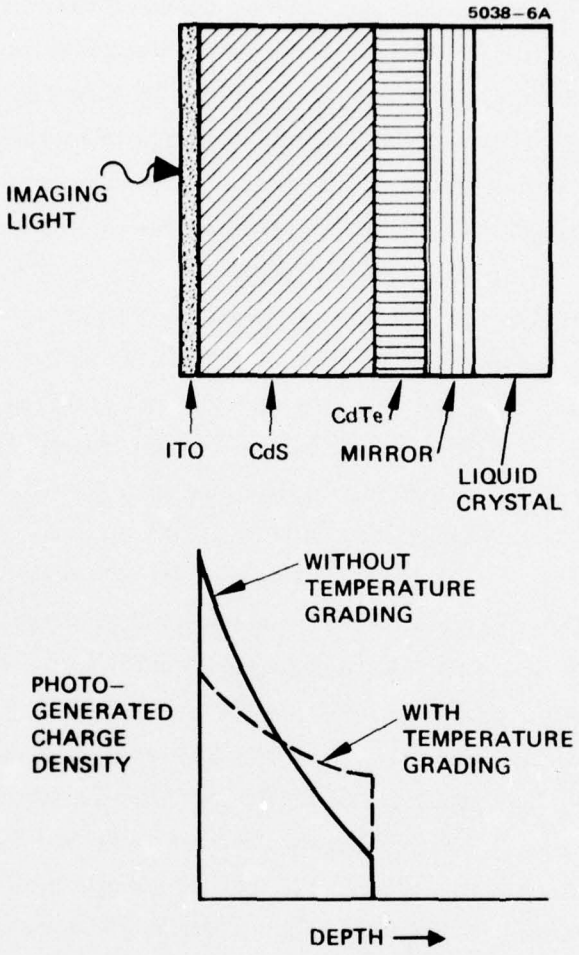

Figure 9. Configuration and absorption characteristics of graded temperature CdS photosensor.

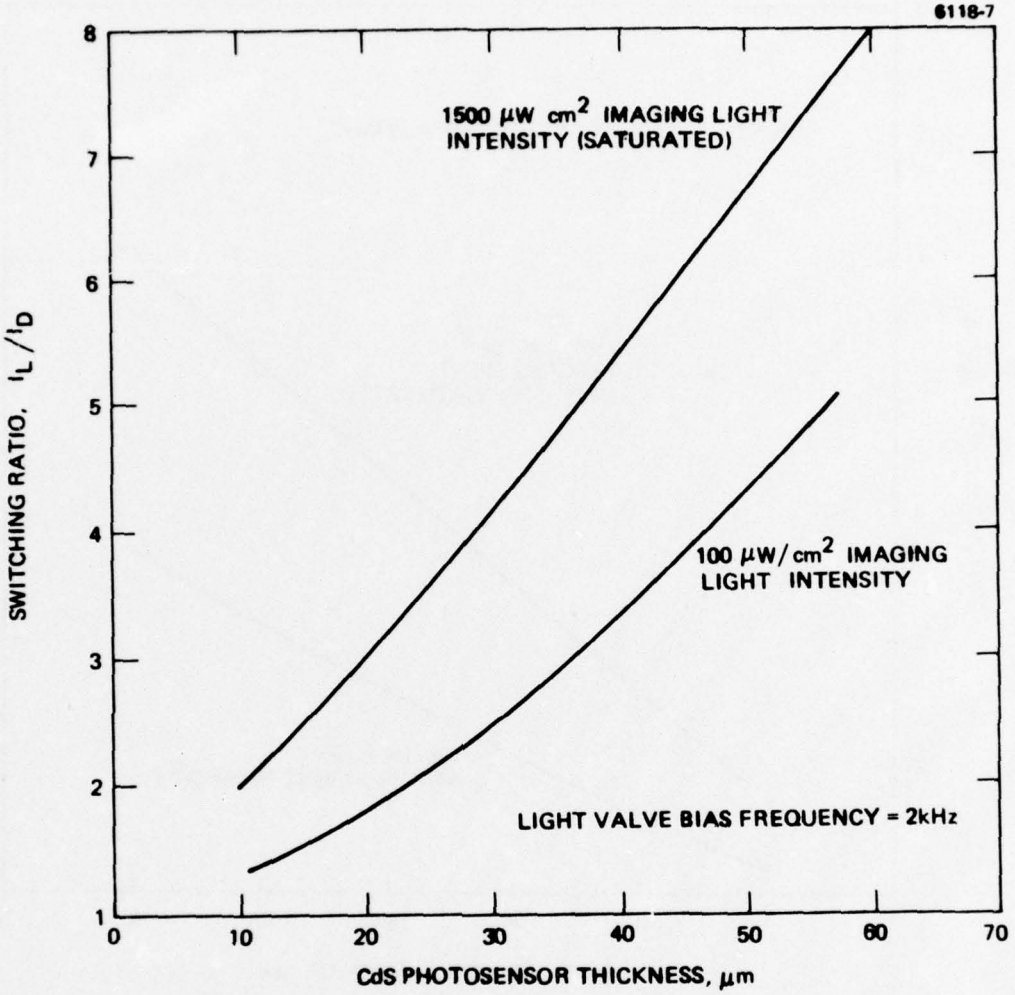

Figure 10. CdS graded absorption photosensor switching ratio as a function of film thickness. Light valve bias frequency = 2 kHz.

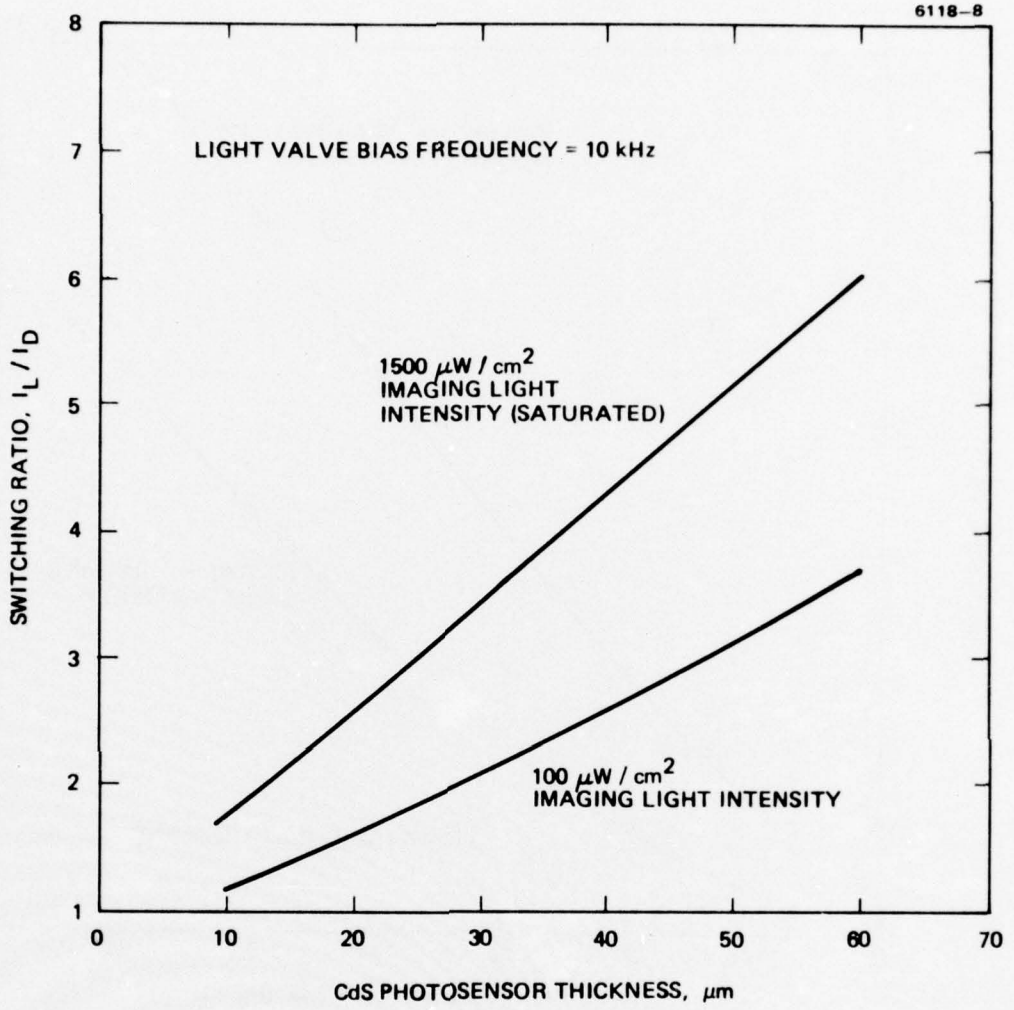

Figure 11. CdS graded absorption photosensor switching ratio as a function of film thickness. Light valve bias frequency = 10 kHz.

In addition to granularity, the very thick films showed increased image retention effects; we attributed these to deep electron traps, which play an increasingly important role in the thick films. Because of these factors, a practical limit of 30 μm thickness was established for the present development of the color-symbology light value. With the 30 μm thick photosensor, the switching ratio was increased from 1.5 to 2.5 (100 $\mu W/cm^2$, 2 kHz), which allowed us to linearize the homeotropically aligned color-symbology light value. More importantly, it also gave us the additional switching ratio required to made practical the HFE color-symbology light value developed in Phase II of this program.

b. Application of the Graded Band Gap Photosensor to the Color-Symbology Light Valve

In a parallel Hughes IR&D program, we developed an improved high-switching-ratio photosensor consisting of three layers of different band gaps. The layers, shown schematically in Figure 12, are CdZnS (next to the ITO back electrode), CdS (in the center), and CdS Se (next to the CdTe light-blocking layer). The relative band gaps of the three layers are shown in Figure 12. Different band gap materials were used to allow light to penetrate uniformly through the entire thickness of the photosensor and thus to improve the efficiency of photocurrent generation. This is an improvement over the temperature-graded band gap approach used in the thick CdS films just described because it allows greater penetration of light to the CdTe interface, where it is most efficiently used.[2] The switching ratio of the graded band-gap photosensor as a function of frequency is shown in Figure 13. Large increases in saturated switching ratio are obtained at 100 $\mu W/cm^2$ with less than proportional increase. One drawback to using these films is the anomolously slow time response of the CdSSe (which dominates the response of the three layers) – its response time is not predicted by the accepted theoretical model of photoconductivity in II-VI compounds.[8]

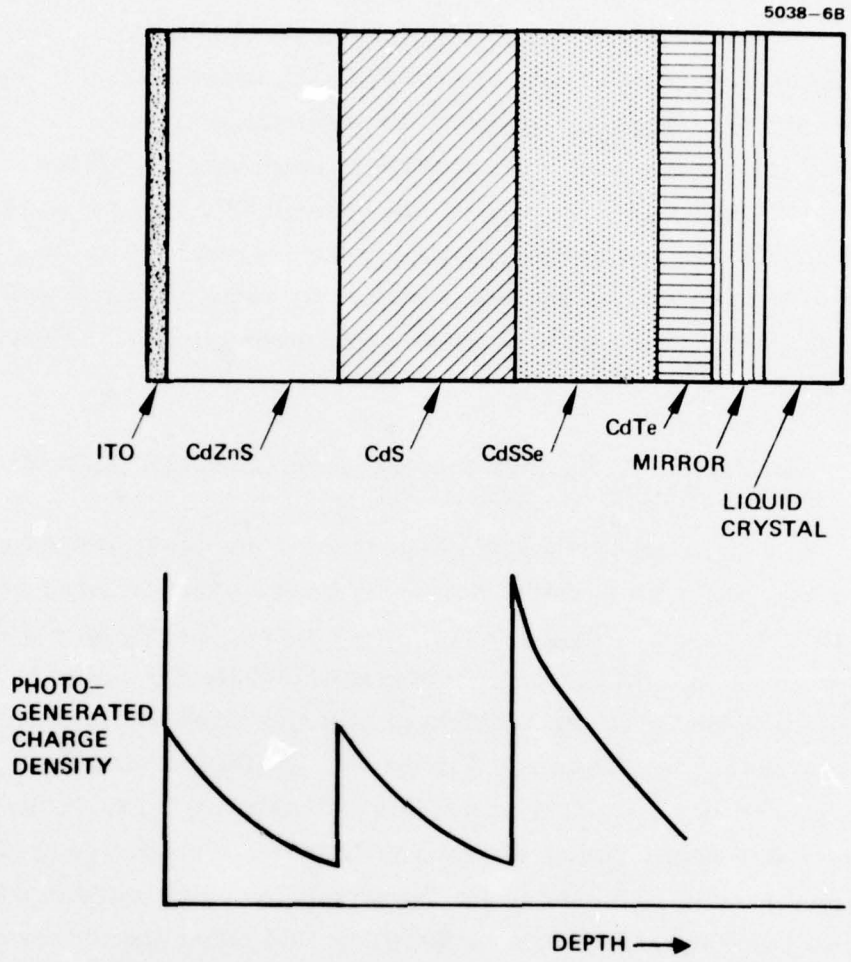

Figure 12. Configuration and absorption characteristics of three layer composite photosensor.

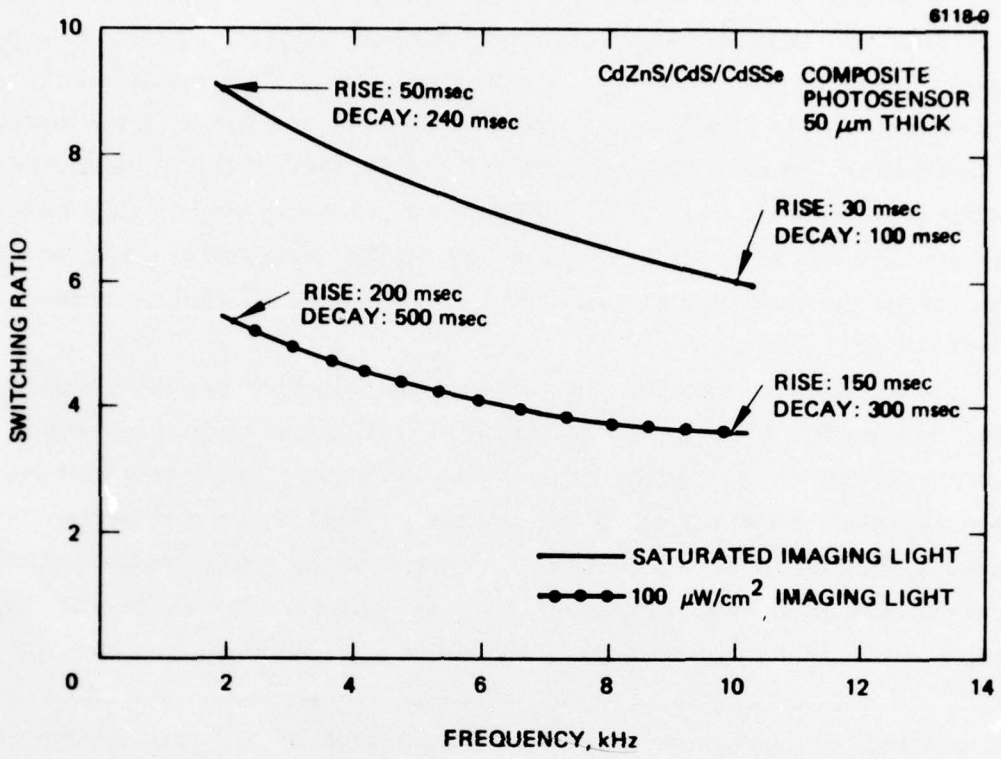

Figure 13. Composite photosensor switching ratio and response time as a function of voltage bias frequency.

The results reported for the switching ratio of the graded band gap composite photosensor were measured on films that had not been given the standard light valve polishing process. This mechanical polishing process provides an optically flat surface for uniform device performance and also removes the diffuse surface of thick, polycrystalline photosensor film. The mechanical polishing step is followed by the chemo-mechanical process which removes the damaged surface layer created by the mechanical polish and restores the photoelectronic properties.

On graded composite films given this polishing process, the high switching ratios were severely degraded. A measurement of each component film indicated that the CdSSe top layer completely lost its photoresponse after the polishing process. This was not expected because the chemical behavior with respect to the iodine in the polishing process of CdSSe should be similar to that of CdS. It was beyond the scope of the present program to develop a new polishing process for the CdSSe. Because of this polishing problem, we were not successful in integrating the composite graded band gap photosensor into the complete light-valve structure. Also, using a dual structure of CdZnS and CdS provided no particular advantage over the thick CdS layer described above. And the slow response of the CdSSe layer indicates that more developmental effort is required in the deposition of this material before it can be incorporated into the color-symbology light valve.

C. LIQUID CRYSTAL TECHNOLOGY

This section reports the results of our program to develop liquid-crystal materials and alignment techniques suitable for a practical tilted perpendicular color-symbology light valve. At the conclusion of the previous NAVY light-valve program, we had demonstrated the uniform tilted perpendicular alignment of the liquid-crystal MBBA/EBBA using a Hughes-developed alcohol-amino liquid-crystal alignment. (See the Final Report of Contract N00024-75-C-1185 for details.) The principal liquid-crystal technology problems remaining at that time

were the relatively slow response times required to display color symbols and the lack of environmental and photochemical stability of the liquid crystal and alignment. In the present program, we made substantial gains in understanding the mechanisms involved in these instabilities and also gained an appreciation of the difficulty of achieving high birefringence liquid-crystals suitable for use in the tilted perpendicular color-symbology light valve. However, we were not able to solve these problems completely during the initial phases of the program. This and the emergence of the HFE mode light valve caused a change in the direction of the program and the cessation of this work. But, for any application which specifically requires a tilted perpendicular alignment, this line of investigation could be continued and would provide a strong basis for the application.

1. Liquid Crystal Materials for Tilted Perpendicular Alignment

A liquid crystal with high birefringence and low viscosity is required for a practical color-symbology light valve. The effective birefringence (Δn_{eff}) of the liquid-crystal layer is a function of the intrinsic birefringence (Δn) of the material, the thickness of the layer, and the orientation of the liquid-crystal molecules within that layer. Activating the light valve causes a change in the effective birefringence ($\Delta\Delta n_{eff}$), which is limited further by the switching ratio of the substrate. For a given switching ratio, $\Delta\Delta n_{eff}$ can be increased by increasing either Δn or the thickness. Since response time increases as the square (or even higher powers) of thickness, the maximum response time that can be tolerated places an upper limit on thickness. A decrease in viscosity can raise this upper limit slightly, but response time varies only as the first power of the viscosity. After considering the various tradeoffs, we have concluded that a high Δn (>0.25) is a practical necessity for obtaining the full range of colors, given the other parameters of the device.

As a result of this analysis, HRL undertook a company-funded program to develop a high birefringence liquid crystal for the tilted perpendicular color-symbology light valve. Since the liquid crystals

would have to withstand exposure to the intense light of the projection beam for long periods of time, they would have to absorb very little or no visible light. The only classes of nematics that appeared to fulfill this requirement were the biphenyls, the phenyl benzoate esters, and the tolanes. But none of these seemed capable of meeting the other requirements by themselves. A strongly negative dielectric anisotropy is essential for a light valve with a tilted perpendicular alignment, but the only known biphenyls with a nematic phase at room temperature have a strongly positive dielectric anisotropy. Some tolanes have negative dielectric anisotropies, but a careful analysis of the available data indicated that it would be extremely difficult to prepare a room-temperature nematic mixture for which this property was sufficiently negative. Satisfactory dielectric anisotropies could be obtained by using esters, but the phenyl benzoate esters do not have the necessary high birefringence. Therefore, we sought to obtain the appropriate combination of properties by combining compounds or groups from each of these classes.

The four most promising materials were formulated from mixtures of tolanes and biphenyl esters, and were designated HRL-34N1 to -34N4. Tolanes comprised more than 80% of these mixtures and gave them high birefringence; the biphenyl ester components were chosen to provide a highly negative dielectric anisotropy without strongly detracting from the birefringence. Melting ranges, clear-points, and birefringences are shown in Table 4. All of these mixtures melted well below room temperature, although only HRL-34N2 had the sharp melting point characteristic of a eutectic. Some experiments were carried out to determine whether their properties were suitable for use in light valves, although light valves containing these materials were never constructed. A complete characterization was interrupted when it was discovered that they were too unstable photochemically to maintain the tilted perpendicular alignment.

Birefringences were measured by a method that involved applying an electrical field across a 0.5 mil liquid-crystal cell with a tilted

Table 4. Some Properties of Liquid-Crystal Mixtures of Tolanes and Biphenyl Esters

Liquid Crystal	Melting Point, °C (solid → nematic)	Clearpoint, °C (nematic → isotropic)	Δn at 545 nm
HRL-34N1	-8 to -3	69	0.23
HRL-34N2	-5	67	0.31
HRL-34N3	-20 to -6	68	----
HRL-34N4	-9 to +7	75	0.21

perpendicular alignment. The light transmission of this cell was determined as a function of voltage with the cell located between crossed polarizers and with the tilt direction forming an angle of 45° with the plane of polarization of the light. The birefringence (Δn) was calculated from the equation

$$\Delta n = \frac{\lambda \left(k - \frac{1}{2}\right)}{d \left(1 - \frac{2E}{\pi S}\right)},$$

where

λ = wavelength of the light

k = number of transmission peaks

d = thickness of the liquid-crystal layer

S = switching ratio, or V/V_{th}, where V_{th} is the threshold voltage and V is the applied voltage at the k^{th} transmission peak

E = elliptical integral with a numerical value of ~ 1 when $S \geq 2$.

Using this method, we obtained values of 0.27 for MBBA and 0.32 for HRL-1N2, an MBBA-EBBA mixture, at 545 nm. Values of 0.215 and 0.23 are reported in the literature[9,10] for MBBA at 589 nm and 25°C.

Response times were measured for HRL-34N1, -34N2, and -34N4 in test cells with nematic film thicknesses ranging from 2.4 μm to 12.7 μm. The results are summarized in Table 5. The data for HRL-34N1 illustrates the very strong dependence of response time on the thickness of the liquid-crystal layer. Least squares log-log plots reveal that the delay and rise times are proportional to approximately the cube of the thickness ($d^{2.8-3.3}$), while the decay time is proportional to $d^{2.2-2.5}$. In conventional equations[11] for rise decay times, these quantities are proportional to the square of the thickness. The difference lies in the method of measuring response times, since in our measurements both switching ratio and thickness were changed. The threshold voltage (V_{th}) and the voltage at the first

Table 5. Response Times of HRL-34N1, HRL-34N2, and HRL-34N4 Cells of Various Thicknesses

Liquid Crystal	Cell Thickness, μm	Threshold Voltage,[a] V_{th}	Off-State Voltage[a]	Applied Signal Voltage (Voltage at First Transmission Peak)[a,b]	Response Times, msec		
					Delay	Rise	Decay
HRL-34N1	2.4	8.5	0	10.4	30	30	5.5
			0.9 V_{th}		19	21	17
	3.9	7.5	0	8.26	60	110	19
			0.9 V_{th}		25	105	80
	6.35 (1/4 mil)	6.6	0	6.87	450	900	100
			0.9 V_{th}		200	1000	450
	12.7	6.5	0	6.74	2750	5250	200
			0.9 V_{th}		2000	4400	1000
HRL-34N2	3.9	8.9	0	9.95	80	100	18
			0.9 V_{th}		45	105	70
	12.7	~7.15	0	7.88	850	2400	325
			0.9 V_{th}		500	2250	1200
HRL-34N4	2.7	~7.2	0	8.66	20	45	12
			0.9 V_{th}		7	40	43

[a] RMS voltages at 10 kHz, except for data on the 2.4 μm cell, which was taken at 1 kHz.

[b] Light passing through a 545 nm interference filter and the cell located between crossed polarizers with the tilt direction at 45° from the electric vector.

transmission peak (V_p) decreased as thickness increased. In part, this was probably because the thickness of the aligning silica layers remained approximately constant when the thickness of the liquid crystal was changed. Therefore, the fraction of the measured voltage drop that was actually applied to the liquid crystal increased as cell thickness increased. However, V_p should also decrease with increasing thickness because the effective birefringence of the liquid-crystal film increases and, therefore, the nematic molecules need not be tilted as far to reach the first transmission peak. Thus, the switching ratio decreases as liquid-crystal thickness increases. As a result, the response times show a power law dependence on the thickness in which the exponent is more than 2.

A rise time of 300 msec has been suggested as a practical goal for a color-symbology device. Using the data in Table 5, we estimate that the thickness of HRL-34N1 would have to be about 5 μm or less to achieve that goal for the first transmission peak. This thickness is not quite enough to provide the desired Δn_{eff}, since a 6 μm thickness is required for a light valve with HRL-1N2, which has a slightly higher Δn than HRL-34N1. If the relationship between rise time and thickness established for HRL-34N1 also holds for HRL-34N2, a rise time of 300 msec should be obtained for cells with a thickness of 5.9 μm or less. Since Δn for HRL-34N2 is almost the same as that for HRL-1N2, this liquid crystal has properties that are marginally adequate for a color-symbology light valve.

2. Tilted Perpendicular Alignment Stability Studies

An extremely dark, neutral off-state can be obtained with a homeotropic (perpendicular) alignment. A very slight uniform tilt must be present, however, to ensure that the liquid crystal will respond to an electric field by tilting uniformly in the predetermined direction. This uniformly tilted homeotropic (or tilted perpendicular) alignment is achieved by shallow-angle ion-beam etching the silica surfaces of the electrodes and then treating them with an alcohol or a mixture of an alcohol and an amine. This process is described in the Final Technical Report of Contract N00024-73-C-1185. Experience with this type of alignment has revealed a tendency for the tilt angle to change substantially over a period of a few days to a few weeks. The objective of this work was to identify and eliminate the causes for this alignment instability, and to improve reproducibility.

Most of the alignment experiments were conducted with the HRL-1N2 liquid crystal, which is a mixture of N-(p-methoxybenzylidene)-p-butylaniline (MBBA) and N-(p-ethoxybenzylidene)-p-butylaniline (EBBA). This material has a nematic range, viscosity, and dielectric anisotropy that are quite satisfactory for application to the color-symbology display. However, its rather strong absorption in the blue region of the visible spectrum caused us to anticipate that it would suffer significant photochemical damage from prolonged exposure to the high-intensity projection light. Nevertheless, since no satisfactory colorless, photochemically stable liquid crystal suitable for tilted perpendicular alignment was available at the beginning of the program, we used HRL-1N2 to determine the factors involved in the alignment instability.

The tilt angle, defined as the angle formed by the liquid crystal director and a line perpendicular to the electrode surfaces, increased as the chain length of the alcohol was decreased (see Figure 14). In cells treated with alcohols selected to induce high tilt angles ($>8^{\circ}$), erratic alignment was often encountered, with domains that tilted in the opposite direction or with twists as well as tilts. However, these abnormal alignments could often be eliminated by heating the liquid

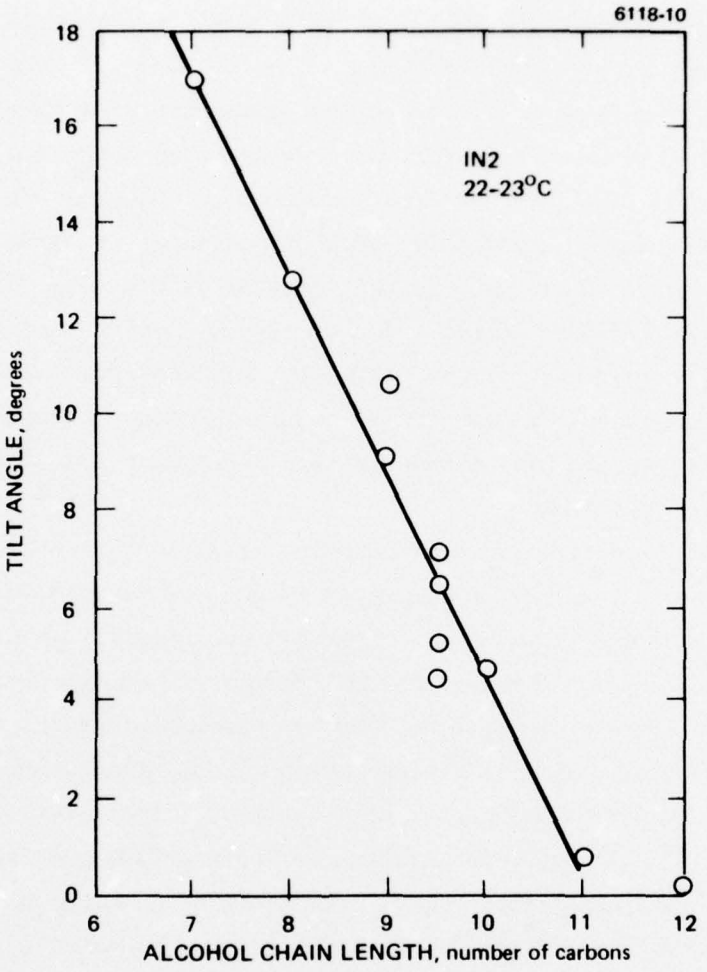

Figure 14. The effect of alcohol chain length on the tilt angle in the alignment of HRL-1N2 on alcohol-treated silica surfaces.

crystal above its clearpoint or by operating the cell for a short period, particularly in the dynamic-scattering (and especially in the "secondary scattering"[12]) mode. For lower tilt angles ($<6^{o}$) in which we were most interested, it was relatively easy to obtain the desired uniform alignment, and the directors always tilted out of the surface toward the ion-beam source. A deviation as high as 2^{o} in fabrication reproducibility can be anticipated when the desired tilt is in the 4^{o} to 6^{o} range. This is shown by the data in Figure 14 for the four duplicate cells in which one electrode was treated with the alcohol $C_9H_{19}OH$ and the other with the alcohol $C_{10}H_{21}OH$. Treating both surfaces with $C_{10}H_{21}OH$ provided the best combination of high contrast and the absence of blackline edge effects.

Tilt angle is also a function of temperature, as shown in Figure 15. In the linear region, the tilt angle increased 0.4^{o} for each $1^{o}C$ decrease in temperature. Therefore, a way of controlling the temperature of the light valve in a display system is needed. This dependence of tilt angle on temperature could also be used to correct for temporal changes in tilt, which would otherwise limit device usability.

Hydrolysis of the Schiff bases can significantly affect tilt angle changes of HRL-1N2. When unsealed cells are left exposed to ambient air, the tilt angle generally decreases with time; in light valves, this leads to black-line edge effects, which indicate too little tilt. (See the Final Report of Contract N00024-73-C-1185.) Similar cells stored in a desiccator change more slowly, and the tilt angle of stored cells sometimes increases. Tilts were also lower when cells were prepared with a batch of 1N2 that was repeatedly exposed to air than with a similar mixture that was protected in a desiccator. As a result of these observations, long-term tilt stability tests were carried out with cells that were stored in a desiccator to simulate the essentially anhydrous condition of a perfectly sealed light valve. We also modified our liquid-crystal storage and cell assembly techniques to decrease substantially the exposure of the liquid crystal to moist air. Improvements were also made in the light-valve package to eliminate silver paste and epoxies from those areas

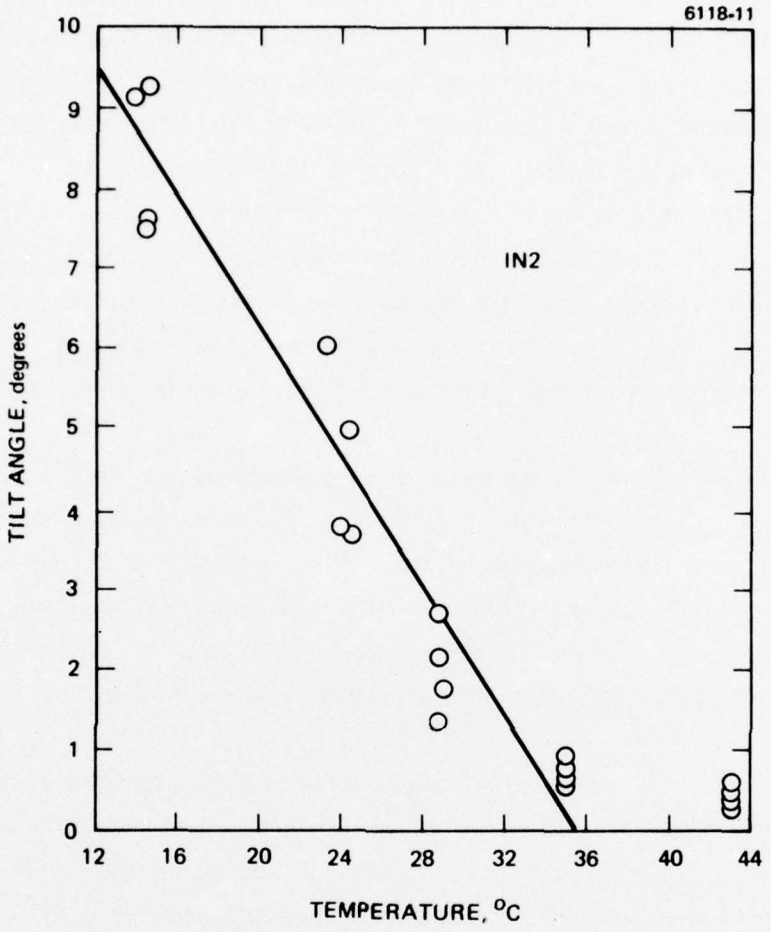

Figure 15. The effect of temperature on the tilt angle of HRL-1N2 aligned on alcohol-treated silica surfaces.

where any release of volatile organics could contaminate the liquid crystal and affect the stability and quality of the alignment.

We also studied the effect of ion-beam etching angle on alignment reproducibility. The silica surfaces had usually been etched with the ion-beam forming an angle of 20^{o} with the surface. We found, however, that the tendency to form erratically aligned domains increased when the ion beam formed an angle of 10^{o} with the electrode surface and decreased when the angle was 30^{o}. These tests were carried out with three sets of cells; in each cell, one electrode was treated with 1-nonanol and the other was treated with 1-decanol. When the etch angle was 10^{o}, every cell of a set of three had two domains; with an angle of 20^{o}, two out of six cells had two domains; and with an angle of 30^{o}, none of three cells had two domains. Therefore, the tendency to form the unwanted second domain decreased as the etch angle was increased within this range. Nevertheless, erratic alignment was encountered so infrequently in actual light valves, where a small tilt angle was employed, that we continued to use the 20^{o} etch angle for general device production.

As a result of these reproducibility tests, a substantial number of the tilt stability tests were carried out with electrodes that were etched at 30^{o}. We assumed that the etch angle would have no effect on the temporal stability of the tilt angle. This assumption proved to be wrong, as illustrated in Figures 16, 17, and 18. All of the cells represented in these figures were prepared from the same batch of liquid crystal, and all were stored in a desiccator. Nevertheless, there were striking differences in the stability of the tilt angle among these cells. As shown in Figure 16, the cells with the 20^{o} etch underwent a significant decrease in tilt during the first three weeks, then settled down to a very slow decrease over the next seven months. In contrast, the other two sets, which had the 30^{o} etch, had substantial increases in the tilt angle over a period of 11 or 12 weeks. We know of no reason for this relationship between etching angle and tilt angle stability, but it appeared to be a general one. Fifteen cells with electrodes etched at an angle of 30^{o} had unstable tilt angles, with the angle increasing with time in each case, and none were stable. In contrast, 15 of the cells with electrodes etched at 20^{o} were reasonably stable, while only two showed unexplained instability.

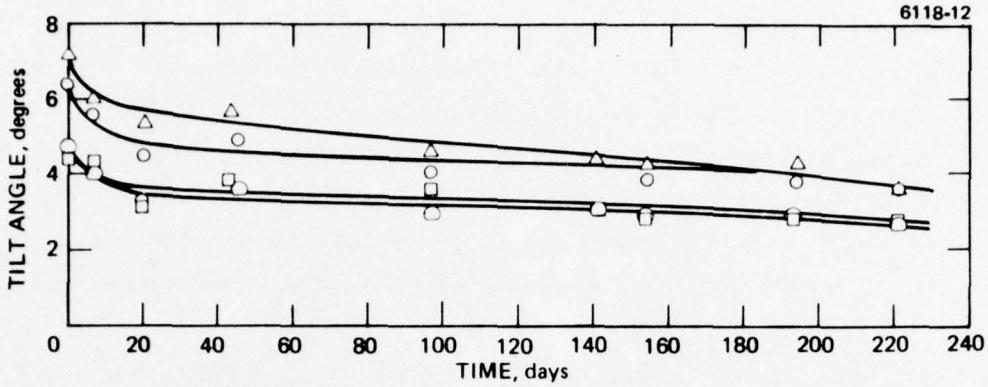

Figure 16. Temporal stability of the tilt angle in cells stored in a desiccator. (Etch angle, 20°; alcohol treatment, $C_9H_{19}OH$ and $C_{10}H_{21}OH$; liquid crystal HRL-1N2.)

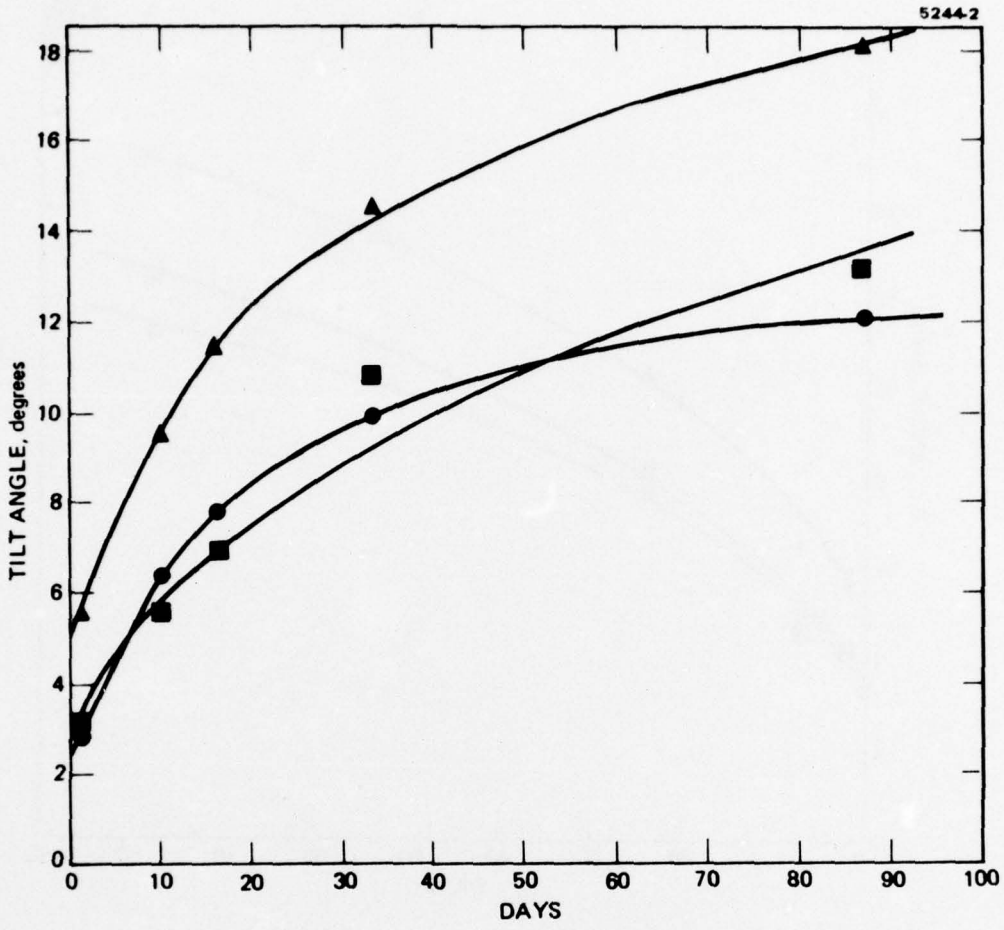

Figure 17. Temporal stability of the tilt angle in cells stored in a desiccator. (Etch angle, 30°; alcohol treatments, $C_9H_{19}OH$ and $C_{10}H_{21}OH$; liquid crystal HRL-IN2.)

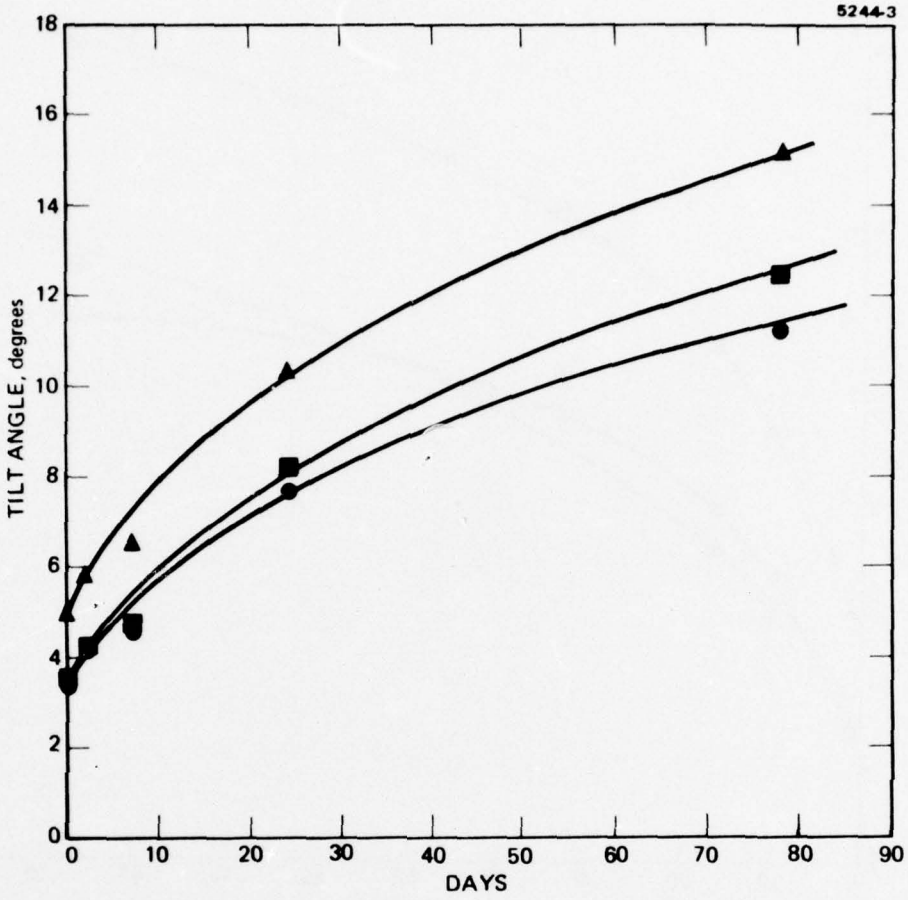

Figure 18. Temporal stability of the tilt angle in cells stored in a desiccator. (Etch angle, 30°; alcohol treatments, $C_9H_{19}OH$ and $C_8H_{17}OH$; liquid crystal HRL-IN2.)

"Reasonable" tilt angle stability was defined as remaining within the acceptable range of 2^{o} to 5^{o} for at least six months, or, if the initial tilt was more than 5^{o}, changing no more than 2^{o} in six months. All tilt angles were measured at $23^{o}C$, or corrected for temperature using a factor of 0.42^{o} tilt/^{o}C deviation (but only if the measured tilt was greater than 2^{o}). The initial change, which occurred during the first few days to three weeks, was ignored. This aging period appeared to be required for the newly assembled cell to come to a stable condition in equilibrium with its environment in the desiccator.

Although the test cells that had electrodes etched at 20^{o} and were stored in a desiccator generally had a reasonably stable alignment, experience with 1N2 light valves had demonstrated that their useful lifetime was considerably less than six months. Moreover, they always failed by starting to show black line edge effects, which indicated that the tilt angle had decreased. The cause was found on a parallel company-funded program which was investigating the photochemical stability of liquid crystals. HRL-1N2 cells with a tilted perpendicular alignment underwent photochemical damage that irreversibly decreased the tilt angle when exposed to near ultraviolet or even blue light. Data illustrating the effect are provided in Table 6. The alignment stability was greatly enhanced by eliminating wavelengths shorter than 420 nm, but the useful lifetime was still substantially less than 100 hr at the intensity of the test apparatus. No new components could be detected in the liquid crystal by gas or thin-layer chromatography, although there were small changes in the ratio of starting components. Irradiating the treated electrode surfaces before assembling the cell had no effect on alignment, which indicated that the photochemical degradation was due to the liquid crystal and not to the surface coating.

Photochemical instability had been anticipated for HRL-1N2, but the HRL-34N series was expected to be more stable. Unfortunately, this was not true, and irradiation with wavelengths longer

Table 6. Effect of Light on Tilt Angle of Test Cells with a Tilted Perpendicular Alignment

Liquid Crystal	Exposure Time, hr[a]	Cutoff Wavelength, nm	Tilt Angles, deg	
			Initial	Final
HRL-1N2	17	330	10.64	1.38
	183	420	10.84	2.19
	18.5	330	3.00	0.47
HRL-34N2	16	420	3.86	0.87

[a]Light from a xenon arc lamp with a light intensity of about 166 mW/cm^2 at the surface of the test cell.

than 420 nm caused the alignment tilt angle to decrease even more rapidly for HRL-34N2 than for HRL-1N2 (see Table 6). Furthermore, the photolysis of HRL-34N1 formed products that were strongly surface-active and could readily be detected by thin-layer chromatography.[11] Such materials, which either have polar groups or are polymeric, would concentrate on the surface of the electrodes where they would undoubtedly alter the alignment.

In summary, the tilted perpendicular alignment was found to have adequate stability in a desiccator with limited exposure to light, but it tends to be unstable if the liquid crystal is photochemically degraded. The mixtures of both MBBA and EBBA and of tolane and biphenyl esters were too sensitive to visible light to permit using them in a color-symbology light valve with tilted perpendicular alignment. To make a practical light valve of this type, more stable liquid crystals will have to be found. Since doing so could be a difficult, time-consuming task, it seemed judicious to pursue the alternative approach offered by the HFE mode. With this approach, the more stable cyanobiphenyl liquid crystals and a twisted parallel alignment can be used.

D. LIGHT VALVE PACKAGING/SEALING

The goal of achieving a stable, uniform color-symbology light valve is critically dependent on the quality of the cell packaging. With the ac light valve development work done under Contract N00024-73-C-1185, we devised a cell holder that mechanically clamped the substrate and counterelectrode to provide the required rigidity of the structure. There was no provision made for adjusting the liquid-crystal thickness ("fine tuning") to improve the uniformity of the device after the cell had been assembled. Hermetic sealing was accomplished by epoxy bonding the substrate and the counterelectrode to the metal holder. Then the metal holder components were also epoxy sealed. Finally, the intervening space between the substrate edges and the holder was flushed with an inert gas and the filling holes sealed off.

In improving this design for the color-symbology light valve, we had two criteria:

- To provide for the fine adjustment of the liquid crystal thickness after assembly
- To provide a sealing technique that avoids direct exposure of the liquid crystal to organic vapors during the curing process, and that also avoids continued exposure of the liquid crystal to high-vapor-pressure organic materials after assembly.

We arrived at a cell-holder design which incorporates these features; it is shown in Figure 19. The cell is sealed hermetically with low organic vapor pressure Viton O-rings and gaskets. As could be done with the previous holder design, the inter-holder cavity can be flushed and back-filled with an inert gas. However, the liquid crystal is not exposed to the organic vapors resulting from the curing of the epoxy. To further reduce any organic contamination of the liquid crystal, we eliminated the use of epoxy for bonding the leads and of silver paste for contacting the electrical leads to the substrate and counterelectrode. They were replaced with an indium soldering process that contacts the lead to the contact pad on the edge of the

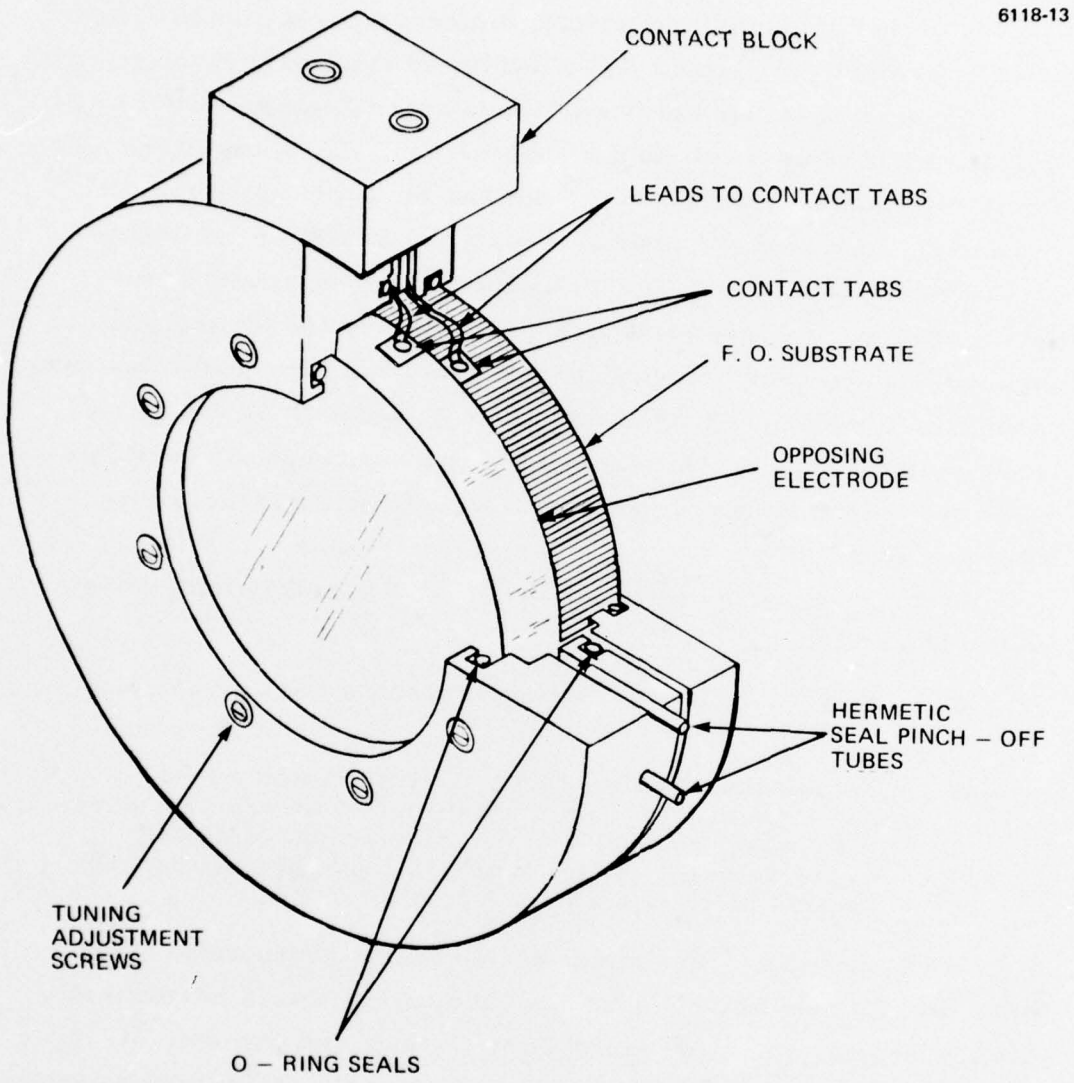

Figure 19. Cell holder design that provides hermetic sealing and liquid-crystal thickness tuning of LCLV.

substrate. Thus, the holder provides an environment devoid of organic vapors, except for the low-vapor-pressure Viton gaskets. Lifetest measurements are still needed to determine if this low-level organic vapor has any long-term effect on the liquid-crystal material or on its alignment stability.

The cell can be fine tuned for uniformity with adjusting screws on the circumference of the aperture. This is illustrated in Figure 19. These screws press the two parts of the holder against the resilient Viton gaskets, and thus provide a highly sensitive means of applying pressure to the substrate/counterelectrode sandwich. This pressure is useful in eliminating a wedge in the liquid-crystal thickness (sometimes caused by large particles in the liquid crystal or imbedded in the spacer pads). However, this tuning cannot eliminate a "bullseye" thickness nonuniformity caused by curvature that is inherent in the substrate or counterelectrode. This class of nonuniformity must be eliminated before cell assembly by the techniques discussed in Section 2. B above.

E. PROPERTIES OF INTERIM TILTED PERPENDICULAR COLOR-SYMBOLOGY LIGHT VALVES DELIVERED TO NELC

In this section, we list the properties of the interim devices Nos. 1 and 2 delivered to NELC under the terms of the contract. The measurement procedures and equipment used are those described in the Final Technical Report, NavSea Contract N00024-73-C-1185 Section III. D.

1. Interim Device No. 1 (delivered 9 December 1975)

- Cell Designation H2480-22-A
- Physical Description
  - Fiber Optic Faceplate Physical Diameter 2.10 in.
  - Working Aperture 1.85 in.

- Thickness:
  - Substrate 0.50 in.
  - Counterelectrode 0.50 in.
- Substrate:
  - Type: Galileo Electrooptics Corp. Fiber Optic Type D-14 with EMA
  - Photoconductor: 12 μm thick Sputtered CdS
- Liquid Crystal: HRL-1N2 (EBBA-MBBA) 3.1 μm thick
- Liquid Crystal Alignment: Homeotropic Tilted
  - Technique: Angle Ion Beam Etched Alcohol Amine Treated
- Dielectric Mirror: Sputtered TiO_2/SiO_2 SiO_2 Alignment Film Liquid Crystal

- Measured Performance
  - Operational Conditions: 15 Vrms at 20 kHz
  - White on Black Symbology: (Measured with 100% MTF input image)
    - Contrast Ratio 80:1 (Measured with Photo-optic Response)
    - Resolution 60 lines/mm
    - Input Imaging Light Power 100 $\mu W/cm^2$ at 525 nm
    - Response Time
      - Rise 400 ms
      - Decay 300 ms
    - Color on Black Symbology: (Measured with 100% MTF input image)

Color	Input Imaging Light Power, $\mu W/cm^2$	Resolution lines/mm	Response Time	
			Rise (ms)	Decay (ms)
Yellow	120	20	400	300
Magenta	200	20	350	300
Blue	450	20	300	300
Green	800	20	200	300

2. Interim Device No. 2 (delivered 14 May 1976)

- Cell Designation LXX1-956-IN2
- Physical Description
  - Fiber Optic Faceplate Physical Diameter 2.10 in.
  - Working Aperture 1.85 in.
  - Thickness:
    - Substrate 0.50 in.
    - Counterelectrode 0.50 in.
  - Substrate:
    - Type: Galileo Electrooptics Corp. Fiber Optic Type D-14 with EMA
    - Photoconductor: 15 μm thick Sputtered CdS
  - Liquid Crystal: HRL-1N2 (EBBA-MBBA), 6 μm thick
  - Liquid Crystal Alignment: Homeotropic Tilted
    - Technique: Angle Ion Beam Etched Alcohol Amine Treated
  - Dielectric Mirror: Sputtered TiO_2/SiO_2

- Measured Performance
  - Operating Conditions 11 Vrms at 10 kHz
  - White on Black Symbology: (Measured with 100% MTF input image)
    - Contrast Ratio 125:1 (Measured with Photopic Response)
    - Resolution 60 lines/mm
    - Input Imaging Light Power 6 $\mu W/cm^2$ at 525 nm
    - Response Time:
      - Rise 700 ms
      - Decay 700 ms
  - Color on Black Symbology: (Measured with 100% MTF input image)

Color	Input Imaging Light Power, $\mu W/cm^2$	Resolution lines/mm	Response Time*	
			Rise (ms)	Decay (ms)
Yellow	12	22	600	700
Magenta	30	22	500	600
Blue	60	22	400	600
Green	100	22	400	600

*Response limited by liquid crystal thickness.

- Color Uniformity: Grades from Magenta to Blue across aperture with uniform 100 $\mu W/cm^2$ input intensity at 10 kHz
- Cosmetic Defects: ~10 point defects and several small scratches from reassembly of cell

SECTION 3

THE SECOND PHASE: THE HYBRID FIELD EFFECT MODE COLOR-SYMBOLOGY LIGHT VALVE

We entered a new phase of color-symbology development with the reduction to practice, late in this program, of the HFE mode color-symbology LCLV.[4] This device, which followed the monochrome symbology and optical data processing HFE light valves,[3] holds the promise of a practical solution to the requirement for a single-channel color-symbology projector. This device became realizable with the development of higher switching ratio photosensors (discussed in Section 2. B), which allowed us to switch higher voltages to the liquid crystal. Another critical factor was the discovery of a dark neutral-color off state, above the liquid-crystal threshold, that allowed high contrast ratios to be achieved in the projected imagery.

This section describes the HFE mode, emphasizing color-symbology applications. The properties of the final LCLV device delivered to NELC are also summarized. *This is the first HFE mode* device delivered to the Navy for color-symbology purposes. This particular device, although still far from optimized, exhibits impressive performance combined with stability and operating lifetime.

A. THE USE OF THE HFE MODE FOR COLOR-SYMBOLOGY APPLICATIONS

The HFE mode combines the twisted nematic electro-optic mode with a pure optical birefringence effect. The twisted nematic effect is used to produce a dark off-state for the light valve and the birefringence effect is used to produce the bright on-state, including the birefringent color peaks.

Although we use the twisted nematic alignment in the off-state, it is not the 90° twist generally reported in the literature[13] (and used in most watch displays). The 90° twist configuration cannot be used in the light valve because the light valve will not operate effectively with a polarizer between the liquid-crystal layer and the dielectric

mirror. Thus, to implement HFE, the liquid crystal layer is fabricated with a 45^{o} twist angle between the preferred alignment directions on the two electrodes, which causes the liquid crystal molecules to assume the same twist. This is shown schematically in Figure 20. The twisted configuration causes the polarization direction of linearly polarized incident light to rotate exactly through the 45^{o} twist angle as the light passes through the layer.

The operation of the HFE electro-optic effect is now described. Consider the off-state first. As shown in Figure 21(a), a crossed polarizer/analyzer pair is situated between the light valve and the read-out light source. The polarizer is placed in the incident beam with its direction of polarization oriented so that the direction of polarization of the incident light is parallel to the direction of the long axis of the liquid-crystal molecules as they are aligned on the surface of the entrance electrode. The analyzer is placed in the reflected beam, oriented with its polarizing direction at 90^{o} with respect to that of the polarizer. This arrangement produces a dark off-state because the direction of polarization of the linearly polarized incident light is rotated through 45^{o} after its first pass through the liquid-crystal layer. But after being reflected from the dielectric mirror, the light passes a second time through the liquid crystal, and its polarization is rotated back to the same direction as that of the incident light. Thus the light is blocked by the (crossed) analyzer. As discussed above, the off-state of the device is determined entirely by the twisted nematic effect. However, when the liquid-crystal thickness is within a factor of 10 of the wavelength of the read-out light, the off-state transmission of the layer increases because of a residual birefringence which is intrinsic to the twisted nematic configuration. This off-state transmission, which is wavelength dependent, can seriously limit the maximum contrast ratio achievable with the device – particularly if the device is used with white light. Fortunately, we have found that a transmission null exists at which all wavelengths of white light have a low value of transmission. (This effect occurs when the liquid-crystal thickness is greater than 3 μm for a liquid crystal of

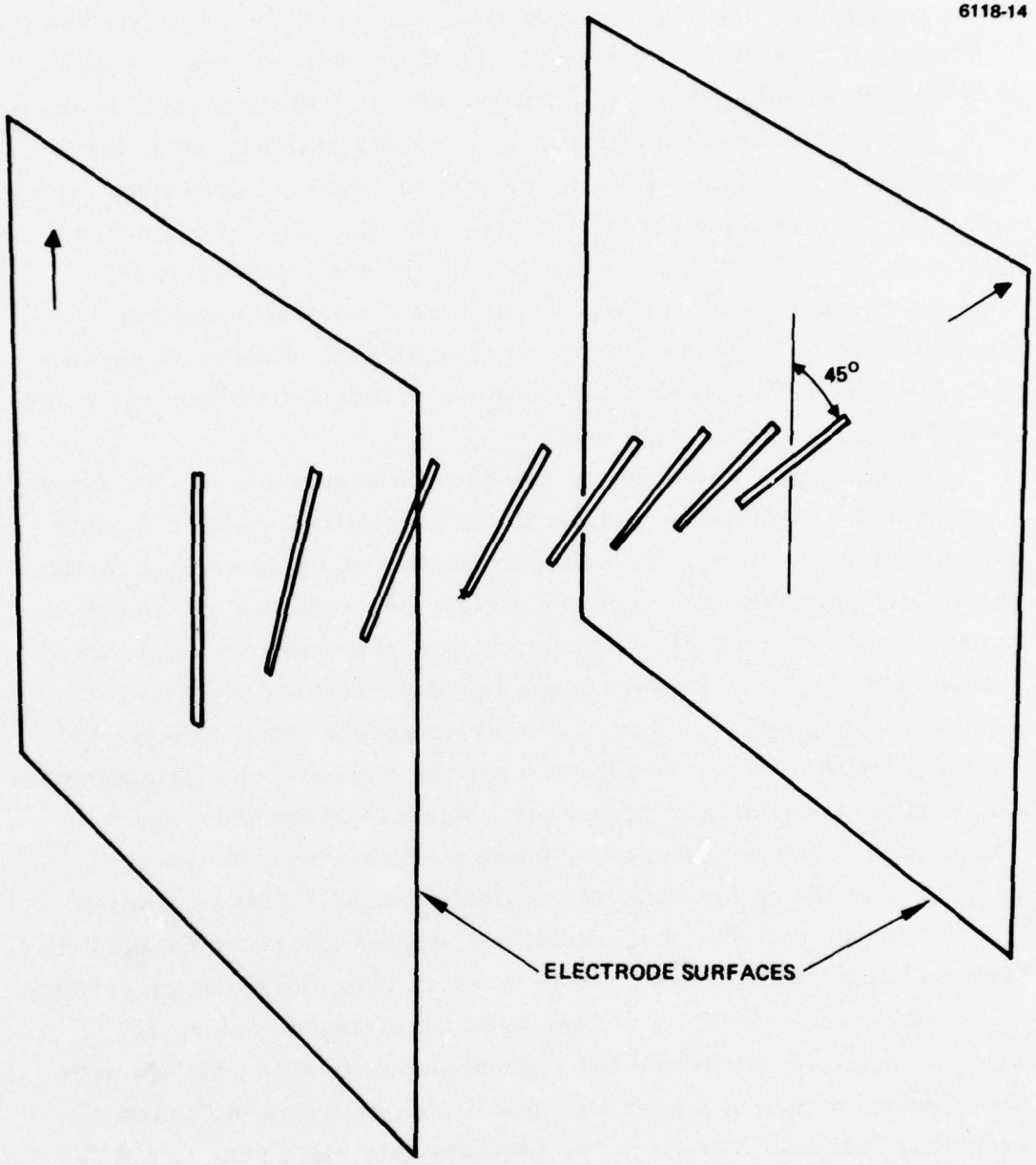

Figure 20. Schematic of 45° twist liquid-crystal alignment.

birefringence $\Delta n=0.23$.) This null state occurs at a voltage (applied to the liquid crystal) that biases the liquid crystal past the voltage threshold to a voltage level between the off-state transmission level and the main transmission peaks. This is shown in Figure 22 for the transmission versus voltage curve of the final delivery light valve with a 6 μm thick liquid-crystal layer. The null state is identified on this figure. Thus, even though the off-state transmission is relatively high for white light, we can bias the device above the liquid-crystal threshold and thereby operate in the null as an equivalent off-state. We thereby achieve a low-transmission, neutral-color background for color symbology.

Consider now the on-state as shown in Figure 21. As we apply an even higher voltage bias to the liquid crystal and excite it beyond the null point described above, the molecules of liquid crystal continue to rotate from nearly parallel to the electrode surfaces to a more perpendicular orientation. As this occurs, the twisted nematic effect lessens and the birefringence of the liquid crystal becomes the dominant electro-optic effect. The birefringence effect changes the polarization of the incoming light, creating a cross-polarized component, and the transmission increases. Because of the wavelength dependence of the birefringence, color peaks are successively generated as the polarization of the light changes. This is similar to what occurs with the perpendicularly aligned color-symbology cell. However, the order of selection is inverted from the tilted perpendicular device. In the HFE mode, the color birefringent peaks are selected at low voltages and the superposition of color peaks to produce white, occurs at higher voltages. This is shown in Figure 22. A further increase in voltage can increase this white peak to a 90% transmission level across the visible spectrum. Then, as the molecules are driven still closer to perpendicular (to the electrode surfaces), the birefringence decreases until it becomes zero when the long axes of the molecules are oriented perpendicularly to the electrode surface. As a result of this decrease in birefringency, the light

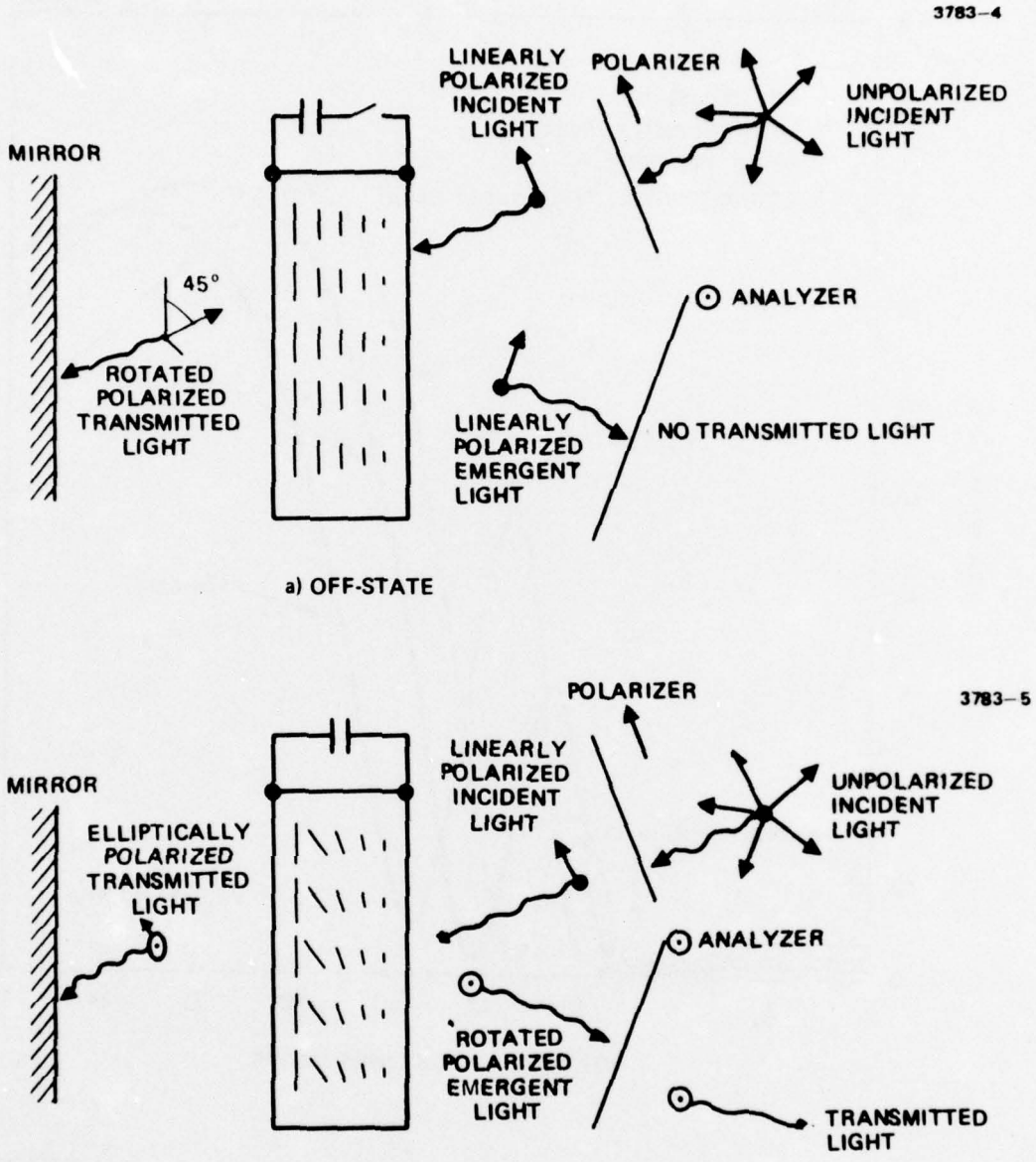

Figure 21. Operation of the HFE mode.

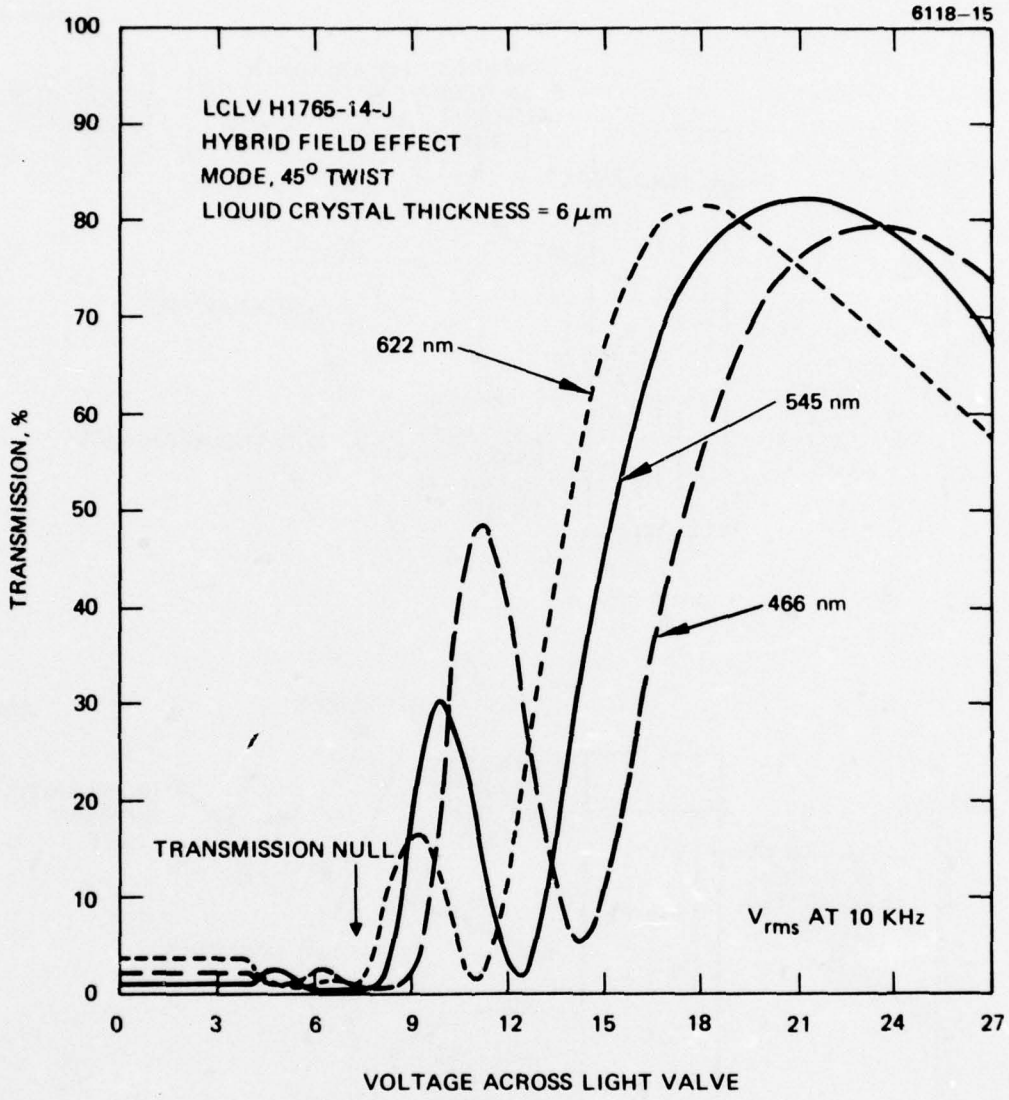

Figure 22. Transmission characteristic of the delivered HFEM liquid crystal light valve

transmission returns to zero, a black on white gray scale region of operation results in this region as the birefringence decreases. In general, we operate the light valve between the null and the transmission peak to give the maximum performance for both monochrome and color symbology. The properties of the black-on-white gray scale region have not been characterized in detail.

In summary, the HFE mode color-symbology LCLV operates by the imaging light intensity selection of liquid crystal birefringent color peaks for symbols from a dark background. In principle, this is the same as the tilted perpendicular color-symbology light valve. The differences between the two modes lie in the fact that white symbols are selected for low imaging light in the tilted perpendicular with higher light levels for the successive color peaks; in the HFE mode, the color peaks are selected first with the white symbols obtained at the highest imaging light level. The other major difference is that the tilted perpendicular dark off-state results from a region of no light modulation by the liquid crystal below the electro-optic threshold; the dark off-state in the HFE mode results from a broad visible spectrum null in the birefrigent characteristics of the liquid-crystal at low voltages above the electro-optic threshold.

B. PROPERTIES OF THE FINAL LCLV DEVICE DELIVERED

This section presents the properties of the final color-symbology HFE light valve device, delivered on 18 February 1977. The measurement procedures and equipment used are those described in the Final Technical Report, NAVSEA Contract N00024-73-C-1185, Section III. D.

- Cell Specification
  - Designation: 1765-14-J
    - Substrate
      - Type: Galileo Electro-optics Corp. Fiber Optic Type D-14 with EMA
    - Photoconductor: 30 μm thick Sputtered CdS

- Liquid Crystal: British Drug House E-7, 6 μm thick biphenyl eutectic
- Liquid Crystal Alignment: 45^{o} Twisted Nematic for operation in Hybrid Field Effect Mode
  - Technique: Shallow Angle Ion Beam Etched
- Dielectric Mirror: Sputtered TiO_2/SiO_2

- Measured Performance
  - Operating Conditions: 7.2 Vrms at 10 kHz
  - Monochrome Symbology (Yellow-white characters on dark neutral background) (Measured with 100% MTF input image):
    - Contrast Ratio: 120:1 (Measured with Photoptic Response)
    - Resolution
      - R_L^*: 51 lines/mm
      - R_M^{**}: 32 lines/mm
    - Input Imaging Light Power: 100 $\mu W/cm^2$ at 525 nm (P-1 phosphor spectrum)
    - Response Time
      - Rise***: 125 msec
      - Decay****: 140 msec

---

*Limiting resolution

**Resolution at which the symbol border is 50% of the element width on the Air Force Resolution Chart

***0 to 90%

****100 to 10%

- Color Symbology (Measured with 100% MTF input image)
- Transmission versus Voltage Characteristics: See Figure 22.

Color	Input Imaging Light Power, $\mu W/cm^2$	Resolution		Contrast Ratio*	Response Time, ms	
		R_L	R_M		Rise	Decay
Yellow	43	51	18	76:1	800	150
Magenta	30	51	18	19:1	1300	200
Blue	21	57	26	31:1	1700	210
Green	12	57	57	51:1	2200	220

*Measured photopically from transmission null.

- Reflectivity — 85%
- Color Uniformity — ~75% of aperture one color
- Intensity Uniformity — 88%
- Cosmetic Defects — 4 point defects: 3 mm, 2.5 mm, 2.5 mm, and 0.8 mm diameter. Small area of fine, low contrast scratches.

REFERENCES

1. T. D. Beard, W. P. Bleha, and S.-Y Wong, Appl. Phys. Lett. 22, 90 (1973).

2. J. Grinberg, W. P. Bleha, A. D. Jacobson, A. M. Lackner, G. D. Myer, L. J. Miller, J. D. Margerum, L. M. Fraas, and D. D. Boswell, IEEE Trans. Electron Devices ED-22, 775 (1975).

3. J. Grinberg, A. D. Jacobson, W. P. Bleha, L. J. Miller, L. M. Fraas, D. D. Boswell, and G. D. Myer, Opt. Eng. 14, 217 (1975).

4. W. P. Bleha, J. Grinberg, A. D. Jacobson, and G. D. Myer, 1977 SID International Symposium Digest of Technical Papers 8. To be published.

5. J. Grinberg and A. D. Jacobson, J. Opt. Soc. Am. 66, 1003 (1976).

6. L. M. Fraas, W. P. Bleha, J. Grinberg, and A. D. Jacobson, J. Appl. Phys. 47, 584 (1976).

7. L. M. Fraas, J. Grinberg, W. P. Bleha, and A. D. Jacobson, J. Appl. Phys. 47, 576 (1976).

8. R. H. Bube, Photoconductivity of Solids (Wiley, N. Y., N. Y., 1960).

9. M. Brunet-Germain, C. R. Acad. Sci. 271B, 1075 (1970).

10. I. Haller, H. A. Huggins, and M. J. Freiser, Mol. Cryst. Liq. Cryst. 16, 53 (1972).

11. J. Robert, G. Labrunie, and J. Borel, Mol. Cryst. Liq. Cryst. 23, 197 (1973).

12. A. Sussman, Appl. Phys. Lett. 21, 269 (1972); R. Chang, J. Appl. Phys. 44, 1885 (1973).

13. M. Schadt and W. Helfrich, Appl. Phys. Lett. 18, 127 (1971).

PRECEDING PAGE BLANK-NOT FILMED

APPENDIX A

HFE LCLV OPERATING PROCEDURE AND MOUNTING DIAGRAMS

A. LCLV OPERATING PROCEDURES

- Mount the fiber-optic faceplate LCLV on fiber-optic faceplate CRT using mounting components described in this appendix. Align polarization reference mark on cell holder with direction of polarization of projection light.
- Connect audio frequency oscillator to output mini-bnc connector. Set frequency to 10 kHz. Increase voltage bias supplied to cell until dark null state appears on screen (approximately 7.2 Vrms).
- Turn up CRT brightness until highest input intensity level successfully produces white symbols set value. Adjust and set lower input intensity levels to select yellow, magenta, blue, and green symbols.
- Light valve is now ready for dynamic operation.

B. CELL HOLDER DESIGN AND SYSTEM MOUNTING

A new cell holder has been designed and fabricated so as to retrofit to the OSG Optical System. The design provides for pneumatic sealing while still providing spring tension for applying pressure to join the light valve to the CRT. It does so through the use of three separate spring-loaded holding clamps. The same slide plate as was used in the previous design was modified only slightly to accommodate the new design and still stops against the existing photochromic film registration stops.

The cell holder assembly consists of three basic parts: the cell base, cell hold-down and slide plate. These components can be seen in Figures 23, 24, and 25. The light valve cell assembly (fiber optic substrate and opposing electrode) drops into the cell base and the cell hold-down slides over the glandular seal and is held in place with the annular ring of 4 x 40 screws. Viton-A O-rings are also used to seal the fiber optics and opposing electrode to the cell. The interior of the

PRECEDING PAGE BLANK-NOT FILMED

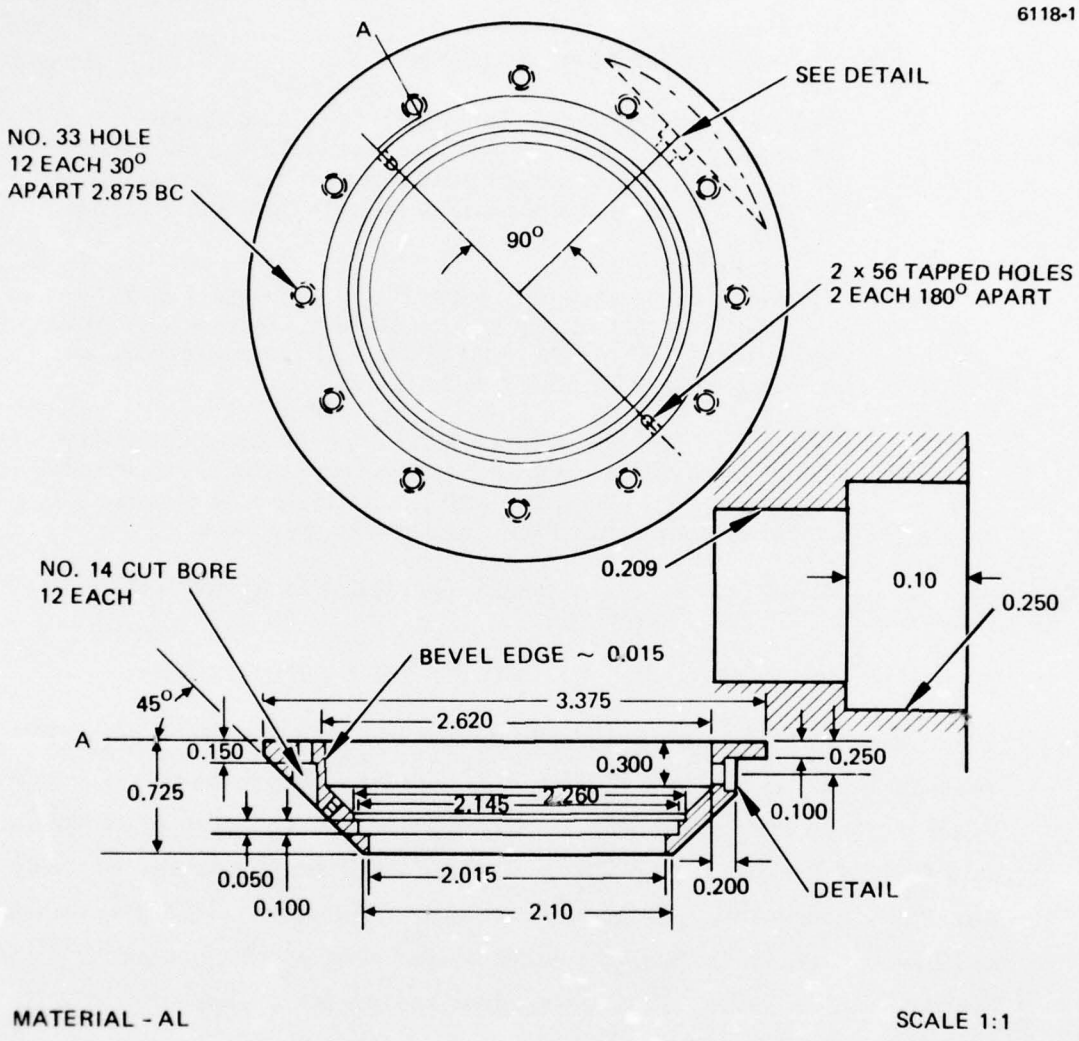

Figure 23. Color cell base.

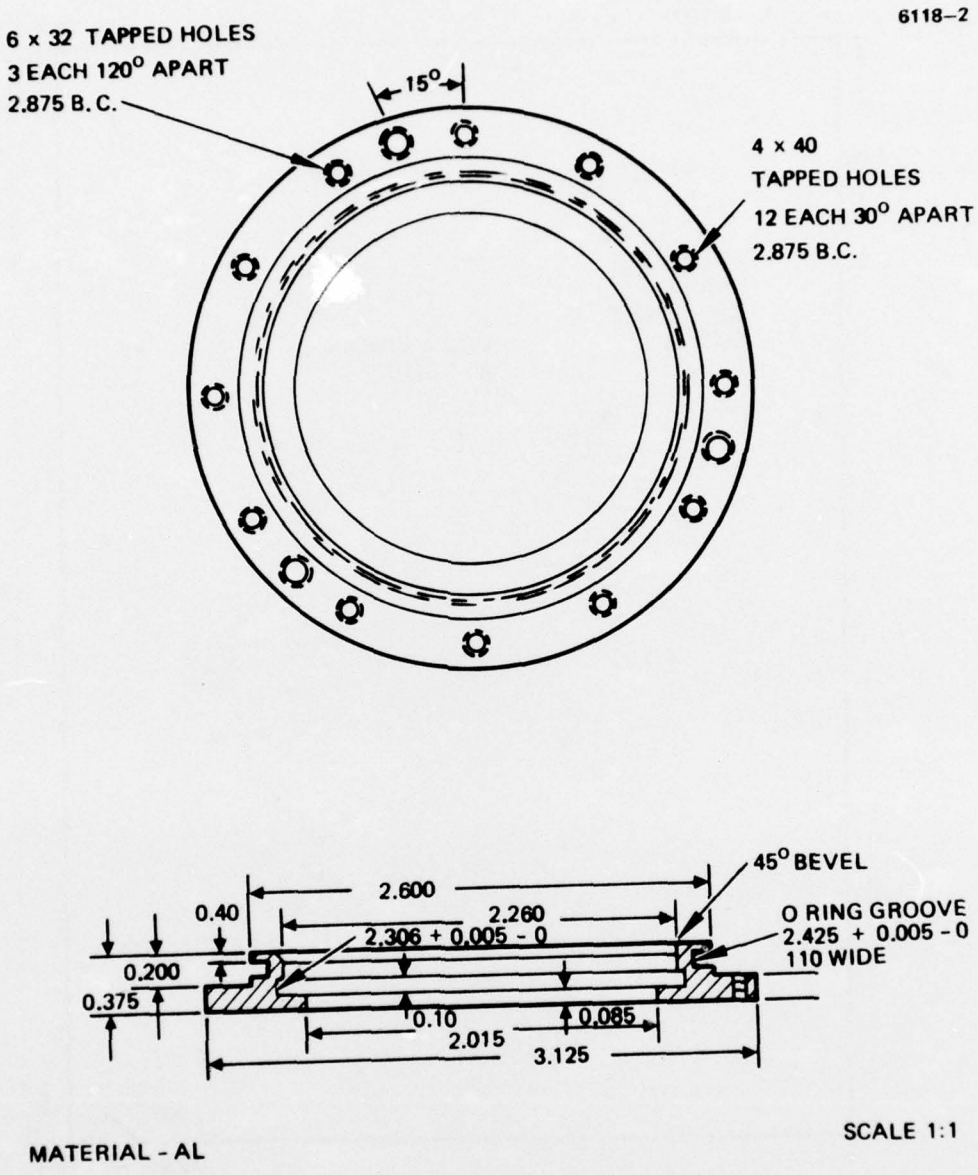

Figure 24. Color cell hold down.

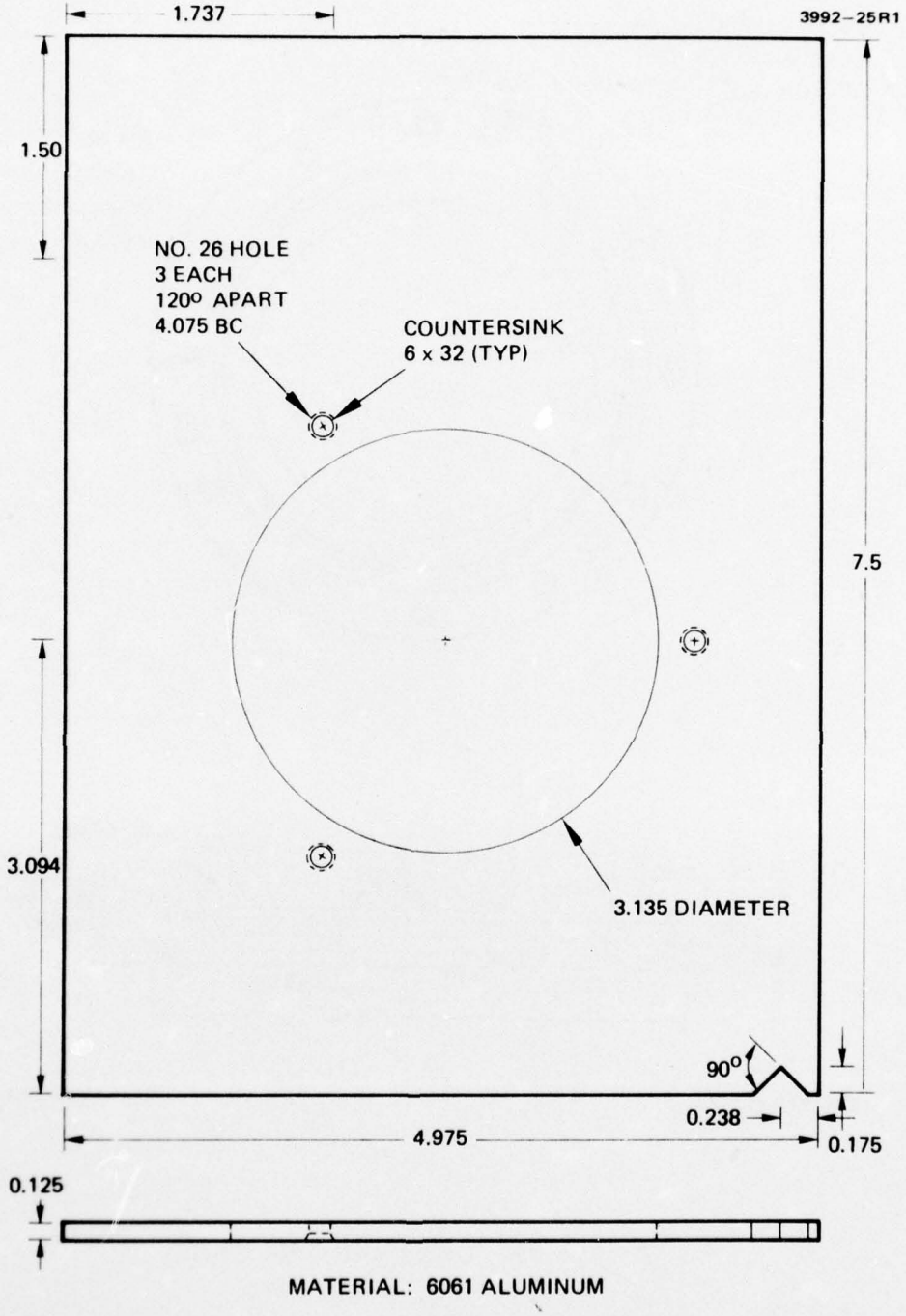

Figure 25. Slide Plate.

completed cell is flushed with dry N_2 through the two small ports and sealed with screws. Sealing has been provided through a miniature BNC real-mount receptacle held in place with the nylon insulator shown in Figure 26. The cell is mounted to the slide plate by the three spring-loaded hold-down clamps already mentioned; these are shown in Figure 26. Spring pressure can be regulated by adjusting the holding nut. The cell is easily removed from the slide plate by pulling out on the hold-down clamps and rotating them 90^{o}. A schematic of this new mounting configuration appears as Figure 27.

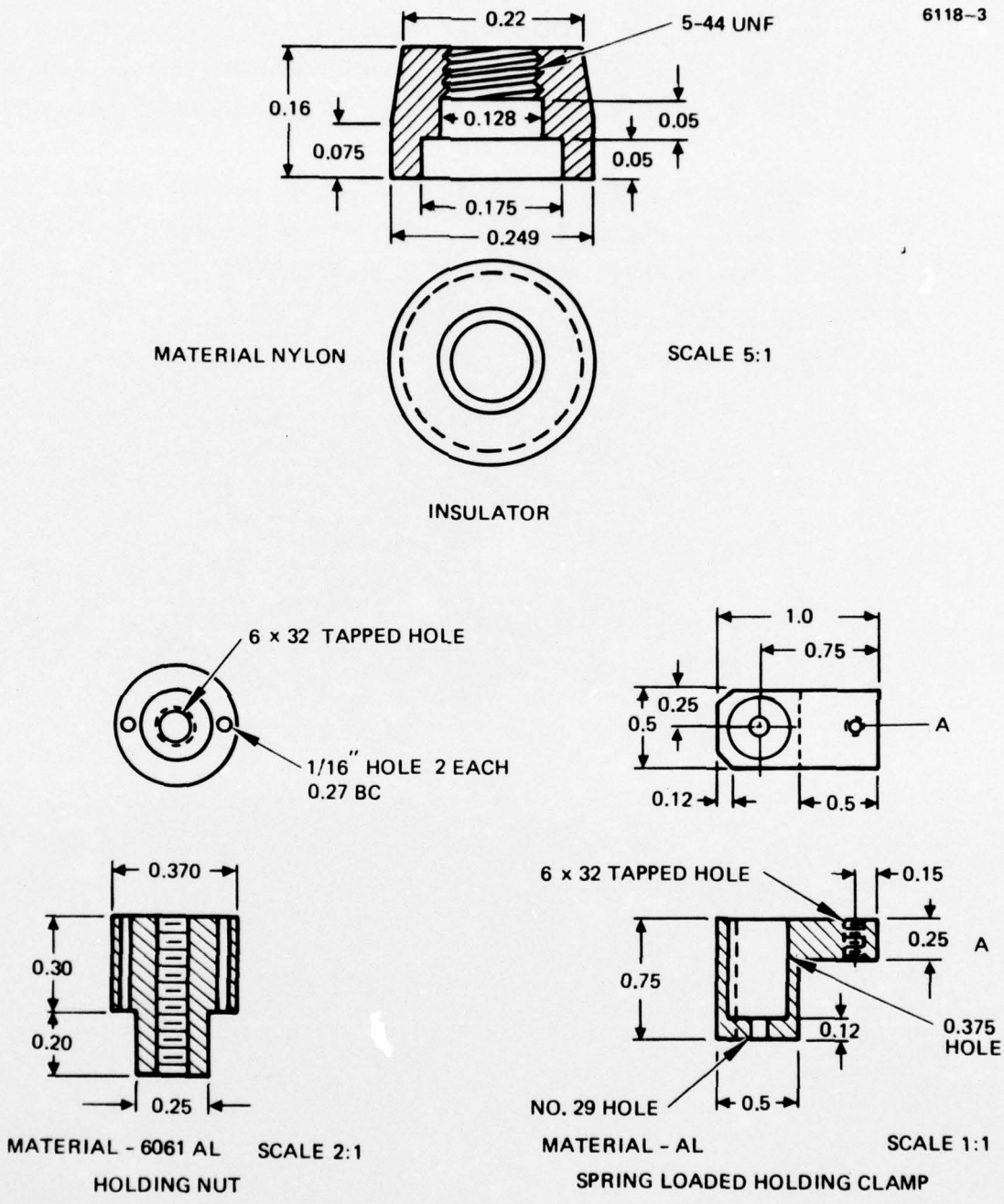

Figure 26. Details of the cell holder.

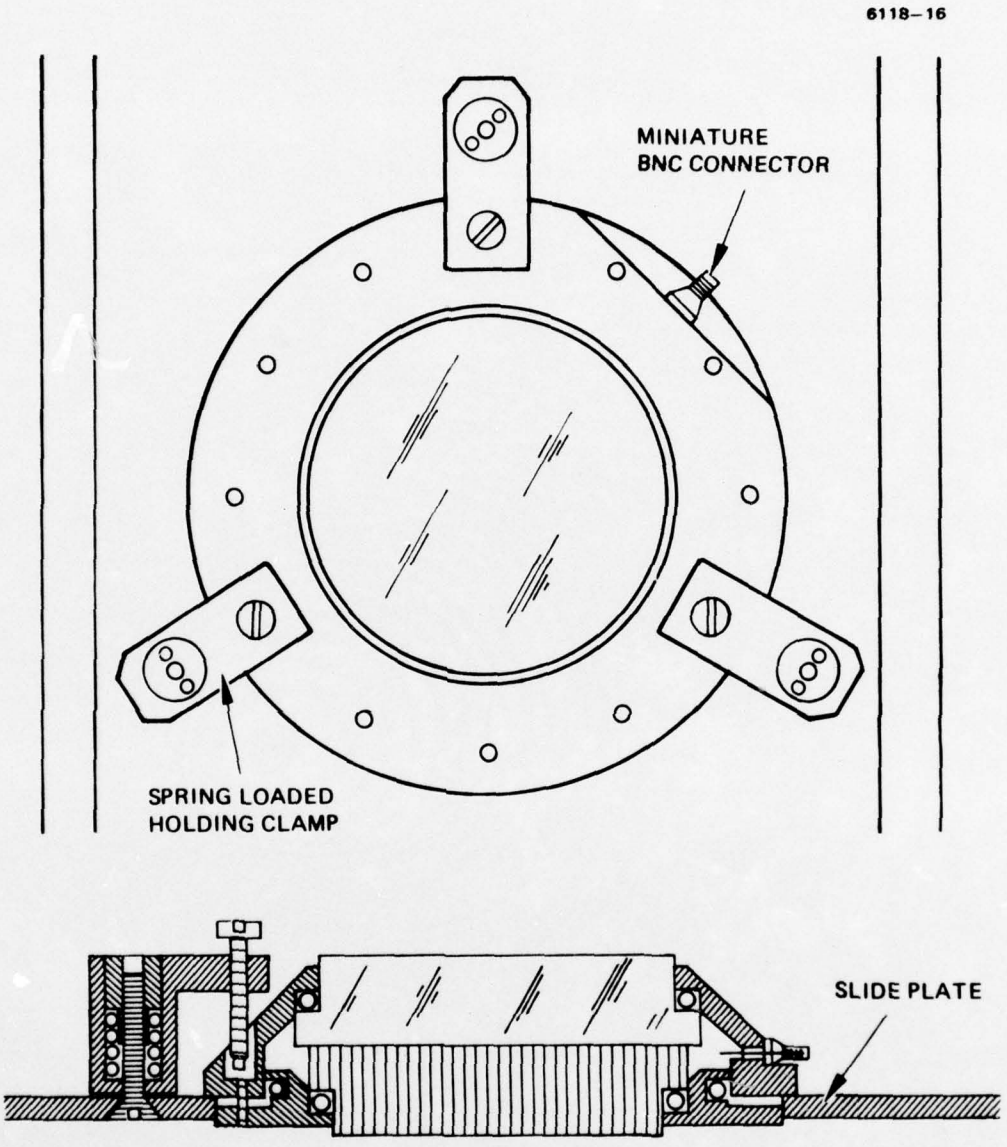

Figure 27. New cell mounting configuration.

APPENDIX B

Novel charge-storage-diode structure for use with light-activated displays

L. M. Fraas, J. Grinberg, W. P. Bleha, and A. D. Jacobson

Hughes Research Laboratories, Malibu, California 90265
(Received 30 June 1975)

A theoretical model is described for the photosensor-substrate structure presently used with the ac liquid-crystal light valve. This structure consists of a thin film (sputter deposited) of *n*-type CdS on which is evaporated a thin film of *p*-type CdTe. The model describes the photosensitivity of this structure in terms of the depletion-width photocapacity of the charge-storage diode formed by these two coatings. The model developed based on this photocapacity effect allows a consistent explanation of the experimentally observed fact that good device photosensitivity is observed at high frequencies (e.g., 10 kHz), contrary to the prediction that would result from a quantum-photodiode model. By assuming an electronic-defect-center structure that consists of fast and slow electron trap levels and a recombination level, as in the case of a photoconductor, the charge stored in the diode is related to image-activating light intensity. This provides descriptive information on device response time, gray scale, and sensitivity. Additionally, the model allows for the identification of those material properties that presently limit photosensor performance.

PACS numbers: 85.60.P, 73.40.L, 72.40., 73.60.F

I. INTRODUCTORY BACKGROUND

A. Photoactivated displays

There are a variety of display devices that consist of a light-sensitive voltage-gating layer and an adjacent layer of some field-activated light-modulating medium, both sandwiched between a pair of electrodes. Two examples of such devices are the ac liquid-crystal light valve[1,2] and the metal-plated ruticon.[3] While Rose[4] has treated the important question of a theoretical lower bound for the writing-light exposure required for such devices, in practice, our work on the ac liquid-crystal light valve has required that we develop a more specific model—one that is amenable to certain practical considerations. In particular, for real-time displays, such a model should provide for the relationship between the writing-light exposure and the photosensor response time; additionally, it should allow the identification of material properties that limit photosensor performance levels to values below the theoretical bound set by Rose's calculation.

The specific model developed here has led to the identification of a new photosensor structure for light-activated displays, an ac light-activated charge-storage diode. In this charge-storage-diode structure, the ac photocapacitance associated with the diode depletion width plays a role of major importance. Although this photocapacity is of specific importance for ac liquid-crystal displays, where ac drive voltages are used to avoid electrochemical degradation,[1] it is also of general importance for real-time field-effect displays, where frames are exposed and voltage erased at finite frame rates.

Within the liquid-crystal display device context, this new charge-storage photosensor has the salient advantage of providing a light-activated current-switching ratio (i_{on}/i_{off}) which is nearly independent of operating frequency. This is a striking advantage because, in order to achieve any reasonable lifetime, the liquid crystal has to be driven by an ac current source and the ac frequency has to be well above TV rates (for TV devices) in order to prevent beat-frequency effects. Under these conditions, the dark capactive current of the thin films increases very significantly. A simple calculation shows that a photodiode substrate with unity (or less) quantum efficiency will have a very limited switching ratio at frequencies of 200 Hz or higher. We obtain almost frequency-independent switching ratios in the range of 10^2 to 10^4 Hz. The described model explains this behavior in terms of stored charge in the depletion layers in the form of holes at recombination centers. The hole lifetimes are much longer than the driving-voltage period. Therefore, an electron flows back and forth many times before recombining with a hole. In fact, if the recombination time is independent of the frequency, the number of hole-electron separations is proportional to frequency. This produces a photocurrent which is proportional to frequency in the same fashion as is the capacitive dark current. As a result, the ratio of these two, which is the switching ratio, is frequency independent. Macroscopically, the effect of photocurrent proportional to the frequency can also be described as a photocapacitive effect and represented by a photocapacitance in the electrical equivalent circuit.

B. Basic model—the ac light-activated charge-storage diode

The ac liquid-crystal light-valve substrate is formed from the following coatings listed in order of deposition:

(1) Substrate formation begins with the deposition of an indium-tin-oxide (ITO) transparent electrode coating on a high-quality optically finished glass plate.

(2) The ITO coating is followed by a 16-μm-thick high-resistivity *n*-type CdS photoconductive coating.

(3) The CdS layer is overcoated with a *p*-type CdTe blocking layer.

(4) Finally, substrate formation is terminated with the deposition of a broad-band dielectric mirror.

When a liquid-crystal layer is sandwiched between this substrate and a second ITO-coated glass counter-

 Copyright © 1976 American Institute of Physics

PRECEDING PAGE BLANK-NOT FILMED

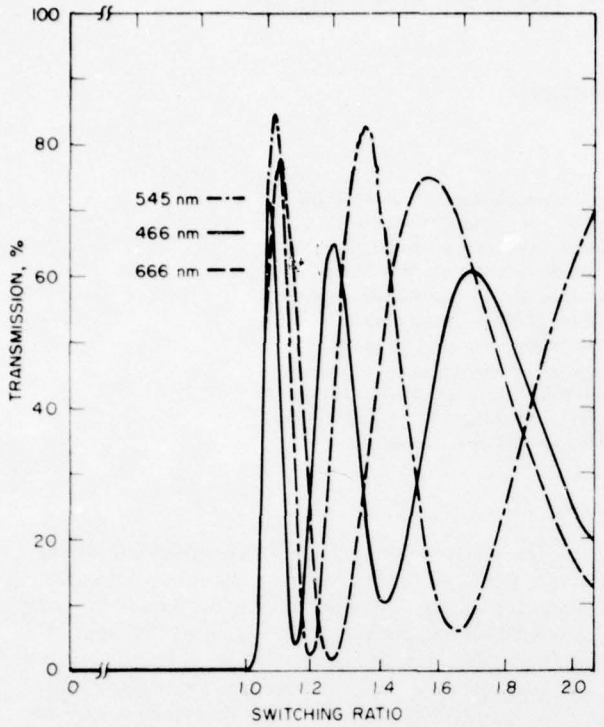

FIG. 1. Three color characteristic transmission curves of a 6-μm-thick liquid-crystal cell. These curves relate to a color-symbology liquid-crystal light value (Ref. 2).

electrode, the ac light valve is formed. This light valve is capable of TV-rate high-resolution high-intensity color-symbology image projection.[2]

The equivalent circuit for a resolution element in this device consists of two parts—a light-sensitive element and a network of passive components. The passive components are represented as an ideal capacitor for the mirror and a parallel resistor/capacitor combination for the liquid crystal. The physics describing the photoelectric properties of the CdS/CdTe light-sensitive element is the topic of this paper.

The light valve functions by switching ac voltage from the light-sensitive element to the liquid crystal when the substrate is illuminated. If we define a switching ratio as the ratio of peak current when the photosensor is illuminated to the peak current in the absence of illumination, then in practice, light-induced switching ratios of 2:1 are quite sufficient to drive a field-effect liquid crystal through a gray scale or color range (see Fig. 1).

This ac voltage switching occurs by means of light-induced ac current flow through the 16-μm-thick CdS film. This current flow can be initially visualized in one of two traditional ways. One can imagine the photosensor to function in either a photoconductor mode or in a heterojunction-photodiode mode.

In the photoconductor mode, light absorbed in the bulk CdS injects electron-hole pairs. The holes are captured almost immediately while many of the electrons are left in the conduction band free to move, thus increasing the film conductivity. Then current flows by light modulation of bulk conductivity.

In the heterojunction-photodiode mode, light is absorbed in the CdS/CdTe-interface depletion layer. When the diode is back biased, holes are swept through the CdTe and electrons are swept through the CdS film. This charge separation in the depletion layer represents the current-flow mechanism.

When a heterojunction photodiode is placed in series with a capacitor representing the dielectric mirror element and this display device is operated with ac, then the net flow of charge through the photodiode will be zero. Thus for a small portion of each ac cycle, the photodiode will be forward biased. During this time, current flows forward in a strong current pulse for which the integrated charge equals the light-activated charge flow during back bias. However, most of the time, the diode is back biased.

It turns out that neither of these traditional models correctly represent the CdS/CdTe thin-film ac-light-valve structure. However, some of the features of each model can be incorporated to formulate a new model of the photoelectric-device structure.

In the following discussion, a qualitative description is given of this new charge-storage-diode model and this model is contrasted with the photoconductor and photodiode models. A more quantitative description of the charge-storage model is then presented in Sec. II.

The band diagram for this new photoelectric-device structure is shown in Fig. 2.

In our model of this structure, we hypothesize that light injects electron-hole pairs in the highly absorptive orange region of the CdS near the CdTe interface. The injected holes are captured almost immediately at recombination centers in the CdS, as would be the case for a photoconductor. However, the impedance of the photosensor is not controlled resistively, but capacitively. The impedance is controlled by the back-bias

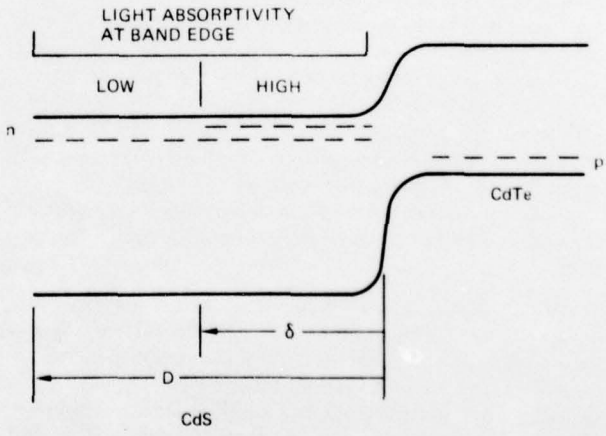

FIG. 2. Band diagram for the CdS/CdTe charge-storage-diode structure. The higher-absorption-coefficient region of CdS near the CdTe interface acts as the major charge-storage region.

TABLE I. Switching ratio for a 4-μm liquid-crystal cell.

Wavelength	Switching ratio	
Red—6000 Å	1.05	2 kHz
Green—5260 Å	1.77	100 μW/cm^2

ac photocapacity associated with a depletion region that spreads from the CdS/CdTe interface. The width of this depletion region and, therefore, the photocapacitance is controlled by a modulation of the effective donor concentration by means of light-injected electrons captured at shallow-trap centers in the highly absorptive CdS region.

This photosensor model is similar to a photoconductor in that holes are captured in the CdS bulk. Thus the substrate spectral-response region is near the CdS band edge (Table I) and the device in ac operation exhibits gain. Gain occurs because an electron-hole pair may be separated more than once. In fact, electrons flow back and forth from the CdS/CdTe interface to the CdS/ITO interface under the influence of the alternating field (e.g., 2 kHz) several times until they recombine with holes at CdS recombination centers (e.g., 30 msec). These recombination events are governed by statistics similar to those of a photoconductor.

The photosensor is unlike a photoconductor in that the ac impedance is controlled by a photocapacitive element, not the photoresistivity. Like the photodiode, the device operates most of the time in back bias.

The hypothesized charge-storage-diode model is made more explicit in Sec. II. This is accomplished in three parts. First, it is noted in Sec. II A that device performance curves follow from charge-vs-voltage (Q-vs-V) curves derived from a depletion width versus voltage calculation for various donor concentrations. This contention is supported by comparing the experimentally determined Q-vs-V curve (Fig. 3) with the theoretical Q-vs-V curves derived in Sec. II A (Fig. 4). Second, it is noted in Sec. II B that the charge-storage-diode operating curve for the diode/display combination follows from equivalent-circuit considerations. Finally, it is noted in Sec. II C that photoconductor recombination statistics link the effective donor concentration, the parameter in the Q-vs-V curves of Sec. II A, with light intensity forming a loop providing a quantitative description of the photosensor device.

In Fig. 2, the region near the CdTe interface of width δ is shown as highly absorptive due to additional shallow-trap levels. Given the above explanation of device operation, it can be seen that this readily enhances sensitivity. Light is absorbed in the depletion region for maximum injection efficiency. The donor concentration is varied most dramatically where it is most effective in changing the depletion width from 16 μm (total CdS film thickness) in the dark to some appreciably smaller value for low light levels.

II. THEORY OF LIGHT-ACTIVATED CHARGE-STORAGE DIODE

A. Charge-distribution equations

The characteristic curves for the charge-storage diode are the Q-vs-V curves. Here Q is the total separated charge and V is the back-bias voltage. To calculate these curves, referring to Fig. 2, one makes the following simplifying assumptions. First, one assumes that the light is absorbed primarily in the highly absorptive orange region ($0 \leq x \leq \delta$). Second, one assumes that the light-modulated donor concentration is uniform in the orange region. Third, that the donor concentration is always zero in the yellow region ($\delta \leq x \leq D$). Given these assumptions and from Gauss's equation, $\int E\,dA = \int \rho\,dV/\epsilon_0$, one calculates the Q-vs-V curves given in Fig. 4. These curves are represented by the following equations:

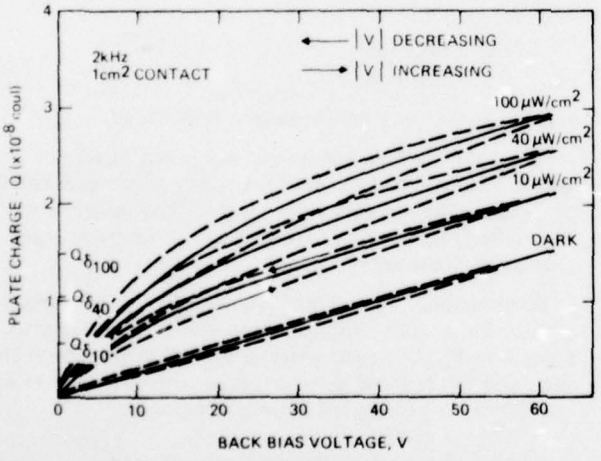

FIG. 3. Experimental plate-charge—vs—back-bias-voltage curves for the charge-storage diode. Data are presented for various light levels. The dashed curves represent scope curve traces for the $|v|$-increasing and $|v|$-decreasing cases. The solid curves represent the averaged case.

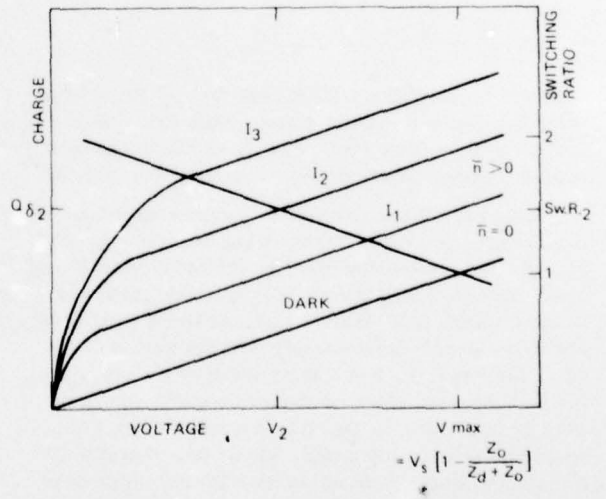

FIG. 4. Plate-charge—vs—back-bias-voltage theoretical curves as per Eqs. (1) and (2). Incident-light intensity I is a parameter. The operating curve for the ac light value as per Eq. (3) is also shown.

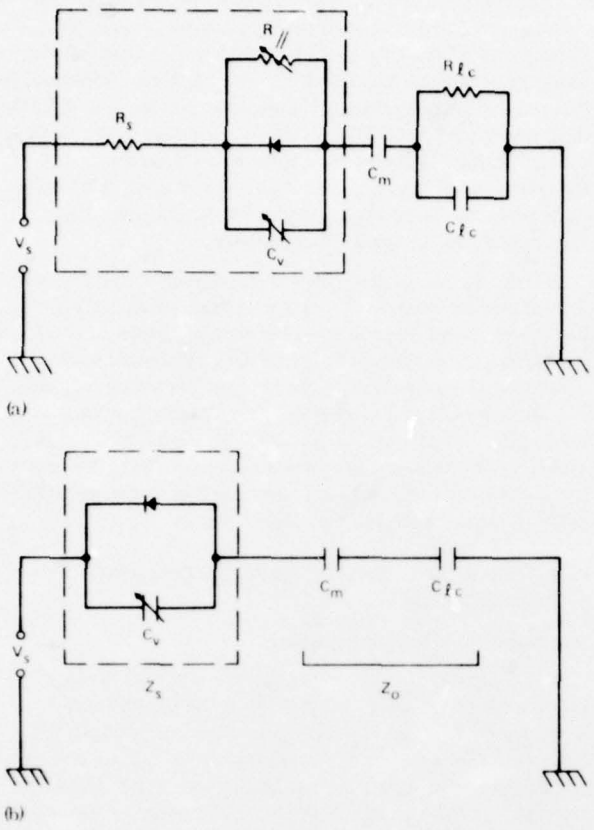

FIG. 5. (a) Equivalent circuit of a resolution element in the ac light value. The portion in the dashed square represents the CdS-CdTe photosensor element, while the portion in series with this represents the impedances of the dielectric mirror and the liquid-crystal elements. (b) A simplification of circuit (a) which is a useful first approximation.

$$V = \frac{Q^2}{2\epsilon\bar{n}}, \quad Q \leq Q_\delta(\bar{n}), \tag{1}$$

$$V = \frac{\bar{n}\delta^2}{2\epsilon} + \frac{(Q - \bar{n}\delta)D}{\epsilon}, \quad Q \geq Q_\delta, \tag{2}$$

where D is the CdS thickness and $Q_\delta = \bar{n}\delta$ represents the total charge in donor states. Note that $\bar{n}$ is the light-intensity-dependent density of filled donor states in the orange region. These curves are plotted in Fig. 4.

Physically, these curves can be understood as follows. In the dark, the filled-donor-state density $\bar{n}$ is zero; Eq. (1) is not effective and Eq. (2) reduces to $V = QD/\epsilon$. The CdS film charges as a 16-μm-thick capacitor. The Q-vs-V curve is a straight line. At finite light levels, the filled-donor-state density $\bar{n}$ is not zero and the CdS, for small V, has a very small depletion width. As V increases, the film depletion width grows as in a diode according to Eq. (1). When the orange region is completely depleted (Q_δ), the device charges with a constant slope given again by a 16-μm-thick capacitor.

B. Operating curve for ac light valve

The equivalent circuit for the ac light valve is shown in Fig. 5(a). In this figure, the region in the dashed square represents the equivalent circuit of the CdS/CdTe light-sensitive element. Series resistivity is represented by R_s in the nondepleted region of CdS and R_v represents the residual resistivity of the CdS in the depleted region. Sec. II A has described the light and voltage variations of the depletion-width capacity C_v. It has been assumed that $R_s \cong \infty$. These assumptions are reasonable first approximations. However, in a second approximation they are important as they can lead to the hysteresis observed in Fig. 3. These deviations will be treated in a later experimental publication.[5]

In standard light-valve operation, approximately 60-V peak-to-peak sinusoidal ac voltage is applied across a cell. A varying fraction of this voltage is applied across the CdS/CdTe charge-storage element. This fraction varies with input-image light level. In other words, as the light level increases, the impedance of the CdS/CdTe element drops and more current flows through the liquid crystal; thus more voltage is switched to the liquid crystal. The voltage on the liquid crystal actuates an electro-optic effect that modulates the projection light to give various levels of gray (or color) in the output image. Calculating the voltage switching ratio as a function of input-image light level is then of interest because this translates to projected-image gray scale.

Recalling that the switching ratio Sw. R. is defined as the ratio of peak current in the light to peak current in the dark, and simplifying the equivalent circuit in Fig. 5(a) to that of 5(b), then the voltage on the CdS/CdTe element in light versus switching ratio is found to be a straight line given by

$$V = \frac{Z_s V_s}{Z_s + Z_0} = V_s \left(1 - \frac{Z_0}{Z_{sd} + Z_0}\,\text{Sw. R.}\right),$$

$$V = V_s \left(1 - \frac{Z_0 \text{Sw. R.}}{Z_{sd} + Z_0}\right), \tag{3}$$

where

$$\text{Sw. R.} = \frac{Z_{sd} + Z_0}{Z_s + Z_0}$$

and Z_{sd} is the dark-state-sensor impedance.

This straight line can be plotted on the family of Q-vs-V curves of Fig. 4. These curves are generated by varying the incident light level I. The intersects of the various light-level curves with this straight line give gray-scale information.

For example, for incident light level I_2, the voltage across the charge-storage diode will run periodically from 0 to V_2. The peak voltage V_2 will define the switching ratio Sw. R.$_2$ and the charge Q_{δ_2} will be swept in and out of the orange charge-storage region.

C. Charge generation-recombination equations

The charge Q_δ is a function of light level. To define this charge requires a model for the generation and recombination of carriers in the highly absorptive orange CdS region. Figure 6 defines a level structure for such a model.

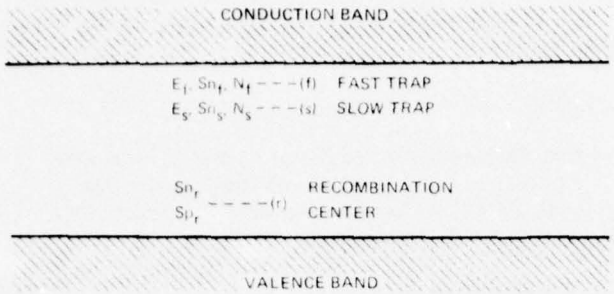

FIG. 6. Band-structure diagram for the CdS charge-storage region. The traps and recombination centers are typical of a photoconductor material like CdS.

The level structure of Fig. 6 is similar to that of a photoconductor. The model possesses the basic features necessary for a first-order description of both single crystals and thin films. However, the thin-film case can be expected to be somewhat approximate because a multitude of levels are probably involved.

The nomenclature of Fig. 6 parallels that of a photoconductor model developed by Bube.[6] In the dark, the recombination level r is assumed filled, and the slow-trap level s and the fast-trap level f are assumed empty. The population of the fast-trap level f in the illuminated state is the quantity of interest. This level defines the charge Q_b. Fast centers are defined as the donor centers that can empty and fill with the period of the applied ac voltage. Thus the filled-donor-state density $\bar{n}$ in Eqs. (1) and (2) will become the space-averaged density of filled fast traps, $\bar{n}_f$, in the remainder of the paper, and this quantity $\bar{n}_f$ will be related to exposure-light intensity and device on and off response times.

The symbols to be used for the band diagram of Fig. 6 have the following definitions. N_i is the density of states i, n_i is the density of filled states i, S_{n_i} is the capture cross section of states i for electrons, S_{p_i} is the capture cross section of states i for holes, n is the density of free electrons, p is the density of free holes, F is the density of electron-hole pairs created per second by optical excitation across the band gap, β_{n_i} is the capture coefficient for an electron by center i, $E_{i=f,s}$ is energy difference between bottom of conduction band and level i, $\mathbf{J}_n$ is the free-electron current, E is the electric field strength, and $P_{i=f,s}$ is the probability per unit time for thermal ejection of an electron in level i into the conduction band.

$$P_i = N_c S_{n_i} V_{\text{th}} \exp(-E_i/kT),$$

where N_c is the effective density of states in the lowest kT-wide part of the conduction band and V_{th} is the thermal velocity for an electron.

Given these definitions, the detailed balance equations can be written for the various level populations:

$$\frac{\partial n_s}{\partial t} = \beta_{n_s} n(N_s - n_s) - n_s P_s \cong \beta_{n_s} n N_s - n_s P_s, \tag{4}$$

$$\frac{\partial n_f}{\partial t} = \beta_{n_s} n(N_f - n_f) - n_f P_f \cong \beta_{n_f} n N_f - n_f P_f, \tag{5}$$

$$\frac{\partial n_r}{\partial t} = \beta_{n_r} n(N_r - n_r) - \beta_{p_r} n_r p, \tag{6}$$

$$\frac{\partial p}{\partial t} = F - p\beta_{p_r} n_r - \frac{1}{q}\nabla \cdot \mathbf{J}_p \cong F - p\beta_{p_r} n_r, \tag{7}$$

$$\frac{\partial n}{\partial t} \cong F - n[\beta_{n_r}(N_r - n_r) + \beta_{n_f} N_f + \beta_{n_s} N_s] + n_s P_s + n_f P_f - \frac{1}{q}\nabla \cdot \mathbf{J}_n. \tag{8}$$

These equations are semirigorously correct. The approximation in Eqs. (4), (5), and (8) is that the fractional filling of the fast- and slow-trap centers is small. Thus $n_{f,s} \ll N_{f,s}$. This is valid at the low light levels in the range of interest for the light valve. The approximation in Eq. (7) is the statement that holes are captured rapidly at recombination centers.

However, for the charge-storage diode, these equations are very difficult to solve in closed form. The quantities n, n_r, n_s, and n_f are functions of position and time, and they are strongly voltage and light dependent. To arrive at an approximate solution of these equations, it is interesting first to solve them for the photoconductor case. Then for the steady-state case, the time dependence is removed; also voltage terms can be neglected as quite small. Finally, spatially uniform distributions through the depth of the film can be assumed. Thus one solves for steady-state average populations as a function of light intensity only. Then Eqs. (4)–(8) reduce to

$$\beta_{n_s} n N_s - n_s P_s = 0, \tag{4'}$$

$$\beta_{n_f} n N_f - n_f P_f = 0, \tag{5'}$$

$$F = \beta_{n_r} n(N_r - n_r). \tag{8'}$$

The two Eqs. (4′) and (5′), indicate that the free-electron and fast- and slow-trap populations, n, n_f, and n_s, are in thermal equilibrium with one another. Thus,

$$n = \frac{N_c}{N_s} n_s \exp\left(-\frac{E_s}{kT}\right), \tag{4''}$$

$$n = \frac{N_c}{N_f} n_f \exp\left(-\frac{E_f}{kT}\right), \tag{5''}$$

and

$$n_f = \frac{N_f}{N_s} n_s \exp\left(\frac{E_f - E_s}{kT}\right). \tag{9}$$

This thermal-equilibrium statement implies that for approximately equal shallow- and deep-trap densities ($N_f \sim N_s$), then $n \ll n_f \ll n_s$. This condition combines with charge neutrality, i.e., $n + n_s + n_f = p + (N_r - n_r)$, to yield

$$n_s \cong N_r - n_r. \tag{10}$$

Thus the density of holes in recombination centers

$N_r - n_r$ is approximately equal to the density of electrons in slow-trap centers n_s, while the density of carriers free or in shallow donor sites is small compared to n_s or $N_r - n_r$. This condition couples into Eq. (8′) to define the slow-trap occupation density as a function of light level. Thus

$$F = \beta_{n_r} n n_s. \tag{8′}$$

The β's can be defined from studying Eq. (4). The first term on the right-hand side represents the growth of population of level s by free-electron capture. This capture term can be written as $(N_s - n_s) S_{n_s} V_{\text{th}} n$, i.e., [the inverse of the distance a free electron moves until capture $(N_s - n_s) S_{n_s}$] times (the distance an electron moves per unit time, V_{th}) times (number of electrons involved n). This equation implies that $\beta_{n_i} = S_{n_i} V_{\text{th}}$ for a photoconductor.

Now, a solution for the charge-storage diode can be attempted. From the solution of the photoconductor problem, we can expect n_s and $N_r - n_r \gg n_f$ and n. Charge neutrality will not hold, but as the fluctuations will be of the order of n_f, we might expect

$$\int n_s \, dV \sim \int (N_r - n_r) \, dV.$$

We can expect nonuniform population densities, but as this does not give easily solvable equations, we will assume that n_s and n_r are spatially uniform. We define $\bar{n}_s$ and $\bar{n}_r$ as spatial averages of n_s and n_r.

Equations similar to Eqs. (4′) and (8′) can be derived by time averaging Eqs. (5) and (6) over a period T of the applied ac voltage. Thus in equilibrium, from Eq. (4),

$$\frac{1}{T}\int_0^T \frac{\partial n_s}{\partial t}\, dt = 0 = \beta_{n_s} N_s \int_0^T n \, dt \, \frac{1}{T} - \int_0^T n_s P_s \frac{dt}{T}.$$

Then

$$(1/T)\,\beta_{n_s} N_s \int_0^T n \, dt - \bar{n}_s P_s = 0. \tag{11}$$

From Eq. (6)

$$\frac{1}{T}\int_0^T \frac{dn_r}{dt}\, dt = 0 = \beta_{n_r}(N_r - n_r)\int_0^T \frac{n\,dt}{T} - \beta_{p_r} N_r \int_0^T \frac{p\,dt}{T}$$

and Eq. (7)

$$\frac{1}{T}\int_0^T \frac{dp}{dt}\, dt = 0 = F - \beta_{p_r} N_r \int_0^T \frac{p\,dt}{T}$$

and eliminating the common term, then

$$F - \beta_{n_r}(N_r - n_r)\int_0^T \frac{n\,dt}{T} = 0. \tag{12}$$

An approximate solution of the integral

$$\int_0^T (1/T)\, n \, dt$$

follows by noting that during each cycle all the electrons in the fast traps become free for some time τ representing a fraction α of a cycle before being swept out of the film. During that time τ, they can interact with recombination centers and deep-trap centers. Then setting

$$\frac{1}{T}\int_0^T n\, dt = \frac{\tau}{T}\,\bar{n}_f = \alpha \bar{n}_f$$

in Eqs. (11) and (12), and recalling that $Q_\delta = \bar{n}_f \delta$, the approximately valid generation-recombination Eqs. (11)–(13) close the loop linking the charge Q_δ to the light intensity F. In summary

$$\beta_{n_s} N_s \alpha \frac{Q_\delta}{\delta} = \bar{n}_s P_s, \tag{11′}$$

$$F = \beta_{n_r}\overline{(N_r - n_r)}\,\alpha\,\frac{Q_\delta}{\delta}, \tag{12′}$$

$$\bar{n}_s = \overline{(N_r - n_r)}. \tag{13}$$

These equations provide the parameter (I_1, I_2, and I_3) information for Fig. 4. It is interesting to note that Eqs. (11′) and (12′) for the charge-storage diode parallel Eqs. (4′) and (8′) for the photoconductor when n is replaced by $\alpha \bar{n}_f$.

III. MODEL PERFORMANCE PREDICTIONS

In Sec. II, the basic theory describing the charge-storage-diode photosensor structure was derived. In this section, the discussion of Sec. II is applied to make predictions relating to the ac-light-valve display device. The predictions derived in this section are compared with experimental device performance measurements in a sequel paper.[5] Reasonably good agreement is found.

A. Sensitivity and gray scale

Equations (11)–(13) can be used to derive the following formula relating F to $\bar{n}_f$:

$$F = \left[\beta_{n_r}\alpha^2 \frac{N_s}{N_c} \exp\left(\frac{E_s}{kT}\right)\right](\bar{n}_f)^2. \tag{14}$$

The term in brackets is a measure of sensitivity. The smaller this term, the higher the sensitivity. This shows that sensitivity improves with (i) smaller recombination cross section—β_{n_r}; (ii) smaller α; (iii) smaller deep-trap densities—N_s; and (iv) smaller deep-trap energy—E_s. Equation (14) also shows that the light intensity varies quadratically with the stored charges, $Q_\delta = \bar{n}_f \delta$. Thus in Figs. 3 and 4, $I_2 \cong 4I_1$ and $I_3 \cong 9I_1$. Now, Fig. 4 completely describes the substrate Sw. R. for liquid-crystal gray-scale calculations. It is clear that even below the saturated switching ratio (maximum possible Sw. R. given Z_0) in the range where the film is depleted every cycle, the gray scale will be compressed at higher light levels and expanded at lower light levels.

B. Response times for storage diode

When light is first turned on, there will be some time before the diode current will build up to its equilibrium value. This turn-on time is just the time to build up charge in the diode. Since $\bar{n}_s$ is the major charge element, this rise time will be

$$T_{\text{rise}} = \frac{\bar{n}_s}{F} = \frac{1}{\beta_{n_r} \alpha \bar{n}_f} . \tag{15}$$

This rise time is longer for lower light levels and larger deep-trap densities.

The treatment of the storage-diode turn-off time is somewhat more complex. However, intuitively, it can be seen that one of two physical conditions will dominate the charge decay. Thus if the initial recombination time is slow enough, the free-charge density will remain in thermal equilibrium with the deep-trap density during decay and the charge decay will be governed by the recombination cross section.

On the other hand, if the initial recombination time is quite fast, then the free-charge density will initially fall rapidly to a level where the thermal-detrapping rate equals the recombination rate, and then the decay rate will be governed by the deep-center thermal-detrapping rate. These intuitive statements can be expressed more formally by referring to Eqs. (4) and (6) for $\partial n_s/\partial t$ and $\partial n_r/\partial t$. To begin, note that when the light is turned off, F goes to zero and $\partial n_r/\partial t$ is no longer equal to zero as in equilibrium. Time averaging Eq. (6) gives the time-averaged decay of $\bar{n}_r$. Thus

$$\frac{\partial(\overline{N_r - n_r})}{\partial t} = \beta_{n_r} \alpha \bar{n}_f (\overline{N_r - n_r}).$$

Although $\bar{n}_f$ is a function of $\overline{N_r - n_r}$, the instantaneous decay time for $(\overline{N_r - n_r})$ can still be written[7]

$$\tau_{\text{decay}} = \frac{1}{\beta_{n_r} \alpha \bar{n}_f} = \frac{N_s \exp(E_s/kT)}{N_c \beta_{n_r} \alpha (\overline{N_r - n_r})} . \tag{16}$$

Now it is clear that the decay time of $N_r - n_r$ will relate to the current decay in the case that n and $\bar{n}_f$ remain in thermal equilibrium with $\bar{n}_s$ during decay. In that case, $\bar{n}_f$ will remain proportional to $\bar{n}_s$ and, in any case, $\bar{n}_s \cong \overline{N_r - n_r}$. So $\bar{n}_f$ will decay with the same decay constant as $\overline{N_r - n_r}$.

The nonthermal-equilibrium case can be examined by referring to Eq. (4). The origin of the thermal-equilibrium condition is simply the statement that $\partial n_s/\partial t = 0$. During decay this statement is no longer valid.

$$\frac{\partial(N_r - n_r)}{\partial t} \cong \frac{\partial n_s}{\partial t}$$

is always valid. So, the thermal-equilibrium condition becomes the condition that

$$\bar{n}_s P_s \gg \frac{\delta(\overline{N_r - n_r})}{\delta t} .$$

In the event that this condition is not satisfied, it is still valid that

$$\left| \frac{\delta n_s}{\delta t} \right| = \left| \frac{\delta(\overline{N_r - n_r})}{\delta t} \right| \leq n_s P_s \cong (\overline{N_r - n_r}) P_s .$$

The conclusion is that there is a lower bound on the decay rate. The decay rate cannot be faster than the thermal-detrapping rate P_s^{-1}.

Finally, consider the case of thermal equilibrium during decay. In that case, as $\bar{n}_f$ will be a decreasing function of time delay after turn off, Eq. (16) says that peak current will not decay exponentially. The time constant for decay will get slower the longer the delay. However, for the instantaneous decay constant immediately after turn off, one substitutes the equilibrium value of $\bar{n}_f$ from Eq. (14). The result is that the initial turn-off time will be faster for higher light levels. However, $Q_b \tau_{\text{decay}}$ will be approximately constant. [Eq. (16) becomes identical to Eq. (15).]

C. Resolution

In general, device resolution should be quite high. First, the image is stored in the high-absorption region of the CdS near the liquid crystal. This can be a relatively thin layer, e.g., 4 μm. Second, considerable field focusing can be expected in the stoichiometric region. Therefore, this layer can be relatively thick to lower the capacitive dark current while not deteriorating resolution.

D. Varied ac frequency characteristic

An explicit expression for the effect of operating ac frequency on diode sensitivity cannot be written for the thin-film case. This results because the quantities α, β_n, N_{n_s}, N_s, and P_s in Eq. (14) all depend implicitly on ac frequency. The implicit variation in β_{n_s}, N_s, and P_s results from the definitions of levels s and f as slow and fast relative to the period of the ac field. Fast centers, by definition, can respond during a period. Thus in thin films with a multitude or continuum of trap levels, a fast center at 200 Hz may become a slow center at 20 kHz. However, in general one can expect N_s to increase with frequency. Statements about β_{n_s} and P_s are more difficult to make. The quantity α can be expected to increase with frequency. This follows because delay times for donor emission become more important when compared to shorter periods. From this statement and the statement about N_s increasing with higher frequency, Eqs. (14) and (15) predict lower sensitivity and slower rise times at higher frequencies.

In addition to the above variations, higher frequency generally gives better image uniformity. This follows because material variations in R_s and $R_{\parallel}$ [Fig. 5(a)] are less important and the capacity terms are more important. And since the capacities are controlled primarily by film thicknesses that can be made extremely uniform, the voltage switched to the liquid crystal is closely related to the image-light intensity. Finally, higher-frequency operation gives improved resolution, because the higher-capacitive currents dominate the sheet-resistivity spreading currents.

IV. DISCUSSION

The lower bound of Rose on writing-light exposures[4] is based on a simple capacity calculation. He calculates the field change on a light-modulating medium when all the available writing light is absorbed in the photosensor and all light-generated carriers can be separated by the total photosensor-layer thickness before recombination. In practice, one must consider, in detail, system and material limitations on the 100% writing-light-absorption assumption and on the 100% carrier-separa-

tion assumption, as well as effects of erasure capacitive current via finite frame-updating times.

In the case of the ac liquid-crystal light valve, it is most convenient to focus on the above practical considerations by first noting that the display device is to be CRT addressed and that a CRT phosphor has a fairly large spectral bandwidth (500 Å). This CRT writing light will be either surface or volume absorbed by the photosensor.

If the writing light is surface absorbed, switching ratios are limited in practice, first, by materials, which often have inordinately fast ($\sim \mu$sec) recombination times via high local-carrier densities and high surface-state-recombination-center cross sections, and second, by the fact that capacitive dark currents are already significant at 30 Hz (real-time frame rate), and are already dominant for the ac light valve with operation at 1 kHz. If the writing light is volume absorbed, recombination rates become more optimal (30 msec).[3] However, in this case, an interplay develops between the assumptions of 100% volume-light absorption and 100% carrier separation. The problem is that low deep-trap materials allow 100% carrier separation, but at the expense of narrower band-edge absorption and less than 100% volume-light absorption.[8] It is the conclusion of the present paper that the 100% volume-light-absorption assumption can be more nearly realized if a graded band-gap material is used. In addition, the 100% carrier-separation assumption can be more nearly realized if the volume-absorbed light is absorbed in a high-field region such as a depletion region and also if the effects of deep-trap densities are minimized by a high shallow-trap-density to deep-trap-density ratio.

[1] T. D. Beard, W. P. Bleha, and S.-Y. Wong, Appl. Phys. Lett. **22**, 90 (1973).
[2] J. Grinberg, W. P. Bleha, A. D. Jacobson, A. M. Lackner, G. D. Myer, L. J. Miller, J. D. Margerum, and L. M. Fraas, IEEE Trans. Electron Devices (to be published).
[3] N. K. Sheridon, IEEE Trans. Electron Devices **ED-19**, 1003 (1972).
[4] A. Rose, IEEE Trans. Electron devices **ED-19**, 430 (1972).
[5] L. M. Fraas, W. P. Bleha, J. Grinberg, and A. D. Jacobson, following paper, J. Appl. Phys. **47**, 584 (1976).
[6] R. H. Bube, J. Phys. Chem. Solids **1**, 234 (1957).
[7] S. M. Ryvkin, *Photoelectric Effects in Semiconductors* (Consultants Bureau Enterprises, New York, 1964).
[8] L. M. Fraas, W. P. Bleha, and P. O. Braatz, J. Appl. Phys. **46**, 491 (1975).

AD-A039 118 HUGHES RESEARCH LABS MALIBU CALIF F/G 20/6
DEVELOPMENT OF A COLOR SYMBOLOGY AC LIQUID CRYSTAL LIGHT VALVE.(U)
APR 77 A D JACOBSON, W P BLEHA N00024-75-C-7187
UNCLASSIFIED NL

2 OF 2
AD A039118

END
DATE FILMED
5-77

ac photoresponse of a large-area imaging CdS/CdTe heterojunction

L. M. Fraas, W. P. Bleha, J. Grinberg, and A. D. Jacobson

Hughes Research Laboratories, Malibu, California 90265
(Received 30 June 1975)

Experimental data are presented for the photosensor-substrate structure presently used with the ac liquid-crystal projection light valve. This structure consists of a thin film (sputter deposited) of *n*-type CdS on which is evaporated a thin film of *p*-type CdTe. In an earlier publication, a model was presented which describes the photosensitivity of this structure in terms of the depletion-width photocapacity of the charge-storage diode formed by these two coatings. The experimental data presented here correlate well with this model. Among the data presented are data on light-valve display, photosensor gray scale, and response time. The response-time data are of particular interest because they show that the projection-light-valve photosensor is capable of operation at near-TV rates. The agreement of the experimental data with model and extrapolation from the model imply that large improvements in sensitivity and response time are still quite possible.

PACS numbers: 85.60.P, 73.40.L, 72.40., 73.60.F

I. INTRODUCTION

This paper reports the experimental characteristics of the imaging photosensor used in the ac liquid-crystal light-valve projection display device.[1,2] However, as the light-valve device itself is novel we begin by briefly describing the light valve with the aim of placing the photosensor discussion into the over-all device context. The light-valve device, which serves as a light-imaging amplifier, is shown schematically in Fig. 1.

When a low-intensity writing image from a CRT, for example, illuminates the CdS/CdTe light-sensitive element, the applied ac voltage is spatially gated to the liquid-crystal layer. The liquid crystal, in turn, acted on by this spatially varying voltage, modulates the high-intensity projection light to form a replica image. The total light-valve performance, then, is gauged by two factors: (1) the voltage switching response of the light-sensitive element to the writing light image and (2) the liquid-crystal modulation effect on the projection light in response to the photosensor supplied voltage.

In this paper, the focus is on the experimental response of the light-sensitive element. In an earlier publication, a theoretical model for the light-sensitive element was proposed.[3] Here, after a discussion of photosensor fabrication (Sec. II), the theoretical model is briefly reviewed (Sec. III) and experimental data are presented and evaluated with this model as a base (Secs. IV–VI).

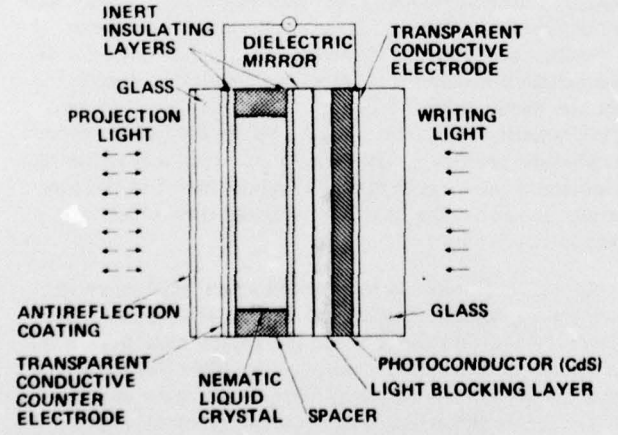

FIG. 1. Schematic diagram of the ac photoactivated light valve used for projection display.

II. PHOTOSENSOR FABRICATION

The photosensor diode used in the ac light valve consists of three film layers deposited in sucession on a glass substrate. These films are, in order of deposition, (i) a 40-nm-thick e-beam-evaporated indium-tin-oxide transparent electrode, (ii) a 16-μm-thick reactively sputtered CdS film, (iii) a 2-μm-thick thermally deposited CdTe film.

The CdS film is prepared by reactive sputtering in a H_2S/Ar atmosphere in a fashion similar to that described by Frazer and Melchior.[4] The sputtering variables have the following values: deposition rate, 1.3–1.5

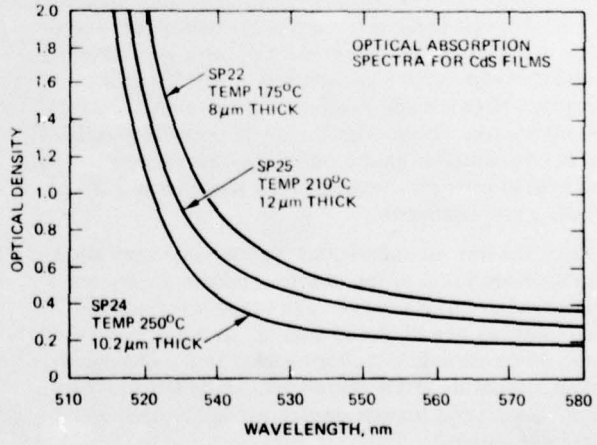

FIG. 2. Shown are optical absorption spectra for sputtered CdS films with substrate temperature as a parameter. Note that as the temperature is lowered, the near-band-edge absorption increases.

 Copyright © 1976 American Institute of Physics

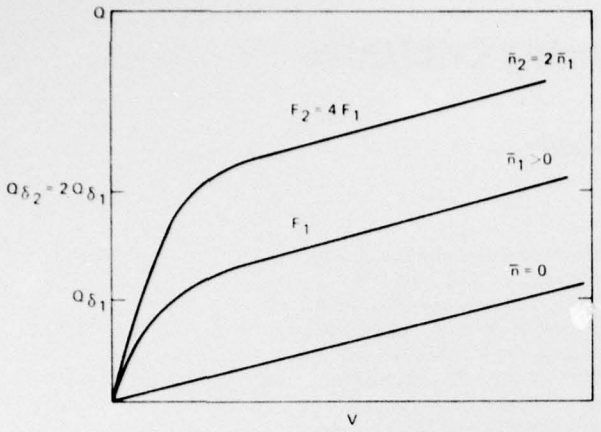

FIG. 3. Shown are theoretical plate-charge—vs—back-bias-voltage curves for a light-activated charge-storage diode. The light-induced electron-hole-pair injection rate is the curve parameter.

μm/h; argon pressure, 14—16 μm; H_2S concentration, 2%; bias, substrates grounded; residual gas pressure, $\leq 2\times10^{-5}$ Torr; substrate temperature, varied during deposition.

Graded absorption films are prepared by varying the substrate temperature during the CdS-film deposition. The initially high (225 °C) substrate temperature produces a highly insulating low trap density and shorter-wavelength absorption-edge layer, while the final low substrate temperature (175 °C) produces a shifted absorption edge and high shallow-trap-density layer. This effect of substrate temperature on the CdS-film optical absorption edge is illustrated by the spectra of Fig. 2.

After CdS-film deposition, the film is chemomechanically polished and a p-type CdTe film is deposited thus forming the n-p diode structure.

III. PHOTOSENSOR MODEL REVIEW

The photosensor element in the light-valve structure of Fig. 1 is the large-area diode formed by the p-type CdTe and n-type CdS films. As has been described in an earlier paper,[3] the key element controlling the operation of this diode structure is the ac capacitive impedance associated with the diode depletion width. It has been postulated that a light-injected charge controls this depletion-width capacity. The way this occurs is briefly reviewed below.

Since the key element in the photosensor operation is the depletion width of the charge-storage diode, the characteristic diode curves are the Q-vs-V curves. These curves are shown in Fig. 3. In these curves, V is the diode back-bias voltage and Q is the charge on the indium-oxide (ITO) Ohmic contact to the CdS film. Light intensity is the parameter producing the family of curves shown.

First we consider the dark state. In this state, the CdS layer in the diode has a resistivity such that the diode depletion width sweeps easily from the CdS/CdTe interface all the way through the CdS film (~16 μm) for very small voltages, V. Thus in the dark the ac impedance of the photosensor is that of a 16-μm-thick CdS dielectric parallel-plate capacitor. So for the dark case the Q-vs-V curve in Fig. 3 is a straight line.

Second we consider the illuminated state. Then when light falls on the diode, the photons create electron-hole pairs in the bulk of the CdS film near the CdTe interface. The injected holes are captured in the CdS at recombination centers forming a stored charge. If the diode is in the zero-back-bias-voltage condition, the light-injected electrons are captured at trap centers in the CdS and the hole charge is compensated. Thus the ITO plate charge is zero at zero voltage. As the voltage varies from zero, however, since some of the electrons are mobile while the holes are not, the shallow electron traps act effectively as donors, and the depletion width varies with voltage in a fashion controlled by an effective donor concentration created by light-injected electrons captured at shallow-trap centers. This is the nonlinear region of each illuminated-diode curve in Fig. 3. When the voltage reaches the point that the shallow-trap centers are depleted, the charge has been removed from the bulk of the film and the film will again charge as a 16-μm dielectric capacitor and the Q-vs-V curve becomes a straight line parallel to the dark-state Q-vs-V curve.

It is clear from the above discussion that the electron population at the shallow-trap centers is the light-dependent quantity which characterizes the photosensor response. This quantity can be related to light intensity and sensor on and off times by assuming a three-level model for the CdS film.[3] These three levels are (1) a recombination center, (2) a shallow-trap center, and (3) a deep-trap center.

The deep-trap center plays an important role in limiting performance. Referring to the earlier discussion, not all electrons trapped are free to move at the frequency of the applied ac voltage. Thus they limit sensitivity, as many of the light-injected electron-hole pairs are then ineffective.

The equations relating to sensitivity and sensor on and off times developed from this three-level model are summarized in Table I. It is worth noting that these equations parallel the equations for a photoconductor if the conduction-band free-electron population density for the photoconductor is replaced by the quantity $\alpha\bar{n}_f$. This quantity arises because all of the electrons trapped at shallow centers $\bar{n}_f$ are free to move for a fraction of a period α each cycle before they are swept to the electrode. So $\alpha\bar{n}_f$ is the effective average free-electron population density.

As was discussed in the preceding paper,[3] there is some advantage in grading the optical absorption coefficient of the CdS film so that the region near the CdTe interface is more highly absorptive. This has the advantage of higher sensitivity because of more uniform bulk carrier injection, a more ideal spectral match to the CRT phosphor, and a higher average collection

TABLE I. Descriptive equations for light-activated charge-storage diode. Symbol definitions are in Sec. VIII.

(1)	$Q_b = \bar{n}_f \delta$
(2)	$V = \frac{Q^2}{2\epsilon \bar{n}}, \quad Q \le Q_b(\bar{n})$
(3)	$V = \frac{\bar{n}\delta^2}{2\epsilon} + \frac{(Q-\bar{n})D}{\epsilon}, \quad Q \ge Q_b$
(4)	$V_0 = V_s\left(1 - \frac{Z_D \text{Sw.R.}}{Z_{sd} + Z_0}\right)$
(5)	$F = \left[\beta_{n_r} \alpha^2 \frac{N_s}{N_t} \exp\frac{E_s}{kT}\right](\bar{n}_f)^2$
(6)	$\tau_{\text{rise}} = \frac{\bar{n}_s}{F} = \frac{1}{\beta_{n_r} \sigma \bar{n}_f}$
(7)	$\tau_{\text{decay}} = \frac{1}{\beta_{n_r} \sigma \bar{n}_f} = \frac{N_s \exp(E_s/kT)}{N_c \beta_{n_r} \alpha (N_r - n_r)} \ge P_s^{-1}$

voltage. It was noted in Sec. II that the grading is accomplished for our CdS/CdTe charge-storage-diode structures by varying the substrate temperature during the CdS deposition process.

IV. PHOTOELECTRIC MEASUREMENT TECHNIQUE

The theory describing the charge-storage CdS/CdTe diode has been reviewed in Sec. III. In the following sections we shall focus on the presentation of experimental data. First, data supporting the postulates of the charge-storage-diode model will be presented in Sec. V and then data pertinent to display-device operation will be presented in Sec. VI.

In this section, the measurement techniques used to acquire the data of Secs. V and VI are described. These techniques center around the idea of an equivalent circuit for the light-valve device.

The equivalent circuit for the ac light-valve device consists of two parts, a light-sensitive element and a set of passive components. The light-sensitive element consists of the CdS photoactive layer overcoated by the electrically blocking CdTe contact layer, while the set of passive components consists of the dielectric mirror and the liquid-crystal layer. The dielectric mirror is represented simply by an ideal capacitor and the liquid-crystal layer is represented by a parallel resistor-capacitor combination. This equivalent circuit is shown schematically in Fig. 4. The portion of this circuit inside the dashed-line square represents the photosensor, as described by the charge-storage-diode model.

The photosensor performance data of Sec. V focus on the region of the equivalent circuit within the dashed-line square. For this type of data, the passive-equivalent-circuit-component effects are minimized. This data is exemplified by experimental Q-vs-V curves similar to those of Fig. 3. The curves of Fig. 3 were used earlier to explain the operation of the charge-storage diode. The samples used to collect experimental data consist of the standard ITO/CdS combination. However, the electrically blocking contact is formed by a $\frac{1}{2}$-cm^2 Ag-paint contact, rather than the usual CdTe blocking contact layer. Tests have shown the two types of contacts to be equivalent. Experimentally, then, the Q-vs-V curves are taken by placing the ITO/CdS/Ag sample in series with a large capacitor and driving the combination with a 60-V peak-to-peak sawtooth voltage waveform. Scope traces generate the Q-vs-V curves; when the scope y axis monitors the voltage on the large series capacitor, the scope x axis monitors the voltage supplied to the photosensor. The Q-vs-V curves are measured at frequencies, light levels, and voltages of interest to device performance.

The gray-scale and response-time data of Sec. VI focus on the equivalent circuit for the whole light-valve device. For the collection of these data, the ITO/CdS/Ag sample is set in series with impedances representing a dielectric mirror and a 4-μm-thick liquid-crystal layer. All impedances representing a dielectric mirror and a 4-μm-thick liquid-crystal layer are scaled to the $\frac{1}{2}$-cm^2 Ag-electrode-contact area. This equivalent-circuit-data collection procedure has been found to be valid by comparing equivalent-circuit data with actual liquid-crystal light-valve data.

V. VERIFICATION OF PRINCIPAL PHOTOSENSOR MODEL ASSUMPTIONS

First, it is important to verify the two principal assumptions made in the charge-storage-diode model reviewed earlier. These are as follows: (i) that only light absorbed in the CdS film, not the CdTe, contributes to the diode stored charge, and (ii) that the ac capacitive impedance associated with the CdS-diode depletion-width is the dominant light-dependent impedance component.

The first assumption is verified by the following experimental observations:

(1) The peak diode spectral response lies at the CdS band edge and falls off rapidly in the red. The data of Table II is typical for ac-light-valve response. If electron-hole pairs generated in the CdTe were important, red spectral response would be comparable to the green.

(2) The high-frequency switching ratio is higher than the theoretical valve for unity gain and this switching ratio, to a first approximation, is independent of frequency. In fact, the theoretical unity-gain switching ratio at 2 kHz, 100 μW/cm^2, and 50 V peak-to-peak is 1.1. This is much lower than observed (e.g., 1.77 from Table II); higher than unity-gain and frequency-independent characteristics follow naturally from the hypothesis of hole capture in CdS.

TABLE II. Switching ratio—4-μm liquid crystal.

Wavelength		Switching ratio
Red—6000 Å	1.05	2 kHz, 100 μW/cm^2
Green—5260 Å	1.77	2 kHz, 100 μW/cm^2

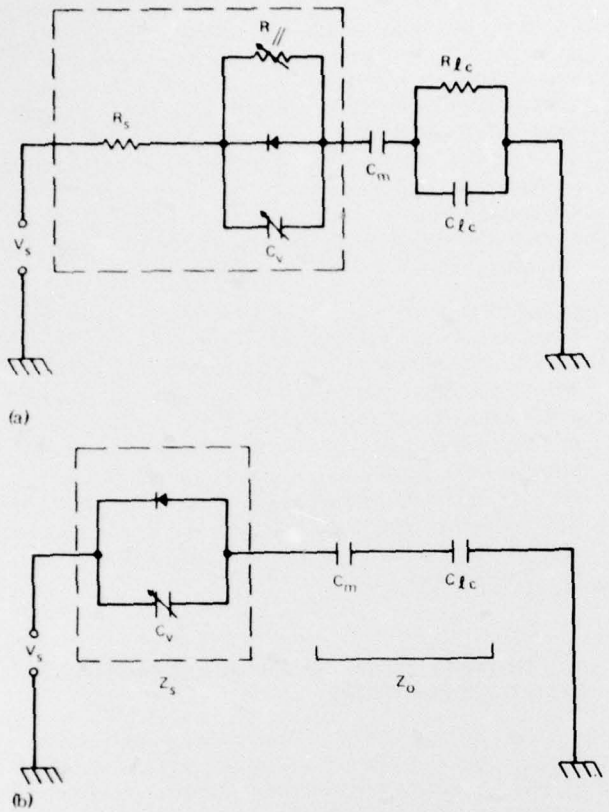

FIG. 4. (a) Equivalent circuit of a resolution element in the ac light valve. The portion in the dashed square represents the CdS/CdTe photosensor element, while the portion in series with this represents the impedances of the dielectric-mirror and the liquid-crystal elements. (b) A simplification of circuit (a) which is a useful first approximation.

(3) The Ag blocking contact is equivalent to the CdTe blocking contact. This implies again that the CdS film properties control the photosensor performance.

The second assumption that the depletion-width photocapacity dominates ac photosensor performance can be restated by referring to the generalized charge-storage-diode equivalent circuit shown in Fig. 4. If this assumption is valid, then

$$R_s \ll \frac{1}{\omega C_v}$$

and

$$R_{\parallel} \gg \frac{1}{\omega C_v}.$$

The quantity R_s represents the undepleted CdS-film photoresistivity. From dc peak-spectral-response measurements utilizing Ohmic contacts, an approximate value for R_s can be calculated. From this computed value of R_s from a photoconductor model, one would expect a diode switching ratio of better than 10 to 1 measured through a capacitive short if the capacitive depletion width could be ignored. Then, based on the charge-storage-diode model, one would expect the capacitive depletion width to become less important at lower voltages. Then the ac switching ratio should exceed 10 for a capacitive short as the applied peak-to-peak voltage approaches zero. This trend is observed, as is shown in Fig. 5. Furthermore, for a uniform stoichiometric film, one can assume exponential light absorption (e.g., F and n_f fall off exponentially with distance from the ITO/CdS interface). Then a calculation using Maxwell's equation as for Eqs. (2) and (3), assuming an exponential n_f distribution yields the theoretical switching-ratio curve in Fig. 5. This switching ratio is calculated assuming that the capacitive-depletion-width impedance dominates R_s. So then the photocapacity dominates R_s at 200 Hz. This is also true at high frequency and high light levels.

The assumption that $R_{\parallel} \gg 1/\omega C_v$ can be shown to be valid by comparing experimentally measured Q-vs-V curves for a cell with the theoretical Q-vs-V curves of Fig. 3. Experimental Q-vs-V curves are shown in Fig. 6 for 2-kHz and varying light levels. These curves show a small hysteresis from the increasing- to decreasing-voltage cases. However, the averaged curves correlate well with the curves of Fig. 3. The observed hysteresis effect results from a finite $R_{\parallel}$. Physically, $R_{\parallel}$ represents the residual resistivity of the depleted portion of the CdS film. $R_{\parallel}$ is finite in this region because, even though the shallow centers are empty, carriers may still be injected in the depleted region by light absorption and by deep-trap-level emptying. This carrier injection in the depletion region leads to hysteresis because recombination occurs only when electrons and holes are together in the bulk of the film and this occurs mainly near zero voltage. So plate charge accumulation from carrier injection via light absorption and deep-trap emptying lead to a large charge for larger delay-time intervals as measured from the zero-voltage region. Thus more charge is accumulated for the $|V|$-decreasing case than for the $|V|$-increasing case as is seen in Fig. 6.

However, even given the existing hysteresis, the statement that $R_{\parallel} \gg 1/\omega C_v$ is still a good working first approximation. This follows because the low-light-level hysteresis charge is presently no more than approximately 20% of the shallow-center charge, and as the films improve, i.e., as the deep-trap-center density decreases, the hysteresis charge will decrease.

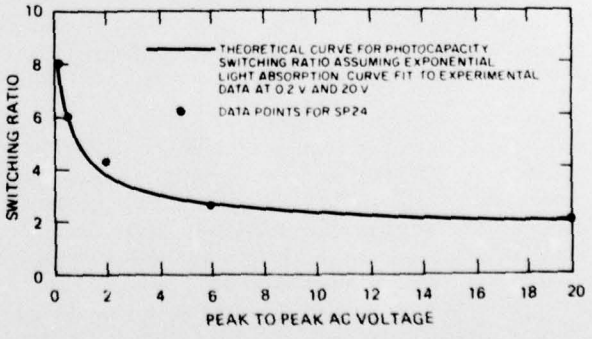

FIG. 5. Switching ratio for a CdS film measured through a capacitive short as a function of peak-to-peak ac voltage amplitude at 200 Hz.

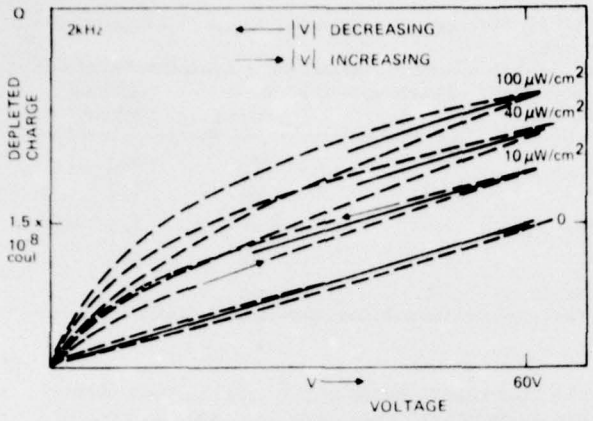

FIG. 6. Experimental plate-charge—vs—back-bias-voltage curves at 2 kHz. Light intensity is the curve-family parameter.

VI. PHOTOSENSOR-RELATED LIGHT-VALVE PERFORMANCE DATA

In Sec. V, the focus was on the narrow objective of charge-storage-diode model verification. In this section, the focus shifts and broadens. Our objectives here are threefold.

First, we wish to present photosensor data pertinent to light-valve-display operation. This has not been presented previously and is of some interest. For example, the response-time data show that the photosensor device is capable of near-TV-rate operation.

Second, we wish to show that these display-device data correlate well with the model.

Third, we wish to show that the small deviations from the model can be attributed to the presence of more than one deep-trap level, and therefore, improvements in the polycrystalline-CdS-film quality will lead to a closer agreement with the model.

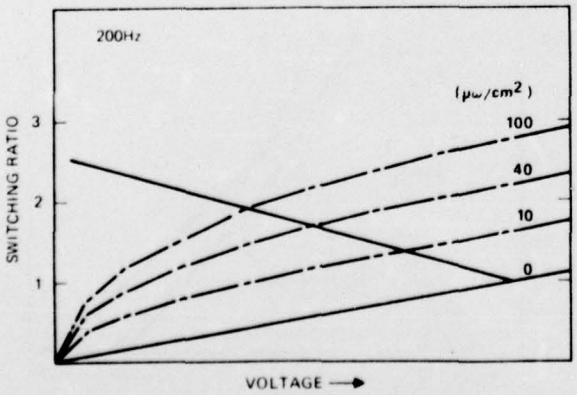

FIG. 7. Shown are averaged experimental Q-vs-V curves for the charge-storage diode at 200 Hz. The straight line crossing the Q-vs-V family of curves represents the charge-storage-diode/light-valve operating curve as derived in Eq. (4), Table I.

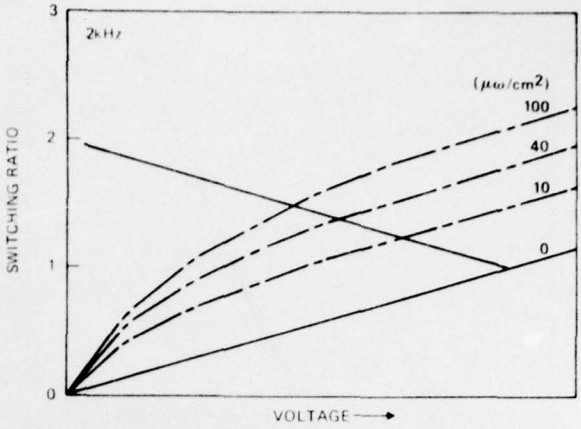

FIG. 8. Shown are averaged experimental Q-vs-V curves for the charge-storage diode at 2 kHz. The straight line crossing the Q-vs-V family of curves represents the charge-storage-diode/light-valve operating curve as derived in Eq. (4), Table I.

A. Gray-scale data

As discussed earlier, experimental Q-vs-V curves were recorded via scope-trace photos with a small-impedance series capacitor. These data were recorded at 200 Hz and 2 kHz. The averaged traces are shown in Figs. 7 and 8 for a $\frac{1}{2}$-cm² metal contact.

Next, impedances representing a 4-μm liquid-crystal layer (scaled to the $\frac{1}{2}$-cm² contact area) were switched into the circuit (forming an ac-light-valve e equivalent circuit) and equilibrium peak-current switching ratios were measured at various light levels. Finally, straight lines were drawn on the averaged Q-vs-V curves representing the photosensor load curves. These straight lines were drawn to conform to measured saturated-light switching ratios. From the straight-line intersections on the Q-vs-V curves, predicted gray-scale switching ratios were determined. These predicted gray-scale data are compared in Table III with the measured equilibrium switching ratios. It can be seen from Table III that theory and measurement agree very well.

Also, from the light-intensity information in the Q-vs-V family of curves in Figs. 7 and 8, it is possible to check the validity of the quadratic Q_b-vs-F dependence shown in Eq. (5). This is done by plotting $\log Q_b$-vs-$\log F$

TABLE III. Theoretical and experimental ac-light-valve gray-scale data.

Light intensity, (μW/cm²)	Predicted switching ratio	Measured switching ratio	
10	1.2	1.1	2 kHz
40	1.37	1.3	
100	1.47	1.5	
10	1.38	1.43	200 Hz
40	1.68	1.7	
100	1.92	1.85	

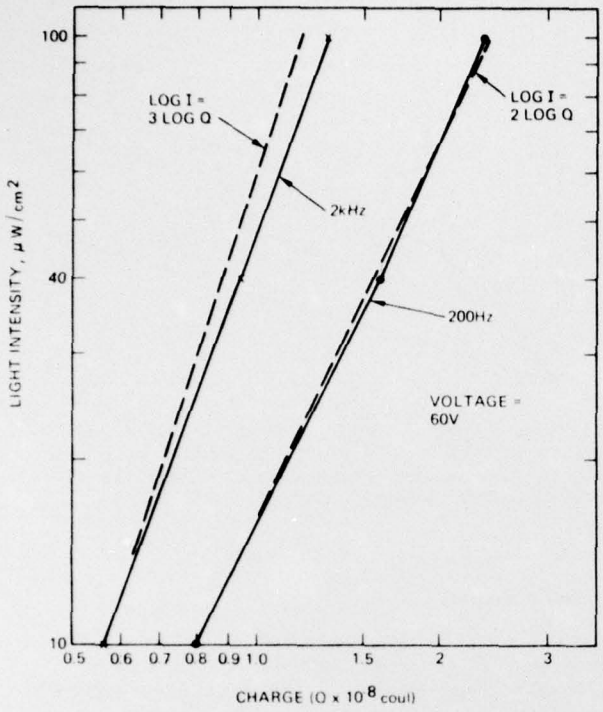

FIG. 9. The depleted charge is plotted versus illumination intensity for a charge-storage diode. Data are presented for diode operation at 200 Hz and 2 kHz. The dashed lines represent constant slopes of 2 and 3.

in Fig. 9. Agreement with the predicted slope of 2 is reasonably good. The deviation at high light levels can be explained as follows: Recall that α is the fractional portion of a period for which an electron remains free in the CdS film before being swept to the electrode. This sweep-out time will be inversely proportional to the drift velocity. In a photoconductor with a multitude of traps, the drift velocity increases at higher light levels.[5] This phenomenon will lead to a decrease in α at high light levels and a slope larger than 2 as observed in Fig. 9. However, this effect can be regarded as a higher-order perturbation on the charge-storage-diode model.

B. Response-time data

Photosensor response times can be measured from the equivalent-circuit peak-current-envelope scope-curve traces as substrate illumination light is turned on or off. Table IV shows the equivalent-circuit measured time-response data for 2 kHz.

It is of interest to compare the measured time-response data of Table IV with the predictions of Eqs. (6) and (7) from Table I.

1. On time

Note that, for the two-trap-level systems described in Table I, the $n_f\alpha$-vs-$F^{1/2}$ dependence in Eq. (5) combines with the τ_{rise}-vs-$n_f\alpha^{-1}$ dependence in Eq. (6) to predict a τ_{rise}-vs-$F^{-1/2}$ dependence. This implies that

TABLE IV. Photosensor response-time data as a function of light level.

Light intenstiy (μW/cm^2)	Switching ratio	On time (msec)	Off time (msec)	
10	1.1	250	30	2 kHz
40	1.3	50	30	
100	1.5	20	50	
400	1.75	10	30	
Saturated	2.1	≤5	15	

a plot of the experimental log$I$-vs-logτ_{rise} data should show a slope of -2. These data are shown in Fig. 10 for the 2-kHz case. Data points for the 200-Hz rise-time case are also shown. In each case, the -2 slope dependence exist for the data above 100 μW/cm^2, but a clear anomaly exists for the data below this light level. The low-light-level data fits more nearly a curve with -1 slope. This -1 slope can occur if a second deep-electron-trap level exists in the sputtered CdS films.

The -1 slope is explained as follows: Equation (6) in Table I describes the photosensor rise time. This equation was derived by noting that the rise time is simply the time needed to charge the CdS/CdTe charge-storage diode. As the major charge element arises from the filling of deep-trap levels, the time is simply n_s/F. The problem is to describe n_s. In the two-electron-trap-level model,[3] the deep-trap-level population is a function of F and in fact varies as $F^{1/2}$. However, if the dark-state Fermi level is quite deep and the films possess a multitude of deep levels, then the lower deep levels must be nearly filled before the shallow centers can fill sufficiently to greatly affect the depletion width. If N_{ss} represents the trapped-electron density, then n_s in the expression for rise time becomes N_{ss}. This N_{ss} is approximately the lower deep-trap-center density, and thus is not a function of F. Therefore, the rise time

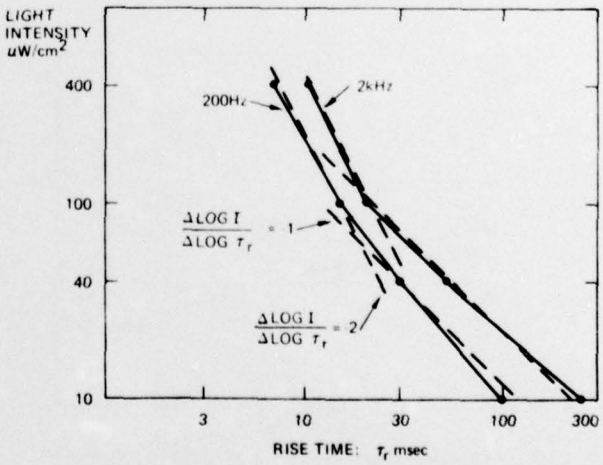

FIG. 10. The photocurrent rise time for a light valve is plotted versus photosensor illumination light intensity. Data are presented for operation at 200 Hz and 1 kHz. The dashed lines represent slopes of -1 and -2.

should vary as F^{-1}. This explains the -1 slope observed for the lower-light-level data in Fig. 10.

2. Off time

Turning now to the photosensor decay time, note that there are two cases implicit in Eq. (7). Decay can be dominated by recombination or by detrapping.[3] Where the decay time is controlled by detrapping, Eq. (7) predicts a constant decay time P_s^{-1} independent of light level. This apparently describes the data at 2 kHz.

VII. CONCLUSIONS

The preponderance of data presented in Secs. II–VI supports the charge-storage-diode model presented. Some deviations from the simple three-level model were observed. These experimental deviations can be summarized as follows: (i) Q-vs-V curve hysteresis, (ii) a prolonged low-light-level turn-on time, and (iii) problems with drift-velocity variations with light intensity and applied ac frequency.

We have noted that these deviations can be regarded as arising from a multitude of deep-electron-trap levels in the CdS films.

The fact that we have developed a viable model to describe the ac photoresponse of CdS/CdTe photosensors allows us to reach the following outstanding conclusion: To the extent that the deep-trap density in films can be reduced, the expected benefits for a display device are (i) faster turn-on time and (ii) higher sensitivity. This conclusion still stands even given the observed deviations.

The extent to which sensitivity and turn-on time can be improved can be quantified by evaluating the present level of performance. Thus from the data of Fig. 7 for the 40-μW/cm^2 curve, the shallow-trap (mobile) charge, n_f can be calculated. We find for that case $n_f = 3\times10^{11}$ electrons/cm^3. From the measured 30-msec on time for 40 μW/cm^2 and 200 Hz from Fig. 10, we calculate the stored charge in deep-trap centers to be 10^{16} electrons/cm^3. The conclusion is that the effective charge, 3×10^{11}/cm^3, is only 3% of the stored charge, 10^{16}/cm^3; only 3% of the injected charge is effective. Considerable room for improvement exists. This improvement can be realized by minimizing deep-trap densities. This in turn can be done by producing a graded absorption structure by utilizing graded bandgap films of, for example, $CdS_{1-x}Se_x$.

VIII. NOMENCLATURE

Q_b	total shallow-trap-center charge in the CdS film
$\bar{n}_f$	space-averaged shallow-trap-center electron population density
δ	thickness of high shallow-trap density, high absorptive CdS-film region
V	instantaneous back-bias voltage on CdS film
Q	instantaneous CdS electrode charge
ϵ	CdS-film dielectric constant
D	total CdS-film thickness
V_s	total peak supply voltage applied to ac light valve
V_0	voltage amplitude across the CdS film
Z_0	impedance seen by photosensor, i.e., the light-valve mirror and liquid-crystal combination (per unit area)
Sw. R.	current switching ratio, i.e., the ratio of peak current when the photosensor is illuminated to peak current in the absence of illumination
Z_{dark}	total dark-state photosensor impedence per unit area
β_{nr}	capture coefficient for an electron by a CdS recombination center
F	density of electron-hole pairs created per second by optical excitation across the band gap
α	the fraction of a cycle an electron from a shallow-trap center is free to move in the CdS film before being swept out to the electrode.
T	temperature
N_s	density of slow deep electron traps in CdS
E_s	energy difference between deep-trap level and bottom of conduction band
N_c	effective density of states in lowest kT-wide part of the conduction band
f	ac frequency
τ_{rise}	light-induced photosensor-current rise time
τ_{decay}	photosensor decay time
P_s^{-1}	thermal escape time
$\bar{n}_s$	space-averaged deep-trap-center electron population density

[1] T. D. Beard, W. P. Bleha, and S.-Y. Wong, Appl. Phys. Lett. **22**, 90 (1973).
[2] J. Grinberg, W. P. Bleha, A. D. Jacobson, A. M. Lackner, G. D. Meyer, L. J. Miller, J. D. Margerum, and L. M. Fraas, IEE Trans. on Electron Devices (to be published).
[3] L. M. Fraas, W. P. Bleha, J. Grinberg, A. D. Jacobson, preceding paper, J. Appl. Phys. **47**, 576 (1976).
[4] D. B. Fraser and H. Melchior, J. Appl. Phys. **43**, 3120 (1972).
[5] R. H. Bube and H. E. Macdonald, Phys. Rev. **121**, 473 (1961).

(9) Final technical rept. 1 Nov 74-12 Jun 76,

UNCLASSIFIED

SECURITY CLASSIFICATION OF THIS PAGE (When Data Entered)

REPORT DOCUMENTATION PAGE	READ INSTRUCTIONS BEFORE COMPLETING FORM
1. REPORT NUMBER / 2. GOVT ACCESSION NO.	3. RECIPIENT'S CATALOG NUMBER
4. TITLE (and Subtitle) (6) DEVELOPMENT OF A COLOR SYMBOLOGY AC LIQUID CRYSTAL LIGHT VALVE.	5. TYPE OF REPORT & PERIOD COVERED Final Technical Report 1 Nov 1974-12 June 1976
	6. PERFORMING ORG. REPORT NUMBER
7. AUTHOR(s) (10) A.D. Jacobson W.P. Bleha	8. CONTRACT OR GRANT NUMBER(s) (15) N00024-75-C-7187
9. PERFORMING ORGANIZATION NAME AND ADDRESS Hughes Research Laboratories 3011 Malibu Canyon Road Malibu, California 90265	10. PROGRAM ELEMENT, PROJECT, TASK AREA & WORK UNIT NUMBERS
11. CONTROLLING OFFICE NAME AND ADDRESS Department of the Navy Naval Sea Systems Command Washington, D.C. 20360 (11)	12. REPORT DATE Apr 77
	13. NUMBER OF PAGES 104 (12) 112 p.
14. MONITORING AGENCY NAME & ADDRESS (if different from Controlling Office)	15. SECURITY CLASS. (of this report) Unclassified
	15a. DECLASSIFICATION/DOWNGRADING SCHEDULE

16. DISTRIBUTION STATEMENT (of this Report)

Approved for public release; distribution unlimited.

17. DISTRIBUTION STATEMENT (of the abstract entered in Block 20, if different from Report)

18. SUPPLEMENTARY NOTES

19. KEY WORDS (Continue on reverse side if necessary and identify by block number)

Projection Display, Liquid Crystal, Thin Film Photoconductor, Dynamic Color Symbology, Birefringence, Hybrid Field Effect Mode, Dielectric Mirror, Liquid Crystal Alignment, Imaging Device

20. ABSTRACT (Continue on reverse side if necessary and identify by block number)

The development of a reflective mode liquid crystal light valve suitable for large screen dynamic color symbology projection display is described. The light valve consists of a sandwich structure of a thin film photoconductor, light blocking layer, broad visible spectrum dielectric mirror and liquid crystal sandwiched between two glass electrodes with transparent conductive electrodes. There are no matrix

DD FORM 1 JAN 73 1473 EDITION OF 1 NOV 65 IS OBSOLETE

UNCLASSIFIED

SECURITY CLASSIFICATION OF THIS PAGE (When Data Entered)

172600

PRECEDING PAGE BLANK-NOT FILMED

elements to define resolution because of the insulating characteristics of the dielectric mirror it is necessary to use ac voltages to operate the light valve. In operation the CdS photoconductor, as a high resolution imaging light activated voltage gate for the liquid crystal. The light blocking layer and dielectric mirror serve to reflect the projection light and prevent this light from reaching the visible sensitive photoconductor. Imaging on the light valve is done with a low intensity P-1 CRT with a fiber optic faceplate and a light valve constructed on a mating fiber optic faceplate.

The report details the development of the ac light valve with two liquid crystal modes: tilted perpendicular birefringent field effect and hybrid field effect (HFE). These field effect modes allow white, yellow, magenta, blue, and green symbols to be projected on a black background. The black background also allows the superposition of static imagery, such as maps, on the color symbology. The various colors and white are selected by the value of the image light intensity.

The development of the light valve proceeded in two phases. The first phase concentrated on the tilted perpendicular device. The development of liquid crystals and alignment techniques, CdS photoconductor development, dielectric mirror fabrication, and light valve device physics are detailed here. Also reported are substrate uniformity and cosmetic quality improvements, and a new cell holder design. Finally, the performance of the two tilted perpendicular light valves, delivered to the Naval Electronics Laboratory Center, San Diego, California, is described.

The second phase continued the work of the first phase but concentrated on the HFE light valve. The application of the HFE mode to color symbology is described. Finally, at the end of this phase the performance of the HFE color symbology light valve that was the final device delivery to NELC is detailed.